

Development of New Analytical Methods Enhancing the Sensitive Detection and
Quantification of N-glycans Derived from Biological and Clinical Samples

by

Yunli Hu, B.S., M.S.

A Dissertation

In

ANALYTICAL CHEMISTRY

Submitted to the Graduate Faculty
of Texas Tech University in
Partial Fulfillment of
the Requirements for
the Degree of

DOCTOR OF PHILOSOPHY

Approved

Yehia Mechref
Chair of Committee

Dimitri Pappas

Paul W Pare

Mark Sheridan
Dean of the Graduate School

December, 2014

Copyright 2014, Yunli Hu

ACKNOWLEDGMENTS

First and foremost, I would like to take this opportunity to thank my mentor Dr. Yehia Mechref. Without his patient guidance and continuous support throughout the past four years, it's impossible for me to finish my Ph.D program. His diligent, persistent and commitment to the highest standards motivated me. He supports me to present my work at several different national conferences. His enthusiasm and passion for research will inspire me all my life.

I would like to thank my committee member Dr. Pappas. I really appreciate his guidance and precious suggestions during my Ph.D study. I appreciate the Dr. Pare for being my committee member and devoted his time for giving me valuable advices.

I wish to express my appreciation to the members of Dr. Mechref group. It's a precious memory to be with you for the past four years. Wish you best of luck in your graduate study and future life.

Last but not least, I want to thank my family for their unconditional support. Their encouragement and love inspired me to finish my Ph.D program.

TABLE OF CONTENTS

ACKNOWLEDGMENTS	ii
ABSTRACT	vii
LIST OF FIGURES	xii
CHAPTER I. INTRODUCTION	1
1.1 Protein Post Translational Modifications (PTMs)	1
1.2 Glycosylation of Proteins	1
1.2.1 O-linked Glycosylation	1
1.2.2 N-linked Glycosylation	3
1.2.3 Aberrant Glycosylation and Human Diseases	4
1.3 Glycomics Strategies.....	6
1.3.1 Glycan Release.....	6
1.3.2 Purification of Glycan Mixtures	9
1.3.3 Derivatization of glycans	9
1.4 Separation Techniques	15
1.4.1 CE Separation	15
1.4.2 High Performance Liquid Chromatography (HPLC) Separation	16
1.5 Detection Methods	18
1.6 Quantitative Glycomics through Isotopic Labeling	19
1.6.1 Stable Isotopic Labeling through Reductive Amination.....	19
1.6.2 Stable Isotopic Labeling through Permetylation.....	20
1.6.3 Stable Isotopic Labeling through Tandem Mass Tags (TMTs)	22
1.6.4 Metabolic Labeling Quantitative Glycomics	22
1.7 Software Tool for MS-based Quantitative Method.....	23
1.8 Outline of Chapter and Goals.....	23
CHAPTER II. COMPARING MALDI-MS, LC-MALDI-MS AND LC-ESI-MS GLYCOMIC PROFILES OF PERMETHYLATED N-GLYCANS DERIVED FROM MODEL GLYCOPROTEINS	26
2.1 Introduction	26
2.2 Experiment	29
2.2.1 Material	29
2.2.2 Release of N-glycans from Model Glycoproteins.....	29
2.2.3 Release of N-glycans from Pooled Blood Serum and Purification.....	29
2.2.4 Reduction of N-glycans	30

2.2.5 Permetylation of N-glycans	31
2.2.6 On-line Solid-phase Purification of N-glycans	31
2.2.7 ESI-MS Acquisitions	32
2.2.8 MALDI-MS Acquisition.....	33
2.3 Results and Discussion.....	33
2.4 Conclusion	48
CHAPTER III. COMPARATIVE GLYCOMIC PROFILING OF ISOTOPICALLY PERMETHYLATED N-GLYCANS BY LC-ESI-MS.....	56
3.1 Introduction.....	56
3.2 Experimental	59
3.2.1 Material	59
3.2.2N-Glycans Released from Model Glycoproteins	59
3.2.3N-Glycans Released from HBS, Esophageal Disease and DF samples.....	59
3.2.4 Purification of N-Glycans Released from Pooled HBS	60
3.2.5 Reduction of N-Glycans.....	60
3.2.6 Permetylation of N-Glycans.....	61
3.2.7 Solid-phase purification of N-Glycans	62
3.2.8 LC-ESI-MS	62
3.2.9 Data Evaluation.....	63
3.3 Results and Discussion.....	63
3.3.1 Comparative quantification of permethylated N-glycans derived from model glycoproteins	65
3.3.2 Comparative quantification of permethylated N-glycans derived from HBS69	69
3.4 Conclusion	78
CHAPTER IV. LC-MSMS OF PERMETHYLATED N-GLYCANS DERIVED FROM MODEL ANDHUMAN BLOOD SERUM GLYCOPROTEINS	79
4.1 Introduction.....	79
4.2 Experiment	81
4.2.1 Material	81
4.2.2 N-glycans Released from Model Glycoproteins	82
4.2.3 N-glycans Released from HBS Glycoproteins.....	82
4.2.4 Desialylation of N-glycans from Fetuin.....	83
4.2.5 Reduction of N-glycans	83
4.2.6 Solid-Phase Permetylation of N-glycans	84
4.2.7 Solid-Phase Purification of N-glycans	84
4.2.8 LC-MS and LC-MSMS.....	85
4.2.9 Data Evaluation.....	85
4.3 Results and Discussion.....	86
4.4 Conclusions	106

CHAPTER V. GLYCOMIC PROFILING OF TISSUE SECTIONS BY LC-MS ..	107
5.1 Introduction	107
5.2 Experiment.....	109
5.2.1 Material	109
5.2.2 On Surface Enzymatic Digestion of Model Glycoproteins and Human Blood Serum.....	109
5.2.3 On-Tissue Enzymatic Digestion of Mouse Brain Section	110
5.2.4 Reduction of N-glycan	110
5.2.5 Permetylation of N-glycan	110
5.2.6 LC-MS/MS Analysis.....	111
5.2.7 Data Evaluation.....	112
5.3 Results and Discussion.....	112
5.3.1 Profiling of Permethylated Glycans Derived from Glycoprotein	116
5.3.2 Profiling of Permethylated Glycans Derived from HBS	119
5.3.3 Profiling of Permethylated Glycans Derived from Mouse Brain Sections .	124
5.4 Conclusion..	135
CHAPTER VI. AUTOMATED ANNOTATION AND QUANTITATION OF GLYCAN BY LC/ESI/MS ANALYSIS USING MULTIGLYCAN-ESI COMPUTATIONAL TOOL.....	136
6.1Introduction.....	136
6.2 Experimental	138
6.2.1 Material	138
6.2.2 N-glycans Released from a Model Glycoprotein Fetusin and HBS	138
6.2.3 Dialysis to Remove Salts	139
6.2.4 Reduction	139
6.2.5 Permetylation	139
6.2.6 Nano LC-ESI-MS	140
6.2.7 Data Processing and Quantitation using MultiGlycan-ESI.....	141
6.3 Results and Discussion.....	141
6.3.1 Quantitation of Glycomics using MultiGlycan-ESI.....	145
6.3.2 Label-Free Quantitation of N-glycans Derived from Fetusin Glycomics	148
6.3.3 Label-Free Quantitation of N-glycans Derived from Fetusin Spiked in HBS Sample.....	148
6.4 Conclusion	151
CHAPTER VII. N-LINKED GLYCAN PROFILING IN NEUROBLASTOMA CELL LINES.....	154
7.1 Introduction	154
7.2 Experiment	156

7.2.1 Materials.....	156
7.2.2 Cell Lysis	157
7.2.3 Release of N-linked Glycans.....	157
7.2.4 Dialysis and Reduction	157
7.2.5 Permetylation	157
7.2.6 LC-MS/MS Conditions	158
7.2.7 Glycan Structural Assignment	159
7.2.8 Glycan Quantitation, Plotting and Statistical Characterization.....	159
7.3 Results and Discussion.....	160
7.3.1 Identification of Glycans in SY5Y and NLF Neuroblastoma Cell Lines ...	160
7.3.2 Quantitative Glycomic Profiling between SY5Y and NLF Cell Lines.....	160
7.3.3 MYCN Amplification Relationship with Monosaccharide Count and Sialylation	171
7.4 Conclusion	174
CHAPTER VIII. CONCLUSION AND FUTURE WORK	176
REFERENCE	179

ABSTRACT

Glycosylation plays important roles in many biological processes and aberrant glycosylation has been linked to many human diseases. The development of new analytical methods for qualitative and quantitative glycomics study is essential to monitor glycan changes associated with disease progress. Mass spectrometry (MS) based glycomics strategies are capable of identifying and quantifying numerous glycans derived from complex biological samples. Thus, the development of reliable and sensitive analytical methods is required.

The second chapter focuses on comparing the glycomic profiling of permethylated N-glycans derived from model glycoproteins and human blood serum (HBS) using MALDI-MS as well as reverse phase (RP) LC-MALDI-MS and RPLC-ESI-MS. In the case of model glycoproteins, the glycomic profiles acquired using the three methods were very comparable. However, this was not completely true in the case of glycans derived from HBS. RP-LC-ESI-MS analysis of reduced and permethylated N-glycans derived from 250 nL of HBS allowed the confident detection of 73 glycans (the structures of which were confirmed by mass accuracy and tandem MS), while 53 and 43 structures were identified in the case of RPLC-MALDI-MS and MALDI-MS analyses of the same sample, respectively. RPLC-ESI-MS analysis facilitates automated and sensitive tandem MS acquisitions. The glycan structures that were detected only in the RPLC-ESI-MS analysis were glycans existing at low abundances. This is suggesting the higher detection sensitivity of RP-LC-ESI-MS analysis, originating from both reduced competitive ionization and saturation of detectors, facilitated by the chromatographic separation. The latter also permitted the separation of several structural isomers; however, isomeric separations pertaining to linkages were not detected.

The third chapter introduced a relative quantification strategy, which employing stable isotopic iodomethane for comparative glycomic profiling by LC-ESI-MS. N-glycans released from model glycoproteins and HBS were permethylated with iodomethane (“light”) and iodomethane-*d*₁ or iodomethane-*d*₃ (“heavy”). The reliability of this strategy was evaluated with model glycoproteins. LC-ESI-MS comparative glycomic profiling of isotopically permethylated N-glycans derived from biological samples and glycoproteins reliably defined glycan changes associated with biological conditions or glycoproteins expression. This strategy permitted the reliable quantification of glycomic changes associated with different esophageal diseases, including high-grade dysplasia, Barrett’s disease, and esophageal adenocarcinoma.

The fourth chapter investigated the chromatogram behavior of permethylated N-glycans. The relationship between retention times *vs.* molecular weight of dextran, dextrin and model glycans and was investigated. Also, non-polar surface area (NPSA) of glycans was calculated and compared with experimental retention time. The trends of these two are similar when intermolecular interaction was included into the calculation. Moreover, the retention time is corresponding to glycan types and branch types. Then, the N-glycans analysis model, which combining the use of high mass accuracy and retention time was applied to confirm serum N-glycans. Totally, there were 70 N-glycans compositions identified with a linear fit for each subgroup. For example, R² for complex types N-glycans were better than 0.98. The linearity allows the prediction of N-glycans structure based on their retention time. Moreover, the retention time could be further applied to distinguish structure isomers as well as linkage isomers.

The fifth chapter described a new glycan sample preparation strategy using minimized sample preparation steps and optimized procedures for N-glycan profiling of mouse brain tissue sections. Tissue sections and spotted samples first undergo on-surface enzymatic digestion to release N-glycans. The released glycans are then reduced and permethylated prior to on-line purification and LC-ESI-MS analysis. The efficiency of this strategy was initially evaluated using model glycoproteins and HBS spotted on glass or Teflon slides. The new protocol permitted the detection of permethylated N-glycans derived from 10 ng RNase B. On the other hand, 66 N-glycans were identified when injecting the equivalent of permethylated glycans derived from a 0.1- μ L aliquot of HBS. On-tissue enzymatic digestion of nude mouse brain tissue permitted the detection of 43 N-glycans. The relative intensities of these 43 glycans were comparable to those from a C57BL/6 mouse reported by the Consortium for Functional Glycomics (CFG). However, the sample size analyzed in the protocol described here was substantially smaller than for the routine method (sub microgram *vs.* mg). The on-tissue N-glycan profiling method permits high sensitivity and reproducibility and can be widely applied to assess the spatial distribution of glycans associated with tissue sections, and may be correlated with immunofluorescence imaging when adjacent tissue sections are analyzed.

In the sixth chapter, an LC-MS based automated data annotation and quantitation software, MultiGlycan-ESI, was utilized for glycan quantitation. Data integrated by the software were first compared with manual integration to evaluate the performance of the automatic quantitation. MultiGlycan-ESI was then applied for quantitation of different concentration of fetuin as well as fetuin spiked in a complex biological sample-HBS. The relative abundance differences between software integration and manual integration were

less than 5%, indicating the reliability of this software tool in quantitation. Automated quantitation resulted in a linear relationship of R^2 higher than 0.93 for all six N-glycans derived from 50 ng to 400 ng fetuin. Spiking N-glycans into 0.02 μ L of HBS also exhibited linear agreement between concentration and intensity. With a variety of options that include mass accuracy, merged adducts, and filtering criteria, MultiGlycan-ESI allows automated annotation and quantitation of N-glycan data acquired by LC-ESI-MS. The software facilitates rapid and reliable high-throughput glycomics studies.

In the seventh chapter, a systematic comparison of N-linked profiles between *MYCN*-non amplified SY5Y and *MYCN*-amplified NLF cell lines with the aim of identifying sugar abundance changes linked to high-risk neuroblastoma was performed. Through a combination of LC-MS and bioinformatics analysis, we identified 16 glycans that show statistically significant changes in abundance between NLF and SY5Y samples. Closer examination revealed the preference for larger (in terms of total monosaccharide count) and more sialylated glycan structures in the *MYCN*-amplified samples relative to smaller, non-sialylated glycans that are more dominant in the *MYCN* non-amplified samples. These results suggest potential biomarker candidates prompting accurate neuroblastoma risk diagnosis.

LIST OF TABLES

1.1 The list of post-translational modifications	2
2.1 Relative intensities of the N-glycan structures commonly associated with RNase B acquired using different analytical techniques and methods	38
2.2 Relative intensities of the N-glycan structures commonly associated with PTG acquired using different analytical techniques.....	42
2.3 Signal-to-Noise ratios and relative intensities of HBS permethylated N-glycans analyzed by LC-ESI-MS, LC-MALDI-MS and MALDI-MS	50
3.1 Intensities and Ratios of N-glycans derived from cancer, Barrett's, HGD and DF HBS samples	71
4.1 Intensity and retention time of dextran, dextrin and N-glycans driven from fetuin ...	89
4.2 Total N-glycans extracted from blood serum and linear equation of each subtype.....	96
4.3 Comparison of the total detected N-glycans of previous published work with this work.	101
5.1 Relative abundances of the N-glycan structures commonly associated with RNase B acquired using different analytical techniques and methods.	118
5.2 Relative abundances of the N-glycan structures from CFG data and this study (Low mass range, mass<3250)	128
5.3 Relative abundances of the N-glycan structures from CFG data and this study (High mass range, mass>3250)	132
6.1 Integrated areas of permethylated N-glycans derived from fetuin, calculated by manual or MultiGlycan-ESI integration	144
7.1 List of of N-glycans derived from NFL and SY5Y, along with derived topologies and p-values from a t-test comparison between groups	165

LIST OF FIGURES

1.1 Workflow of commonly used glycomics strategies	7
1.2 Derivation of glycan by reductive amination	11
1.3 Derivation of glycan by hydrazide formation	12
1.4 Derivation of glycan by permethylation	14
1.5 Experimental flow of incorporating reductive tetraplex tags for quantitative glycomics analysis	21
2.1 LC-ESI-MS base peak intensity (BPI) chromatogram and 2-D overlaid BPI plot of reduced and permethylated N-glycans derived from 100 ng of RNase B. The insets are the mass spectra of each peak	34
2.2 LC-MALDI-MS Extract ion chromatograms of reduced and permethylated N-glycans derived from 100 ng of RNase B. The insets are the mass spectra of each peak.	35
2.3 LC-ESI-MS BPI chromatogram and 2-D overlaid BPI plot of reduced and permethylated N-glycans derived from 100 ng of PTG.....	40
2.4 LC-MALDI-MS extract ion chromatograms of reduced and permethylated N-glycans derived from 100 ng PTG.	41
2.5 LC-ESI-MS 2-D overlaid BPI plot of reduced and permethylated N-glycans derived from 250nL HBS	44
2.6 LC-MALDI-MS extract ion chromatograms of reduced and permethylated N-glycans derived from 250nL HBS	45
2.7 MALDI mass spectra and LC-MALDI-MS extracted ion chromatograms of N-glycans derived from blood serum. The inset depicting the mass spectra associated with the LC analysis	47
2.8 LC-ESI-MS extracted ion chromatograms of some N-glycan isomers derived from HBS	49
3.1 Schematic of sample preparation process	64
3.2 Extracted ion chromatograms (EIC) and MS spectra of Man 5 (a), Man 6 (b), Man 7 (c), Man8 (d), and Man 9 (e) glycans derived from RNase B. Equal amounts of N-glycans released from RNase B were permethylated with iodomethane (ICH_3), iodomethane- d_1 (ICH_2D) and iodomethane- d_3 (ICD_3) reagents and mixed prior to LC-ESI-MS analysis.....	66
3.3 EIC and MS spectra of biantennary monosialylated (a) biantennary disialylated (b), triantennary trisialylated (c), and triantennary tetraesiaylated (d) N-glycans derived from fetuin. Equal amounts of N-glycans released from fetuin were “heavy” and “light” permethylated using ICH_3 , and ICD_3 reagents, respectively	68
3.4 EIC of equal amounts of “heavy” and “light” permethylated (a) H5N2, (b) F1H3N5, and (c) F1H4N5 N-glycans derived from DF samples. EIC of equal amounts of “heavy” and “light” permethylated (d) H5N2, (e) F1H3N5, and (f) F1H4N5 N-glycans derived from cancer and DF samples, respectively	75

3.5 EIC of equal amounts of “heavy” and “light” permethylated (d) H5N2, (e) F1H3N5, and (f) F1H4N5 N-glycans derived from Barrett’s disease and DF samples, respectively	76
3.6 EIC of equal amounts of “heavy” and “light” permethylated (d) H5N2, (e) F1H3N5, and (f) F1H4N5 N-glycans derived from HGD and DF samples, respectively	77
4.1 Comparison of retention time vs. glucose unit and NPSA vs. glucose unit of dextrin and N-glycans derived from fetuin	87
4.2 Retention time of dextran, dextrin and N-glycans extracted from Fetuin <i>vs</i> molecular weight (a); and glucose unit (b). The standard deviations are very small as depicted by the error bars of each structure (N=3).....	90
4.3 Comparison of retention time <i>vs</i> glucose unit and NPSA <i>vs</i> glucose unit of dextrin and high mannose structures derived from RNase B	92
4.4 Retention time of N-glycans extracted from RNase B <i>vs</i> molecular weight. The insect depicts extract ion chromatograms of reduced and permethylated N-glycans derived from RNase B	93
4.5 Glycomic mapping of N-glycans derived from HBS (a). Linear fitting of the retention times of (b) high mannose; (c) complex-type biantennary; (d) complex-type triantennary; and (e) complex-type tetraantennary	94
4.6 Linear plot of different glycan structures with each of the <i>m/z</i> values detected at two different retention times suggesting structural differences	104
4.7 Linear plot of different glycan structures with each of the <i>m/z</i> values detected at two different retention times suggesting structural differences	105
5.1 Workflow of N-glycan profiling of tissue sections and model glycoproteins	113
5.2 Bar graphs of LC-ESI-MS intensities of permethylated N-glycans derived from RNase B and subjected to on-glass digestion for 4 h (green) and 8 h (red). Man 5, Man 6, Man 7 and Man 8 derived from 100 ng RNase B were monitored. Error bars represent standard deviation	114
5.3 Bar graphs of LC-ESI-MS intensities of permethylated N-glycans derived from 100 ng RNase B (a) and 500 ng fetuin (b) and subjected to on-glass digestion using 5 U (green) and 25 U (red) of PNGase F	115
5.4 Bar graphs of LC-ESI-MS intensities of permethylated N-glycans derived from 10 ng RNase B at optimized enzymatic releasing condition Error bars represent standard deviations (N = 3 technical replicates)	117
5.5 Bar graphs of LC-ESI-MS intensities of permethylated N-glycans derived from 500 ng fetuin at optimized enzymatic releasing condition Error bars represent standard deviations (N = 3 technical replicates)	120
5.6 Bar graphs of LC-ESI-MS intensities of permethylated N-glycans derived from model glycoprotein mixtures through on-glass (blue) and in-solution (purple) digestions. Error bars represent the standard deviations (N=3 technical replicated).	121

5.7 Bar graphs of the LC-ESI-MS intensities of permethylated N-glycans derived from analyzing a 0.1 μ L aliquot of HBS (a 0.5 μ L aliquot of HBS was subjected to sample preparation procedure as described in Methods)	123
5.8 Bar graphs of the LC-ESI-MS intensities of permethylated N-glycan derived from mouse brain sections. Error bars represent the standard deviations (N=12 biological replicates). Inset depicts an image of a tissue section with 4 spots of PNGase F.....	126
5.9 Venn plot comparing the CFG data and data of this study in term of the number of N-glycans derived from mouse brain tissues	127
6.1 Workflow of MultiGlycan-ESI based automatic quantitation strategy. a) Permethylated N-glycan preparation workflow; b) Software annotation and quantitation method	142
6.2 Bar graph of different adducts of permethylated N-glycans derived from fetuin.....	146
6.3 Bar graph of six permethylated N-glycans derived from fetuin. Same amount of fetuin was injected at different injection volume. Triplicate injections were made for each group	147
6.4 A plot of the linear relationship of the permethylated N-glycans derived from fetuin. Triplicate injections of four groups from 50 ng-400 ng of fetuin were made	149
6.5 A plot of the permethylated N-glycans derived from fetuin spiked into 0.2 μ L HBS. Triplicate injections of five groups from 0 ng-200 ng fetuin spiked into HBS were made	150
6.6 A plot of the permethylated N-glycans derived from fetuin spiked into 0.002 μ L HBS. Triplicate injections of five groups from 0 ng-200 ng fetuin spiked into HBS were made	152
7.1 Scatter plot of detected glycan abundances (measured as XICs) within and across NLF and SY5Y cell lines. The plot trends along with cross-correlation measures depict high correlation between cell lines (indicative of good reproducibility) and low correlation across cell lines (indicative of change)	161
7.2 Abundance profiles for detected glycans. X-axis shows glycan type and follows a HexNAc-Hex-DeHex-NeuAc format. Y-axis depicts average glycomic abundances (from three replicates per group). Comparisons were compared between NLF and SY5Y cell line samples using the statistical t-test. Glycans denoted by * showed statistical significance in differential expression (p-value < 0.05). In particular, NLF (i.e. <i>MYCN</i> amplified) cell lines show a strong preference for larger and sialylated (NeuAc) structures when compared with SY5Y (i.e. <i>MYCN</i> non-amplified) cell lines	163
7.3 Hierarchical clustering of glycomic abundances. Each column is a glycan indicated as in a X-HexNAc-Hex-DeHex-NeuAc format. As can be observed, there is a split between glycans that are more abundant in SY5Y versus glycans that are more abundant in NLF. This illustrates that this particular glycan signature could be used for detecting <i>MYCN</i> amplification within neuroblastoma, and consequently for risk-stratification	164

7.4 Glycan graph arranged according to total monosaccharide count. Each node is a glycan and two nodes are linked by a directed edge if the difference in monosaccharide count is +1 in only one position in the HexNAc-Hex-DeHex-NeuAc format. The glycan HexNAc7Hex8DeHex1Fuc3 was a single node without any edge connections. Orange boxes do not show significant change between SY5Y and NLF, where yellow boxes indicate glycans that show significant (p -value < 0.05) change in expression. The node color for the yellow boxes indicates if the glycan was more abundant in SY5Y (red) or NLF (blue). From the graph, there is evidence that bigger glycans and glycans with more sialylated structures are more abundant in *MYCN*-amplified NLF cells172

CHAPTER I

INTRODUCTION

1.1 Protein Post-Translational Modifications (PTMs)

Proteins are large biomolecules constructed from 20 amino acids, which are involved in all biological processes. PTMs of proteins are either covalent modifications of amino acid residues or proteolytic cleavage of protein termini. The total reported PTMs are over 200, with phosphorylation and glycosylation are the best characterized.¹ Other common PTMs are acetylation, methylation, ubiquitination, lipidation and proteolysis (**Table 1.1**). PTMs of proteins determine their spatial structures and modulate their functions and activities. Characterization of protein structures with details of PTMs information may facilitate the elucidation of the complex biological processes.

1.2 Glycosylation of Proteins

Glycosylation represents one of the most common PTMs which attributes to protein diversity and functions. More than 50% of mammalian proteins are glycosylated.² Based on the different attachment sites of glycans, they can be divided into two categories. N-linked glycan is attached to the nitrogen of asparagine (Asn or N) while O-linked glycan is commonly linked to protein through hydroxyl group of serine (Ser or S) or threonine (Thr or T).

1.2.1 O-linked Glycosylation

Commonly, O-linked glycosylation initiation occurs in the Golgi apparatus by the addition of single monosaccharide to a Ser or a Thr residue. Subsequently enzymatic elongation will take place by transferases, prompting the formation of several core

Table 1.1 The list of post-translational modifications.

PTM	Amino acids modified	Functional group	Δm (monoisotopic)
Phosphorylation	Tyr, Ser, Thr	PO_4^-	79.9663
Glycosylation	Asn, Ser/Thr	Oligosaccharide	>800
Acetylation	Ser,Lys	CH_3CO	42.0106
Methylation	Arg,Lys	CH_3	14.0157
Ubiquitination	Lys	--	--
Acylation	various	various	various

structures. Further modification and elongation of the core structures by a variety of glycosyltransferases yields a large number of O-linked glycans.

1.2.2 N-linked Glycosylation

N-linked glycosylation is the most common type of glycosylation and plays important roles in protein folding, cell-cell interaction and cell-extracellular matrix attachment. The biosynthesis of N-linked glycosylation process occurs in the endoplasmic reticulum (ER) and Golgi complex.³ In contrast to O-glycosylation, N-glycosylation begins with the synthesis of lipid precursor. An oligosaccharide unit containing two N-acetylglucosamines and five mannoses is first synthesized on the cytosolic surface of the ER membrane and linked to a lipid precursor. Then, the oligosaccharide component of the glycoconjugate is flipped to the luminal side of the membrane and another seven monosaccharides are sequentially added. The formed “core” oligosaccharides are transferred to the asparagine residues of nascent polypeptide chain in the presence of the oligosaccharyltransferase. Terminal glucose and mannose residues are removed by ER glucosidases and mannosidases, respectively. ER-generated glycoforms remain uniform. Further trimming occurs when the glycoprotein reaches the Golgi complex. Golgi-generated glycan forms are highly diverse and differ from each other.

The biological roles of glycans can be classified into two types, i) structural and modulatory functions as well as ii) intrinsic and extrinsic properties.⁴ Structural and modulatory roles of glycans include stabilizing proteins, maintaining tissue structure and protecting polypeptides from recognition by proteases or antibodies. Moreover, incorrectly glycosylated proteins are known to fold improperly or even fail to exit the ER.

There are two different types of glycan receptors. The intrinsic glycan receptors are those that mediate clearance, turnover, and intracellular trafficking of soluble blood-plasma glycoproteins. Glycans act as specific binding sites for a variety of viruses, bacteria, and parasites. They also act as recognition targets for toxins of many plants and bacterial.

1.2.3 Aberrant Glycosylation and Human Diseases

The unusual activities of glycosyltransferase and glycosidases will result in altering the glycosylation patterns, which may influence cell recognition, adhesion, migration, as well as proliferation. Thus, glycosylation changes could result in the formation and progression of some human diseases, including inflammation,^{5,6} rheumatoid arthritis,⁷ Alzheimer disease^{8,9} and especially cancer.¹⁰⁻¹⁴

There is increasing evidence that abnormal glycosylation might allow malignant cells to escape immune surveillance, thus facilitate cancer development and metastasis. In the past decade, a wealth of research focus on revealing the correlation between aberrant glycosylation and the progression of cancer, including breast cancer, colorectal cancer, liver cancer, esophagus cancer, ovarian cancer, pancreas cancer and prostate cancer.

Breast cancer is the second most common cause of woman death. The development and progression of breast cancer have been monitored through native,^{15,16} labeled¹⁷ or permethylated¹⁸⁻²¹ O- and N-glycans. These studies demonstrate the over-expression of sialylated, fucosylated and branched N-glycans on breast cancer cell lines or tissue membrane. The up-regulation of Lewis-type epitopes such as sialyl Lewis A, sialyl Lewis X, Lewis A, Lewis B and Lewis Y have been correlated to the cancer states of many organs.^{22,23} The alternations of glycosylation pattern have been correlated with the

levels of sialyltransferases, fucosyltransferases, N-acetylglucosaminyltransferases and galactosyltransferases.

Colorectal cancer is another major prevalent type of malignant cancer worldwide. The glycosylation expression of patient serum as well tissue has been studied using the targeted approach of immunohistochemistry. In colon carcinoma patient serum, the over-expression of carbohydrate antigens has been observed.²⁴ On the other hand, Tn, Lewis antigen and their sialylated forms were changed in colorectal patient tissue.^{25,26} Liquid chromatography (LC)-mass spectrometry (MS) approach revealed the major changes in enterocyte-type cells are the GlcNAc-ended N-glycans.²⁷

Liver cancer includes different subtypes and the primary liver cancer is hepatocellular carcinoma (HCC). Patient serum has been extensively used for the study of glycosylation changes associate with liver cancer. Several studies using matrix assisted laser dissociation ionization (MALDI),²⁸ LC-electrospray ionization (ESI) and ion mobility spectrometry (IMS)-MS²⁹ demonstrated the change of sialylated N-glycan in patient serum. The up-regulation of several glycans, including Sialyl Lewis X³⁰ and α2-6 linked sialylated³¹ glycans, was observed in hepatocellular cell lines and tissues.

Ovarian cancer is the sixth most common cause of cancer world-wide. The diagnosis of ovarian cancer is based on the use of CA125 marker, which suffers from low sensitivity and specificity at early stage. O-glycosylation of several different ovarian carcinoma cell lines, patient serum and plasma has been studied using MS-based glycomics strategies.³²⁻³⁴ N-glycan profiling of SKOV3 ovarian carcinoma cell line demonstrated the predominantly structures are high mannose type and fucosylated complex type.³⁵

1.3 Glycomics Strategies

Although a variety of glycomics strategies exist, the sample preparation processes have some common features. The workflow of typical glycomics method is depicted in **Figure 1.1**. The first step of sample preparation involves the release of glycans. After digestion, a purification step may require to remove the excess salts and proteins. It is optional to derivatize the glycans. The derivatized or native samples can be analyzed by LC-MS or other techniques. Each of the steps will be described and discussed in detail next.

1.3.1 Glycan Release

There are different releasing strategies for N-linked and O-linked glycans, as they have different attachment sites. Efficient N-glycan release can be achieved by enzymatic digestion. Peptide N-glycosidase F (PNGase F), which is commonly purified from *Flavobacterium meningosepticum*, is the most effective enzyme for releasing N-glycans from glycoproteins. PNGase F can efficiently and specifically cleave the glycosidic bond between asparagine residue and core N-acetylglucosamine (GlcNAc) unless the core GlcNAc contains an $\alpha(1\text{-}3)$ linked fucose monosaccharide residue. After PNGase F cleavage, the asparagine residues from which the oligosaccharides have been removed are deaminated to aspartic acid. Deglycosylation rate will be greatly increased by denaturing glycoproteins with detergent prior to PNGase F treatment. Although PNGase F is the most effective enzyme for releasing N-glycans, other endoglycosidases, including Peptide N-glycosidase A (PNGase A), endo- F1, -F2, -F3, and -H, also exhibit special N-glycan release capabilities.

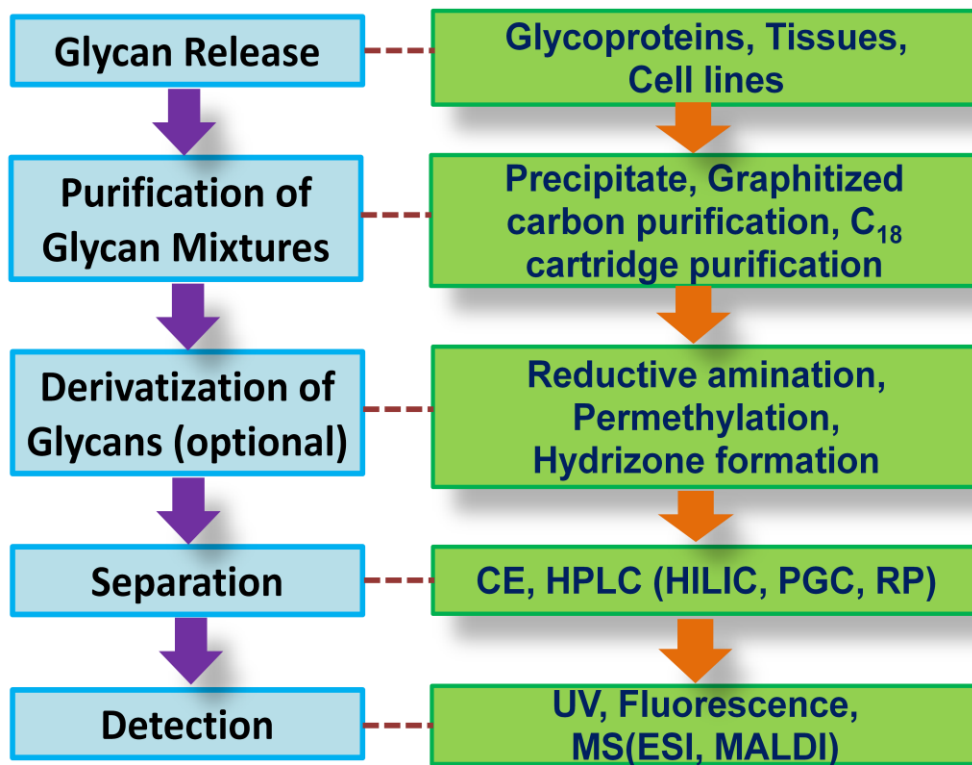


Figure 1.1 Workflow of commonly used glycomics strategies.

PNGase A, which is isolated from almond meal, provides an effective release of α (1-3) linked core fucosylated glycan.^{36,37} However, PNGase A is ineffective for the release of sialic acid containing N-glycans. Endo H cleaves the bond of the chitobiose core of high mannose and some hybrid N-linked glycans. The special cleavage sites of Endo H and Endo F series could be utilized for structure determination and some linkage elucidation.

N-glycans are also released through chemical reactions. However, this is not an attractive approach since releasing N-glycans through chemical reactions may lead to the loss of labile monosaccharides such as sialic acid and fucose as the high temperature (95°C) is always required.³⁸

Enzymatic release of O-linked glycans is still a challenge due to the lack of effective enzyme similar to PNGase F. All available O-glycosidase are highly specific to release O-linked glycans. For example, endo- α -N-acetylgalactosaminidase only enables the release of unmodified Gal β 1-3GalNAc (core 1) and the GlcNAc β 1-3GalNAc (core 3). Any modification of the core structure, such as sialylation, will hinder the action of endo- α -N-acetylgalactosaminidase. Therefore, chemical cleavage is still the most widely used method for releasing O-linked glycans from glycoproteins. Reductive β elimination³⁹ is the most reliable and universal method for releasing O-linked glycans. One issue of alkaline β elimination is that the strong base may cleave off monosaccharide from the glycan. The “peeling” reactions caused by alkaline medium can be minimized by adding a strong reducing agent, which will convert glycans to their alditols form. An alternative way to eliminate the “peeling” reaction is using a mild reagents (ammonia-based β elimination) to perform hydrolysis of O-linked glycans.^{40,41} A new O-linked glycans

releasing strategy, which involves the combination of pronase-E treatment and solid-phase permethylation of glycoproteins, is recently reported.⁴² Although hydrazinolysis⁴³ is an alternative approach to simultaneously release N-linked and O-linked glycans, the widely use of this strategy is hindered by the tedious, moisture sensitive hazardous process.

1.3.2 Purification of Glycan Mixtures

Digested sample contains a mixture of proteins, peptide, buffer salts and released glycans. Removing the proteins and salts in the glycan sample is necessary as the presence of these compounds will suppress the ionization efficiency of glycans. Purification of sample mixtures is based on the different molecular size and different polarity between glycans and protein. A selective organic precipitation/extraction strategy^{44,45} has been introduced to remove the salts and SDS by acetone precipitation. The released glycans are further purified by the precipitation using 50% methanol with adjusted pH to 5.5. Precipitation of proteins involves the use of 80% ethanol has been also reported.⁴⁶ Solid-phase extraction using a graphitized carbon cartridge^{33,47} has been applied to separate glycans from proteins and salts. Not only is the graphitized carbon cartridge is able to remove salts and protein from reaction mixture, it is also capable of fractionating neutral and acidic glycans.⁴⁷ Proteins and peptides can also be removed by passing reaction mixture to C₁₈ cartridge.^{18,48}

1.3.3 Derivatization of glycans

Although mass spectrometric analysis of native oligosaccharides is attainable, underivatized acidic oligosaccharides suffer from low ionization efficiency in positive ion mode. Moreover, due to native glycans lack of chromospheres/fluorophores groups, they

are not compatible with UV/fluorescence detection. To facilitate the UV/fluorescence detection as well as increase the sensitivity of MS detection, various derivatization strategies have been utilized.

1.3.3.1 Reductive Amination

Reductive amination, which involves a reaction between a primary amino group and the carbonyl group of glycan reducing end, commonly introduces a chromophore or fluorophore group into native glycans. In a reductive amination reaction, an unstable Schiff base is first formed by the reaction of an amino group with a carbonyl group. Then, a stable amine derivative is produced by the reaction with sodium cyanoborohydride (**Figure 1.2**).

The most widely used reductive amination reagents are 2-aminopyridine (PA),⁴⁹ 2-aminobenzoic acid (2-AA)⁵⁰ and 2-aminobenzamide (2-AB).⁵¹ PA is first introduced to label glycan by Hase in 1978 for UV and fluorescence detection.⁴⁹ The sensitivity of PA labeled glycan is increased compared to native glycan for MS-based detection. 2-AB is another common fluorescence tag for labeling native glycans.⁵² 2-AA labeled glycan exhibits two times higher fluorescence than 2-AB labeled glycan. Also, 2-AA derivatized glycan is compatible with normal phase and anion exchange LC. Other reductive amination reagents, such as 2-aminoacridone (AMAC),⁵³ 3-aminobenzamide (3-AB),⁵⁴ 3-aminobenzoic acid (3-AA)⁵⁵ and 4-aminobenzonitrile (ABN)⁵⁶ were also reported for labeling native glycans.

Reductive amination is a single site derivatization which takes place at reducing end with high a labeling efficiency. However, a clean-up step is required to remove excess salts and unreacted reagents.

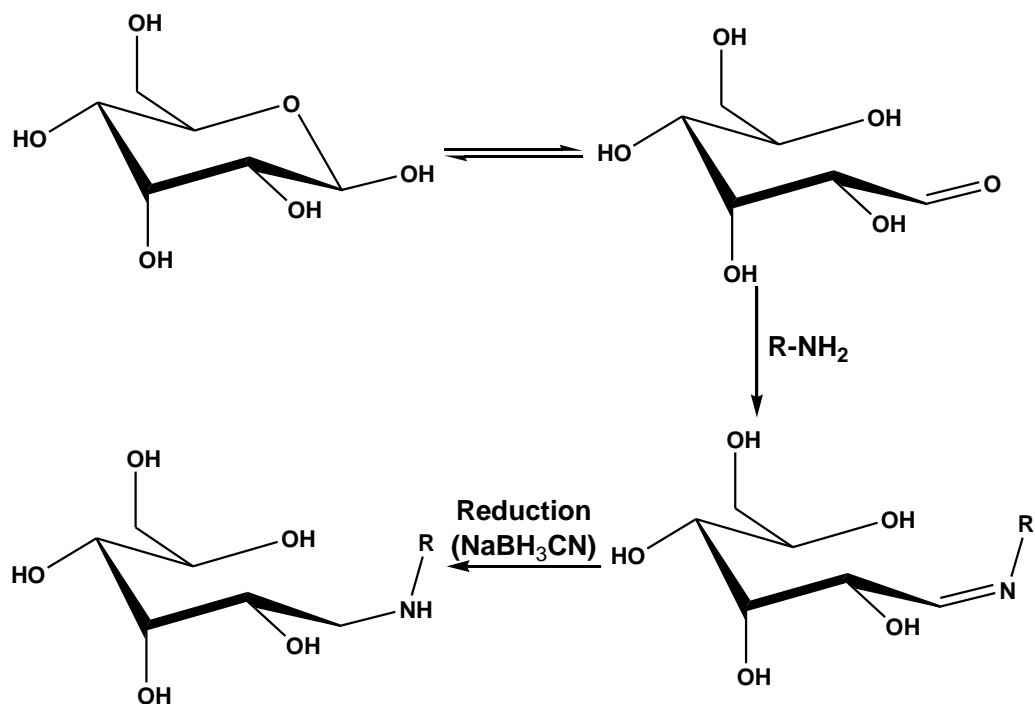


Figure 1.2 Derivation of glycan by reductive amination.

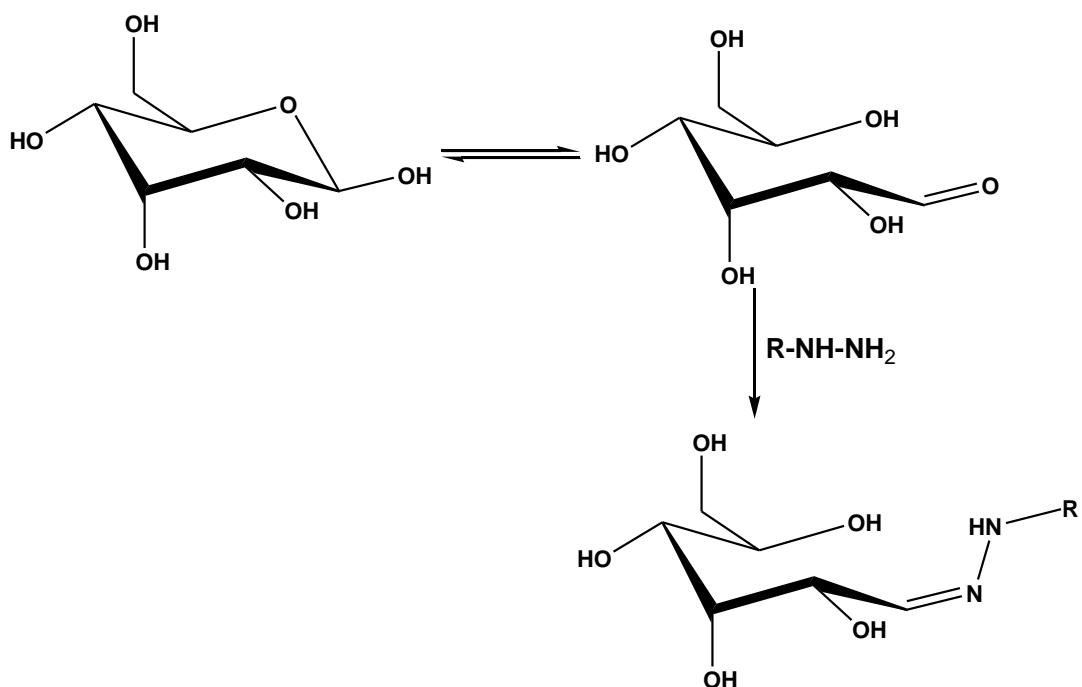


Figure 1.3 Derivation of glycan by hydrazide formation.

1.3.3.2 Hydrazide Derivatization

Hydrazide derivatization is another labeling strategy that occurs at the glycan reducing end (**Figure 1.3**). Compared to reductive amination, hydrazone formation does not require an extra cleaning step after the chemical reaction. That is because no Schiff base is not involved in hydrazide derivatization and excess salts are avoided.

Similar to reductive amination, hydrazide derivatization enables the increase of sensitivity in spectroscopic- and MS-based detection. The commonly used hydrazone formation reagents including 2,4-dinitrophenylhydrazine,⁵⁷ 1-alkoxyamino-1-deoxy alditoles⁵⁸ and pyrenebutyric acid hydrazide.⁵⁹ The labeling efficiency of using phenylhydrazine can reach as high as 100%.⁶⁰ Moreover, the increased ionization efficiency was observed in ESI and MALDI MS of hydrazino-*N,N,N*-trimethyl-2-oxoethanaminium chloride (Girard's T reagent) labeled glycans.⁶¹⁻⁶³ Recently, phenyl-2-GPN reagents were synthesized to introduce hydrophobicity of glycans and increase the sensitivity of MS detection.⁶⁴

1.3.3.3 Permetylation

Permetylation of glycan was first introduced by Ciucan and Kerek.⁶⁵ Permetylation replaces the hydrogen atom in -OH, -NH- and -COOH groups with methyl groups (**Figure 1.4**). This renders glycans hydrophobic with an enhanced ionization efficiency. Moreover, the introduction of hydrophobic groups allows the separation of N-glycan on reverse phase (RP) column. Also, permetylation simplifies structural elucidation by providing comprehensive MSMS information. Although the obvious advantages of this derivatization method, in solution permetylation suffers from oxidative degradation and peeling reaction. Recently, a new permetylation protocol has

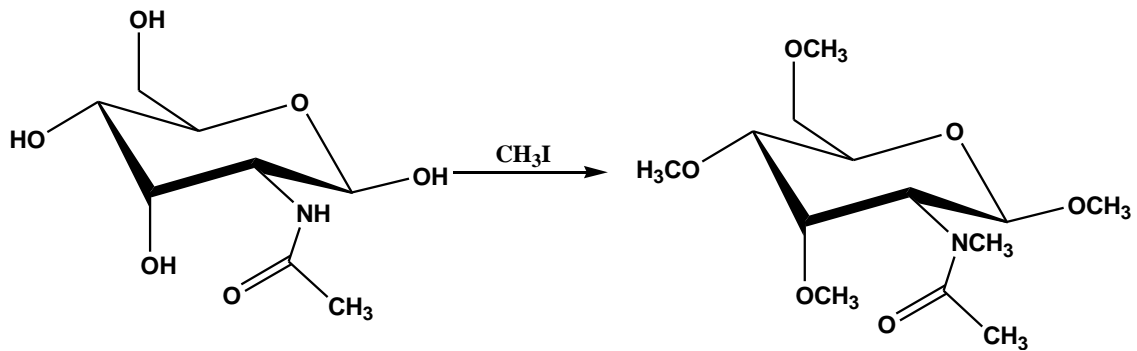


Figure 1.4 Derivation of glycan by permethylation.

been developed.^{48,66,67} Unlike the traditional permethylation, the new strategy involves performing the reaction in sodium hydroxide filled capillary⁴⁸ or spin column.⁶⁶ Oligosaccharides are dissolved in reaction mixture, which contains iodomethane, dimethyl sulfoxide (DMSO) and trace amount of water. The reaction mixture is applied to sodium hydroxide packed spin column or capillary. Highly labeling efficiency is achieved in a short period of time with high reproducibility. Permetylation has been utilized in quantitative glycomics analysis of different diseases.

1.4 Separation Techniques

In complex biological samples, glycan concentration varied and yields a dynamic range of several orders of magnitude. To minimize ion suppression, applying separation techniques prior to detection is necessary. The separation of glycans either based on charge or hydrophobicity. There are several charge based separations techniques, such as capillary electrophoresis (CE), anion exchange chromatography. On the other hand, the separation of glycan on RPLC and normal phase (NP) LC is based on their different hydrophobicity.

1.4.1 CE Separation

CE is an efficient separation method which relies on the different electrophoretic mobility among the different analytes. Labeling glycan with negative charged tags, such as 8-aminonaphthalene-1,3,6-trisulfonic acid (ANTS)^{68,69} and 1-aminopyrene-3, 6, 8-trisulfonic acid (APTS),⁷⁰⁻⁷² is required for CE separation. CE is a rapid separation technique with some isomeric separation ability. CE has been illustrated as a fast separation tool to analysis glycans derived from model glycoproteins, including

ribonuclease B (RNase B),^{70,71,73-75} fetuin,^{70,71} recombinant human erythropoietin,⁷⁰ kallikrein⁷⁰ and monoclonal antibody.⁷⁶

1.4.2 High Performance Liquid Chromatography (HPLC) Separation

HPLC is the dominant separation technique in glycan analysis. A variety of stationary phase, including hydrophilic interaction chromatography (HILIC), RP and porous graphitic carbon (PGC) have been utilized for glycan separation.

1.4.2.1 Hydrophilic Interaction Chromatography

HILIC is a normal phase chromatography and compatible with underivatized as well as labeled glycans. Hydrophilic stationary phases, including silica based ion exchange, zwitterionic, as well as non-ionic phases have been used for the separation of glycans. The primary interaction between the analytes and stationary phase is hydrogen bonding. Ionic interactions and dipole-dipole interactions also play an important role in separation. The mobile phase usually is MS compatible, which contains low concentration of volatile salts and high concentration of organic solvents. Native glycans^{77,78} as well as 2-AB,⁷⁹⁻⁸¹ 1-phenyl-3-methyl-5-pyrazolone (PMP)⁶⁸ and ANTS⁶⁸ labeled glycans have been successfully separated on HILIC column. A database (GlycoBase and autoGU)⁸² has been established which allows the structure assignment of 2-AB labeled glycans. The retention times of 2-AB labeled glycans are normalized by dextran. This strategy permits the assignment of more than 350 N-glycans derived from human blood serum. Although HILIC column is compatible to the polar compounds, there are several disadvantages have been reported. The long retention time, peak fronting and column bleed are the major disadvantages. In addition, the separation efficiency is usually considered inferior to RPLC.

1.4.2.2 PGC Chromatography

Compared to other chromatography column, PGC has unique separation mechanism. Although the separation mechanism still requires more systematic studies, it is widely considered the separation is the combination of hydrophobic interaction, polar and ionic interaction between analytes and stationary phase. Ionic strength is critical in eluting acidic oligosaccharides at a reasonable time with reasonable peak shape. Additives play an important role in the separating of sialylated glycans. The influence of ionic strength, pH, and retention time has been illustrated in a recent study.⁸³ The selection of acidic or basic mobile phases is determined by the MS detection mode. In another study, the rectified retention time and mass has been utilized for glycan isomers assignment.⁸⁴

1.4.2.3 RP Chromatography

RP chromatography is the most widely utilized separation strategy. Due to the hydrophilic properties of native glycans, it lacks interaction with RP column. The derivatization of native glycan with a hydrophobic reagent is required prior to the RP separation. Incorporating hydrophobic tags not only change the retention behavior of glycan, but also enhance the detection sensitivity. Among the various derivatization strategies, permethylation and hydrazine derivatization are most prevalent methods to introduce hydrophobic groups for MS analysis. A recent study conducted the direct comparison between hydrazine labeled glycans and native glycans using RP column and HILIC column, respectively.⁸⁵ This research demonstrated RPLC provides advantages of increasing the peak capacity.⁸⁵ As it mention above, permethylation is a widely used derivatization method. Besides increasing the hydrophobicity of glycans, permethylation

also enhances the ionization efficiency in positive MS mode. This strategy has been applied in the analysis of different biological and clinical samples. The partial isomeric separation of permethylated glycan has also been observed using C₁₈ column.⁸⁶

1.5 Detection Methods

UV and fluorescence detectors are commonly used detectors coupled with CE or HPLC separation. Due to the powerful ability to differentiate species with different *m/z*, MS has become a dominant glycan analysis method in recent years. MS produces a wealth of reliable data and allows for the analysis of glycans associated with complex biological samples. MALDI and ESI are two soft ionization techniques that have been extensively utilized in characterization and quantification of glycans.

MALID is a soft ionization method that has been widely applied in glycomics study. 2,5-Dihydroxybenzoic acid (DHB) is the most suitable matrix for oligosaccharides analysis.⁸⁷ Other matrix, such as 3-aminoquinoline, has also been reported for the glycan analysis and exhibits higher ionization efficiency for sialic acid glycans.^{88,89} MALDI-TOF is a fast analysis method and it only takes few seconds for the analysis of complex biological sample. However, MALDI analysis of native glycans suffers from the low ionization efficiency and instability of sialylated structures. Permetylation is an extensive used strategy to increase the ionization efficiency of negative charged structures. The enhanced stability of sialic acid structures is also observed after permetylation.

ESI is another soft ionization method which can be coupled with different LC. Unlike MALDI-MS, ESI-MS is likely to generate doubly or triply charged ions. As ESI is a relative softer ionization, in-source decay of sialylated glycans is not observed here.

Thus, ESI is an efficient analysis strategy of both sialylated and neutral structures, which allows the interfacing of on-line separation.

1.6 Quantitative Glycomics through Isotopic Labeling

Incorporating stable isotope reagents onto glycans through different derivatization strategies enables the simultaneous MS detection of several samples. Moreover, the different ionization efficiency which originates from sample matrix and instrument instability can be eliminated. Isotopic tags can be incorporated through reductive amination, permethylation, hydrazone formation and tandem mass tag. Introducing the tags *via* metabolic reaction has also been reported.

1.6.1 Stable Isotopic Labeling through Reductive Amination

Reductive amination is one of the widely used glycan derivatization strategy. The reaction occurs only at the reducing end, thus the labeling efficiency of “heavy” and “light” reagent will not be magnified. Introducing isotopic tags through reductive amination does not complicate the sample preparation protocol. The frequent used reductive reagents, such as PA, 2-AA and 2-AB, have been applied for the isotopic labeling of glycans. Labeling glycan with tetradeuterium-labeled PA (d_4 -PA) and d_0 -PA allows the simultaneously analysis glycans derived from recombinant chorionic gonadotropin (rhCG) and human chorionic gonadotropin (hCG).⁹⁰ However, the widely use of this reagent is hampered by the lack of commercially available isotopic PA.

Similarly, d_0 -AA and d_4 -AA have been applied to quantitative glycan profiling of chondroitin sulfate(CS).⁹¹ Another pair of AA isotopic tags, 2-¹²[C₆]AA and 2-¹³[C₆]AA, has been used to label N-glycans derived from RNase B and porcine thyroglobulin (PTG).⁹² Aniline-containing stable isotopes (¹²C₆ and ¹³C₆) have also been applied for

relative quantification of glycosaminoglycans.⁹³ Recently, tetraplex amination isotopic tags were synthesized.⁹⁴ The workflow of utilizing these synthesized isotopic tags for relative quantification of four different samples is shown on **Figure 1.5**. The quantification ability of synthesized tags is evaluated by four enzymatic depolymerization CS mixtures. This synthesized tags were also effective in comparative glycomics profiling of N-glycans derived from four mammalian species.⁹⁵

1.6.2 Stable Isotopic Labeling through Permetylation

As it mentions above, permetylation is a promising labeling strategy. Introducing stable iodomethane reagents through permetylation permits the relative quantification of several samples in one analysis. Comparative glycomic mapping using iodomethane and iodomethane-*d*₃ was reported for the quantification of samples in MALDI analysis.⁹⁶ This method is effective for the relative quantitation study of N-glycans derived from healthy females and breast cancer patients. Also, labeling O-linked glycans derived from cancer cell lines illustrated it is a reliable quantification method.

Quantitation by isobaric labeling (QUIBL) is another relative quantification strategy which involves the isotope reagents of ¹³CH₃I and ¹²CH₂D. This strategy has been shown effective quantification of N-glycans⁹⁷ as well as O-glycan in mucin.⁹⁸ High resolution mass spectrometer is required to differentiated the isotope pairs labeled sample, as the mass difference for each derivatization site is 0.002922 Da. ¹³CH₃I and ¹²CH₃I has also been employed for the relative quantification of N-glycans derived from embryos of *Drosophila melanogaster* at different stages.⁹⁹

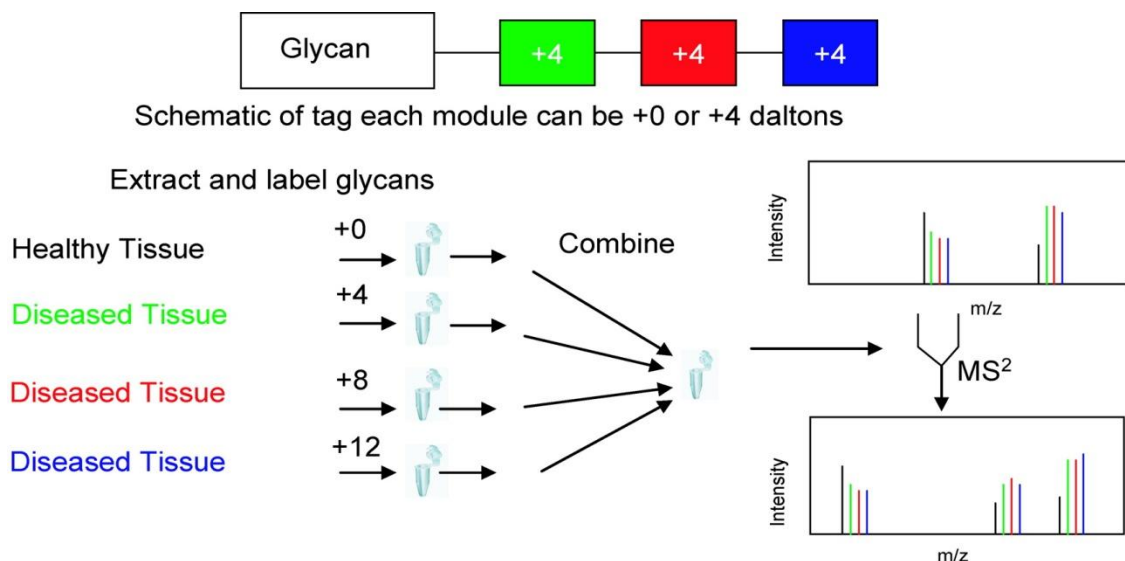


Figure 1.5 Experimental flow of incorporating reductive tetraplex tags for quantitative glycomics analysis. Reprinted and modified⁹⁴ from with permission.

1.6.3 Stable Isotopic Labeling through Tandem Mass Tags (TMTs)

TMTs are originally developed for the quantification of proteins and peptides. The isotope TMTs labeled peptides have same mass and migrate together in LC. The quantification and identification of TMTs is based on the reporter ions in tandem mass spectrometry. Recently, this strategy has been introduced for relative quantification of glycan.¹⁰⁰ The TMTs with hydrazide- and aminoxy-reactive functional groups have been compared. Although the TMTs with aminoxy- reactive functional group shows higher labeling efficiency, analyzing biological samples using this strategy suffers from the low intensity of reporter ions. The quantification is based on the intensity of intact labeled glycans.^{100,101} Thus, although the promising of this quantification concept, reliable MSMS based TMTs quantification has not been achieved.

1.6.4 Metabolic Labeling Quantitative Glycomics

An *in vivo* labeling strategy, isotopic detection of aminosugars with glutamine (IDAWG), has been introduced for glycomic quantitative studies.¹⁰² The concept is originates from stable isotope labeling with amino acids in cell culture (SILAC), which is convenient isotopic labeling strategy for proteomics. IDAWG incorporate ¹⁵N into aminosugars through hexosamine biosynthetic pathway, which produces sugar nucleotides using glutamine. A complete incorporation of ¹⁵N into oligosaccharides has been observed in amide-¹⁵N-Gln media. The reliability of this study has been demonstrated by incorporating ¹⁵N into O-and N-glycans of murine embryonic stem cells. Another *in vivo* labeling strategy has been introduced by Breidenbach *et al.*,¹⁰³ which incorporates GlcNAc or ¹³C₆-GlcNAc counterparts into the oligosaccharides. Although

metabolic labeling strategy is able to minimize the variation introduced by sample preparation, the application of this strategy is limited to live cell.

1.7 Software Tool for MS-based Quantitative Method

Manual annotation and quantification of large set of glycomics data is time consuming. The bottleneck of developing high-throughput glycomics strategy is lacking reliable automated annotation software. Up to now, only a few glycan annotation and quantification softwares have been developed. Among them, the majority of the software tools focus on annotation of MALDI-MS data. Cartoonist¹⁰⁴ is one of the earliest developed glycan annotation tool, which matches the experimental mass to the theoretical glycan mass. The calibration of Cartoonist is based on the 15 most intense ions. After calibration, experiment mass can be matched with the theoretical mass accurately. The final report of Cartoonist is a list of glycans annotated in the MS spectrum. GlycoWorkBench¹⁰⁵ is another software tool allows the annotation of mass spectrometric data. It also provides a glycan drawing tool that enables to define specific glycan structures. Both Cartoonist and GlycoWorkBench require to be combined with quantification tools for glycan quantification.

Recently, software tools that integrate the function of glycan annotation and quantification have become available. GlycReSoft¹⁰⁶ is a software tool that enables the automated annotation and quantification. The LC-MS data is first de-isotope by Decon2LS software tool. Decon2LS¹⁰⁷ are annotated using a default or user-defined glycan library. The output data is the intensity of annotated glycans.

1.8 Outline of the Chapter and Goals

The development of sensitive, reliable and high-throughput glycomics strategy is required for the better understanding of biological processes and disease progress. This thesis consists six projects with the goals of developing sensitive N-glycan quantification methods and employing the glycomics strategy for N-glycan profiling of complex biological and clinical samples.

MALDI and ESI are the widely utilized ionization strategies for glycomics study. In the second chapter, the sensitivity of these ionization methods was compared. To evaluate the necessary of incorporating the separation prior to MS detection, LC-MALDI was compared with MALDI.

In the third chapter, a relative quantification method, which allows the simultaneous detection of four samples in one analysis, was developed. The isotopic tags (iodomethane and deuterium iodomethane) were incorporated into glycans through permethylation.

In the forth chapter, chromatogram behavior of permethylated N-glycans on reverse phase column was investigated. The retention behavior of permethylated N-glycans can be explained using non-polar surface area (NPSA). The relationship between retention time and molecular weight can be used to predict structure of N-glycan. Moreover, the strategy can be utilized for differentiate linkage isomers.

The existing N-glycan profiling methods require relative large amount of samples. In the fifth chapter, a high sensitive method was developed for mouse brain tissue section glycan profiling. The sample preparation steps were minimized to avoid sample loss. This strategy is suitable for N-glycan profiling of small amount of sample.

The current challenge of high-throughput glycomics study is lacking automatic annotation and quantification software tool. Manual annotation of data file is time consuming and makes it impossible for large sets of sample analysis. In chapter six, an automatic software tool, MultiGlycan-ESI, was developed for quantification of glycans. The quantification ability was evaluated by utilizing N-glycans derived from fetuin.

Chapter seven listed an example of N-glycan profiling of biological samples. N-glycan profiling of *MYCN*-non amplified SY5Y and *MYCN*-amplified NLF cell lines was performed. The aim of this study is to investigate the glycan change associate with high-risk neuroblastoma.

Conclusions and future works are described and discussed in Chapter 8 of this dissertation. This Chapter outlines the overall goals attained through the described works. Also, the expected future works are detailed in this last Chapter.

CHAPTER II

COMPARING MALDI-MS, LC-MALDI-MS AND LC-ESI-MS GLYCOMIC PROFILES OF PERMETHYLATED N-GLYCANS DERIVED FROM MODEL GLYCOPROTEINS

Y. Hu, Y. Mechref, *Electrophoresis*, 2012, 33, 1768–1777

2.1 Introduction

A common, intriguing, complex and analytically challenging posttranslational modification of proteins is glycosylation which plays a major role in many biological functions, including protein folding, transport, and targeting.³ Aberrant glycosylation has also been implicated in many human diseases, such as cancer, inflammation, and many immune diseases.^{5,108} Currently, correlation between aberrant glycosylation and disease development and progression is being investigated in search of reliable disease biomarkers that can be effectively employed for disease diagnosis and prognosis. As such, the characterization of protein glycosylation at high sensitivity in biological specimens remains an interesting field of research posing many significant analytical challenges. As such, the characterization of protein glycosylation at high sensitivity in biological specimens remains an intriguing and interesting field of research posing many significant analytical challenges.

Among the various analytical methods routinely employed for glycomics analysis, MS is very effective and powerful, generating a plethora of reliable data. It also permits the effective characterization of glycans derived from purified glycoproteins or biological specimen. Although MS has recently been employed to elucidate glycan structures and their roles in disease progression,^{18,109-111} elucidation of glycan branching and linkages

remains a challenge. Currently, the most reliable analytical tool for structural elucidation of glycans is tandem MS (MS^2 and MS^n), which provides structural information allowing unequivocal glycan structural assignment.¹¹²⁻¹¹⁴ In many cases MS^2 analysis is not sufficient to deduce glycan structures, yet effective identification might not be attainable for many structures, since there are not enough fragments detected. This ambiguity can be somewhat resolved through MS^3 , or MS^n analyses. However, MS^n analysis is not possible for glycans existing at very low levels. Additionally, glycan concentration dynamic range within one sample can extend over several orders of magnitude, prompting saturation of detectors that potentially limit tandem MS use. For glycans existing at low concentrations, chromatographic or electrophoretic separations may overcome such limitations and allow the acquisition of reliable MS^2 and MS^n spectra. Combining LC and MS to elucidate glycan structures offers a means by which glycans of complex samples are effectively identified and quantified. Chromatographic separation of native glycans have been achieved using different types of chromatography, including high-pH anion-exchange chromatography,^{115,116} HILIC using amid-based columns^{77,117-122} and chips^{123,124}, and more recently porous graphitized carbon columns^{45,84,125} and chips.¹²⁶ However, the low ionization efficiencies of native glycan structures, especially sialylated glycans, remains a problem and makes it difficult to simultaneously detect both acidic and neutral glycans in positive-mode MS. The permethylation of N-glycans easily addresses this problem, permitting simultaneous detection of both types of glycans.⁴⁸ Although permethylated glycans ionize and fragment better than native glycans,^{127,128} permethylation of glycans has been considered by many as labor intensive and not highly reproducible when employing Ciucanu and Kerek original procedure.⁶⁵ However, these

limitations were recently overcome by a modified permethylation procedure¹²⁹ and the introduction of solid-phase permethylation method.^{66,67} An attractive feature endured by glycans as a consequence of permethylation is the substantial increase in hydrophobicity. Delaney and Vouros were the first to demonstrate the ability to separate the hydrophobic permethylated glycans by RP chromatography.¹³⁰ They separated unlabeled permethylated maltooligomer ladder, a 2AB-labeled maltooligomer ladder, a complex mixture of 2AB-labeled bi-, tri-, and tetra- antennary standards, and a mixture of recombinant glycoprotein carbohydrates from soluble CD4 with varying sialic acid content.¹³⁰ Six years later, Costello and coworkers reported the RP-LC-MS analysis of permethylated N-glycans derived from RNase B and permethylated O-glycans derived from *C.elegans*.⁴⁵ Recently, permethylated N-glycans derived from HBS were separated using a RP microfluidic liquid chromatography, allowing the resolution of some closely related structures¹⁹; however, only a limited number of glycan structures (20 glycans) were reported in this study.

Recently, we have significantly enhanced the sensitive analysis of permethylated N-glycans through on-line purification prior to RP-LC-MS analysis employing conventional proteomic RP-LC-ESI-MS setting¹³¹. Here, we are qualitatively and quantitatively comparing and evaluating the glycomic profiles of permethylated N-glycans derived from both model glycoproteins (such as RNase B and PTG) and pooled HBS acquired using RPLC-ESI-MS, RP-LC-MALDI-MS, and MALDI-MS.

2.2 Experiment

2.2.1 Material

Ammonia-borane complex, sodium hydroxide beads, DMSO, methyl iodide, DHB, methyl iodide, trifluoroacetic acid (TFA), MS-grade formic acid (FA), RNase B, PTG and pooled HBS were purchased from Sigma-Aldrich (St. Louis, MO). Empty micro-spin columns, graphitized carbon and C₁₈ micro-spin columns were obtained from Harvard Apparatus (Holliston, MA). Acetic acid and HPLC-grade solvents, including methanol and isopropanol, were procured from Fisher Scientific (Pittsburgh, PA), while acetonitrile (ACN) was obtained from JT Baker (Phillipsburg, NJ). HPLC grade water was acquired from Mallinckrodt Chemicals (Phillipsburg, NJ). PNGase F purified from *Flavobacterium meningosepticum* was obtained from New England Biolabs Inc. (Ipswich, MA).

2.2.2 Release of N-glycans from Model Glycoproteins

PNGase F was used to cleave asparagines-linked oligosaccharide (N-glycans) from RNase B and PTG as previously described.¹³² Briefly, RNase B and PTG stock solutions were prepared at a concentration of 1 µg/µL. A 9-µL aliquot of the diluted G7 buffer solution (50mM sodium phosphate buffer, pH 7.5, diluted ten times in HPLC) was added into a 1 µL of glycoproteins and mixed. Then, 1.2-µL aliquot of PNGase F was added into the mixture prior to incubation at 37°C in a water bath for 18h.

2.2.3 Release of N-glycans from Pooled Blood Serum and Purification

A 10-µL aliquot of HBS was mixed with 90 µL G7 (10x diluted) solution. A 1.2 µL aliquot of PNGase F was then added to the sample mixture prior to overnight

incubation at 37°C in water bath. Next, active charcoal macro spin-column was used to purify the pooled blood serum released N-glycans. First, the charcoal spin columns were washed with 400 µL of 100% ACN and followed with additional wash with 85% ACN aqueous solution containing 0.1% TFA. A 5% ACN aqueous solution containing 0.1% trifluoroacetic acid was then applied twice to condition the column prior to applying the sample. The released N-glycans were mixed with a 690-µL aliquot of 5% ACN aqueous solution containing 0.1% TFA and applied to the conditioned charcoal spin-column. Next, the spin-column was washed 5 times with 400 µL aliquots of 5% ACN aqueous solution containing 0.1% TFA. Finally, 40% ACN aqueous solution containing 0.1% TFA was employed to elute N-glycans. The collected eluents were then dried under vacuum.

2.2.4 Reduction of N-glycans

Ammonia-borane complex was used to reduce N-glycans to eliminate their anomeric forms as previously described.¹³³ Briefly, a 10-µL aliquot of freshly prepared ammonium-borane complex (10 µg/µL in water) was added to the N-glycans enzymatically released from RNase B and PTG. The same amount was also added to the purified N-glycans released from HBS. Samples were then incubated at 65°C in a water bath for 1h prior to denaturalization with a 100-µL aliquot of 5% acetic acid aqueous solution. The samples were then dried under vacuum and methanol was applied to the sample to evaporate borate salts, this process was repeated several times until all borate salts were removed. This was assessed by inspecting the bottom of the reaction vial for any white residue which is indicative of the presence of borate salts.

2.2.5 Permetylation of N-glycans

All N-glycans derived from RNase B, PTG and HBS were permethylated as previously described using spin-columns.^{66,67} Briefly, sodium hydroxide beads were packed into the empty micro spin columns to 3 cm prior to washing twice with 50 µL DMSO. Dried samples were then resuspended in 7.5 µL DMSO and 1.2 µL water. A 20-µL aliquot of iodomethane was then applied to the N-glycans released from RNase B, PTG and HBS. The reaction mixtures were then applied to the sodium hydroxide micro spin columns immediately and the permetylation reaction was allowed to proceed for 25 min. An additional 20-µL aliquot of iodomethane was added to each column and the permetylation was allowed to proceed for an additional 15 min. Next, the spin columns were subjected to centrifugation at a low speed (1600 rpm/min) for 30 sec and followed with a wash with a 50-µL aliquot of ACN at the same low centrifugation speed for another 30 sec. The collected eluents of each sample containing the permethylated glycans were then subjected to on-line purification as previously described¹³¹ and briefly detailed next.

2.2.6 On-line Solid-phase Purification of N-glycans

The solution collected at the end of permetylation consist of a mixture of DMSO, ACN, traces of water, excess iodomethane, and reaction by-products. Under vacuum evaporation, the reaction mixture will result in the evaporation of all of the abovementioned except DMSO (ca. 7.5 µL). In order to be able to effectively retain the permethylated glycan on the C₁₈ trapping column of the LC-MS system, the total percentage of organic solvent should not exceed 20%. Therefore, samples are resuspended in a 2% aqueous ACN solution containing 0.1% FA solution to form a 20%

DMSO/ACN aqueous solution. Next, samples were loaded to Acclaims PepMap100 C₁₈ nano-trap column (Dionex, Sunnyvale, CA, USA). The loaded sample was then washed using solvent A, consisting of 98% HPLC-grade water, 2% ACN, and 0.1% FA. This washing step was performed for 10 min at a flow rate of 3 µL/min. The equivalence of permethylated N-glycans derived from 0.1 µg of the model glycoproteins and 0.5 µL of HBS were loaded to the trap. For MALDI-MS analysis, the online purified permethylated N-glycans were eluted with 80% of solvent B at a flow rate of 3 µL/min for 20 min.

In the case of LC-MS analyses, the permethylated glycans purified by the C₁₈ trapping columns were then eluted to a nano reverse phase Acclaim® PepMap capillary column (150 mm x 75 µm i.d.) packed with 100 Å C₁₈ bounded phase (Dionex). The separation was attained using a two-pump system with pump A delivering solvent A consisting of 2% ACN aqueous solution containing 0.1% FA, while pump B delivering solvent B consisting of acetonitrile and 0.1% FA. The flow rate was 350 nL/min and the gradient condition accomplished with 38%-45% solvent B over 32 min. Eluent from the capillary column was collected at each minute and spot on the MALDI plate for LC-MALDI or sprayed directly into LTQ Orbitrap Velos Hybrid FT Mass Spectrometer (Thermo Scientific, San Jose, CA).

2.2.7 ESI-MS Acquisitions

The LTQ Orbitrap Velos Hybrid Mass Spectrometer was operated in an automated data-dependent acquisition mode. The scan mode switched between MS full scan (*m/z* from 500-2000) and CID MS/MS scan which was conducted on the 8 most abundant ions with a 0.250 Q-value, 20 msec activation time, and 35% normalized collision energy.

2.2.8 MALDI-MS Acquisition

MALDI-TOF mass spectrometry analyses were performed using 4800 plus MALDI TOF/TOF (Applied Biosystems, Foster, CA). The instrument was operated in positive-ion reflector mode with a 2000 laser shots employing a mass range of 1500-5000 *m/z*. The LC collected samples were directly spotted on the MALDI plate, while the online purified samples were dried and resuspended in 1.0 μ L of an 80/20%/0.1% water/methanol solution prior to spotting a 0.5- μ L aliquot on the MALDI plate. To each spot a 0.5- μ L aliquot of the matrix solution consisting of 10 mg/mL DHB prepared in a 50% methanol aqueous solution containing 1 mM sodium acetate was added. The inclusion of the sodium acetate was necessary to ensure that permethylated glycans form sodium adducts in the MALDI source. MALDI plate with spotted samples and matrix is then allowed to dry prior to MS analyses.

2.3 Results and Discussion

Recently, we have demonstrated the ability to significantly enhance the sensitive analysis of permethylated N-glycans through online purification.¹³¹ We have also demonstrated the use of conventional proteomic setting without any changes to acquire glycomic profile.¹³¹ However, we only described LC-MS analyses. Here, we are qualitatively and quantitatively comparing RPLC-ESI-MS, RPLC-MALDI-MS, and MALDI-MS glycomic profiles of permethylated N-glycans derived from both model glycoproteins (such as RNase B and PTG) and pooled HBS.

The glycomic profiles of permethylated N-glycans derived from RNase B (model glycoprotein) is depicted in **Figure 2.1** and **Figure 2.2**. The base peak intensity (BPI) chromatogram and 2D overlaid BPI plot of the permethylated N-glycans derived from

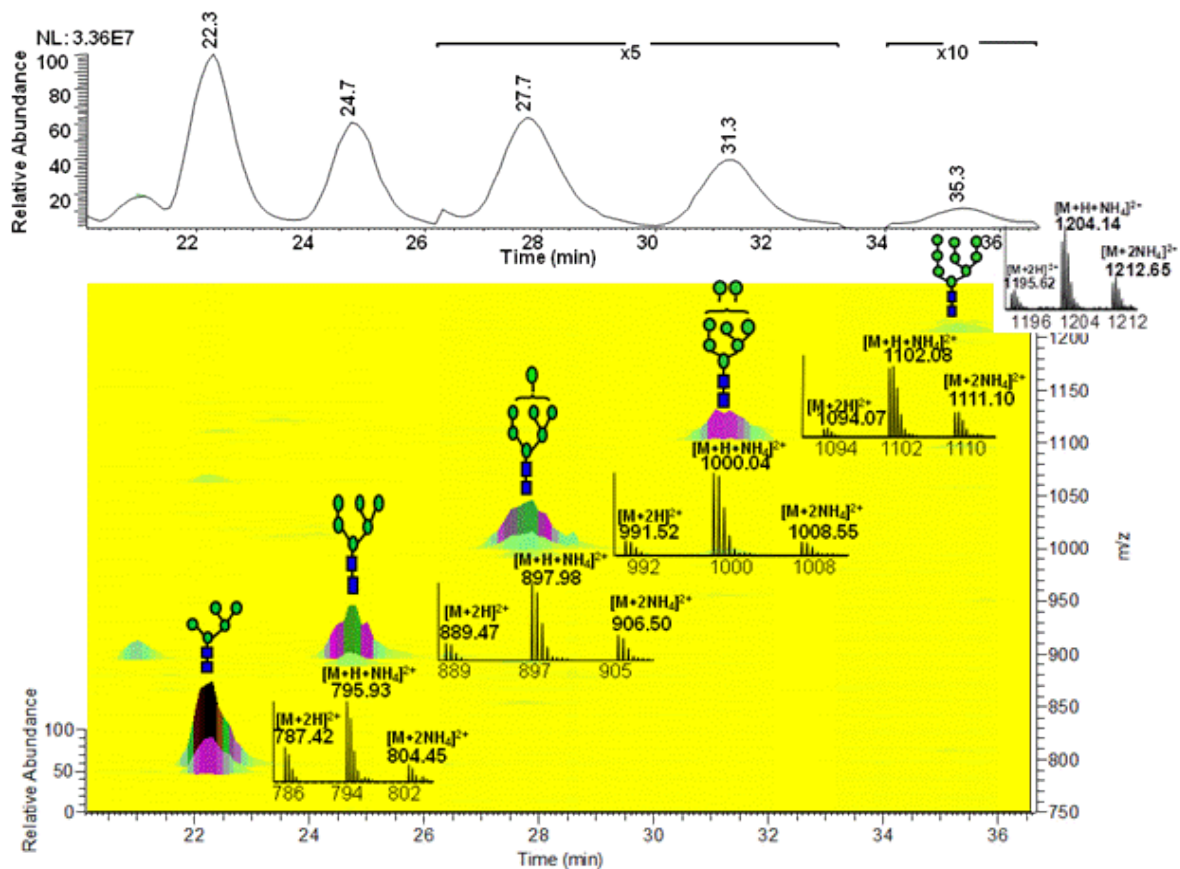


Figure 2.1 LC-ESI-MS BPI chromatogram and 2-D overlaid BPI plot of reduced and permethylated N-glycans derived from 100 ng of RNase B. The insets are the mass spectra of each peak. Symbols: blue square, *N*-acetylglucosamine; green circle, mannose; red triangle, fucose; yellow circle, galactose, purple diamond, *N*-acetylneurameric acid.

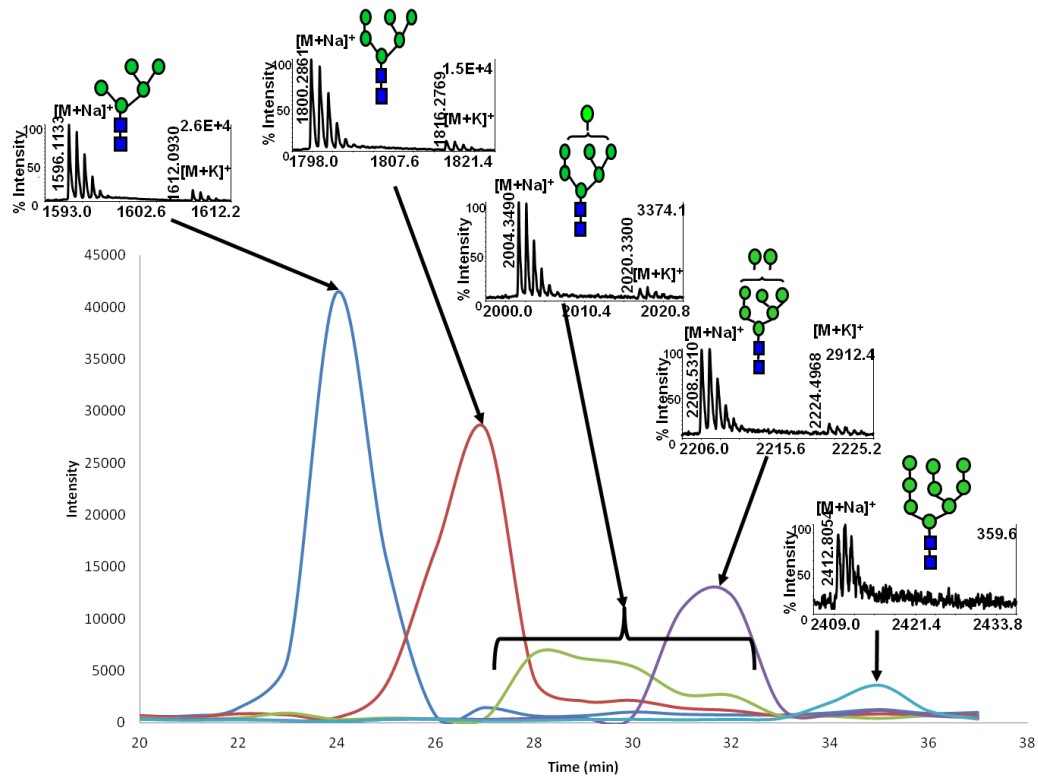


Figure 2.2 LC-MALDI-MS Extract ion chromatograms of reduced and permethylated N-glycans derived from 100 ng of RNase B. The insets are the mass spectra of each peak. Symbols: as in **Figure 2.1**.

RNase B and analyzed by LC-ESI-MS are shown in **Figure 2.1**, while the extracted ion chromatograms (EICs) of the same permethylated glycan generated by LC-MALDI-MS is depicted in **Figure 2.2**. RPLC-MALDI-MS traces here and elsewhere were constructed using Microsoft Excel for smooth line fitting of MALDI-MS ion counts data. Both traces exhibit the endogenous distributions of the different glycans commonly observed on RNase B. Some of the traces shown in **Figure 2.2** do not appear to resemble their counterpart in **Figure 2.1**, especially in the case of Man7. However, we believe that these differences could be partially attributed to the manual deposition that was employed as well as the “sweet spot” limitation of MALDI-MS analysis.

Multiple ions are formed in the ESI source for each permethylated glycan structures as shown in the insets of **Figure 2.1**, including doubly protonated ($[M+2H]^{2+}$), singly protonated and ammoniated ($[M+H+NH_4]^{2+}$), and doubly ammoniated ($[M+2NH_4]^{2+}$). The ammoniated adducts are believed to originate from the reduction step employed to eliminate the anomers. Excessive washing of the loaded samples did not eliminate the formation of these adducts. Also, excessive treatment with methanol and evaporation did not seem to eliminate or reduce the abundance of these adducts. Interestingly, these adducts are more abundant in the case of high mannose and hybrid type of glycans and less abundant in the case of complex type. The formation of these adducts is currently under investigation. The formation of these adducts does not appear to reduce the sensitive analysis of permethylated glycans. The five high mannose glycans of RNase B were also detected (>3 S/N) for permethylated glycans derived from a 10-ng aliquot of RNase using LC-ESI-MS or LC-MALDI-MS. However, this amount was not sufficient to detect all five high mannose glycans of RNase B by MALDI-MS (data not

shown). Accordingly, LC analysis is offering higher sensitivity irrespective of the MS used. This is expected, since the byproducts and impurities associated with a sample are eluted at different retention times than the analytes. These interfering species are all present in the sample in the case of MALDI-MS analysis and adversely influencing the ionization process.

The relative abundances of RNase B glycans acquired using the three methods employed in this study, as well as other analytical techniques such as NMR,¹³⁴ LC-MS of glycans labeled with negatively charged reagent and separated on a reversed-phase column with ion pairing reagent,⁶⁹ and capillary gel electrophoresis of APTS labeled glycans,⁷⁴ are summarized in **Table 2.1**. Although there are differences between the results, such differences might be attributed to the source of RNase B samples. It is not expected that the different studies will have exactly the same numbers. Moreover, the differences shown in **Table 2.1** might be partially contributed to the measurement uncertainties. Nevertheless, the data listed in **Table 2.1** appears to be analytically comparable. The reproducibility of the LC-ESI-MS and MALDI-MS data appears to be substantially higher than that of LC-MALDI-MS. Moreover, the MALDI-MS and LC-ESI-MS data appears to be in a better agreement with the literature data. We believe that this discrepancy might be partially attributed to the manual spotting employed here or to “sweet spot” limitation of MALDI-MS. Although the glycomic profiles of RNase B N-glycans appear to be quantitatively comparable, LC-MS analyses are offering higher sensitivity for the profiling of N-glycans derived from a glycoprotein. This is expected since LC analysis reduced competitive ionization and saturation of detectors.

Table 2.1 Relative intensities of the N-glycan structures commonly associated with RNase B acquired using different analytical techniques and methods (N=3 for all methods with uncertainty numbers).

Glycans	Relative Abundance						
	NMR ^a	CGE ^b	LC-MS ^c	MALDI-MS	MALDI-MS permethylated	LC-ESI-MS permethylated	LC-MALDI permethylated
Man 5	57	51.5	51.9±2	50.9±1	59±0.6	53.49±0.4	49.8±6
Man 6	31	30.3	32.1±2	27.4±0.7	29±0.7	32.46±0.6	29.77±5
Man 7	4	4	6.3±0.6	7.3±1	4±0.2	8.02±0.2	10.82±4
Man 8	7	8.5	7.2±0.8	10.9±0.6	7±0.2	5.21±0.3	7.48±4
Man 9	1	3.7	1.6±0.1	3.5±0.6	1±0.05	0.82±0.06	2.11±1

a) Data is obtained from reference ¹³⁴

b) Data is obtained from reference ⁷⁴

c) Data is obtained from reference ⁶⁹

PTG is a glycoprotein that has N-glycans representing all types, including high mannose, complex and hybrid.¹³⁵⁻¹³⁸ The LC-ESI-MS and LC-MALDI-MS glycomic profiles of PTG are depicted in **Figure 2.3** and **Figure 2.4**. The extracted ion chromatograms of the abundant glycans associated with PTG as well as the 2D overlaid BPI plot of LC-ESI-MS glycomic profiling are shown in **Figure 2.3**. This analysis permitted the detection of 11 glycan structures associated with PTG. The relative distribution of the different glycans observed in the LC-ESI-MS analysis was comparable to what is reported in the literature.^{135,139} The LC-MALDI-MS profile of the same sample is shown in **Figure 2.4**. Less glycan structures were observed in the LC-MALDI profile. In the case of this glycoprotein which has a more heterogeneous glycan profile than that of the RNase B, LC-ESI-MS appears to permit better detection of permethylated glycans. The chromatographic peaks of the sialylated glycan depicted in **Figure 2.3** are broad with shouldering. We believe that these features are common for all sialylated glycans which might be attributed to the presence of multiple isomers (different linkages and location on the antenna) that are not completely resolved under the chromatographic conditions employed here.

The relative abundances of the glycan structures commonly associated with PTG and determined by different analytical techniques are listed in **Table 2.2**. Again as expected, better detection is observed in the case of the LC-MALDI-MS relative to those of MALDI-MS which is attributed to the reduced competitive ionization and saturation of detectors. Due to the high molecular weight of PTG (>650 kDa), the amount of N-glycans analyzed was substantially lower than that of RNase B. The same amount of glycoprotein (100-ng aliquots) was analyzed. Accordingly, a 100-ng aliquot is needed to

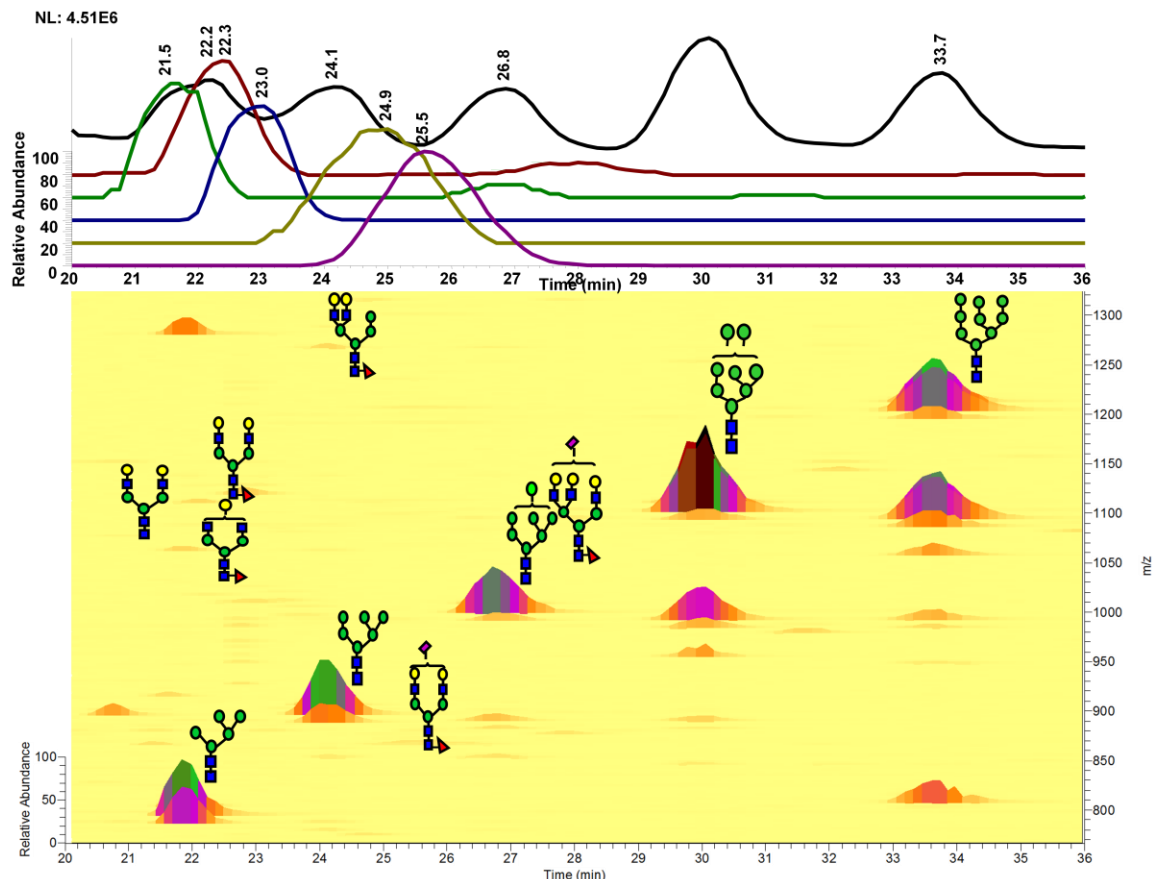


Figure 2.3 LC-ESI-MS BPI chromatogram and 2-D overlaid BPI plot of reduced and permethylated N-glycans derived from 100 ng of PTG. Symbols: as in **Figure 2.1**.

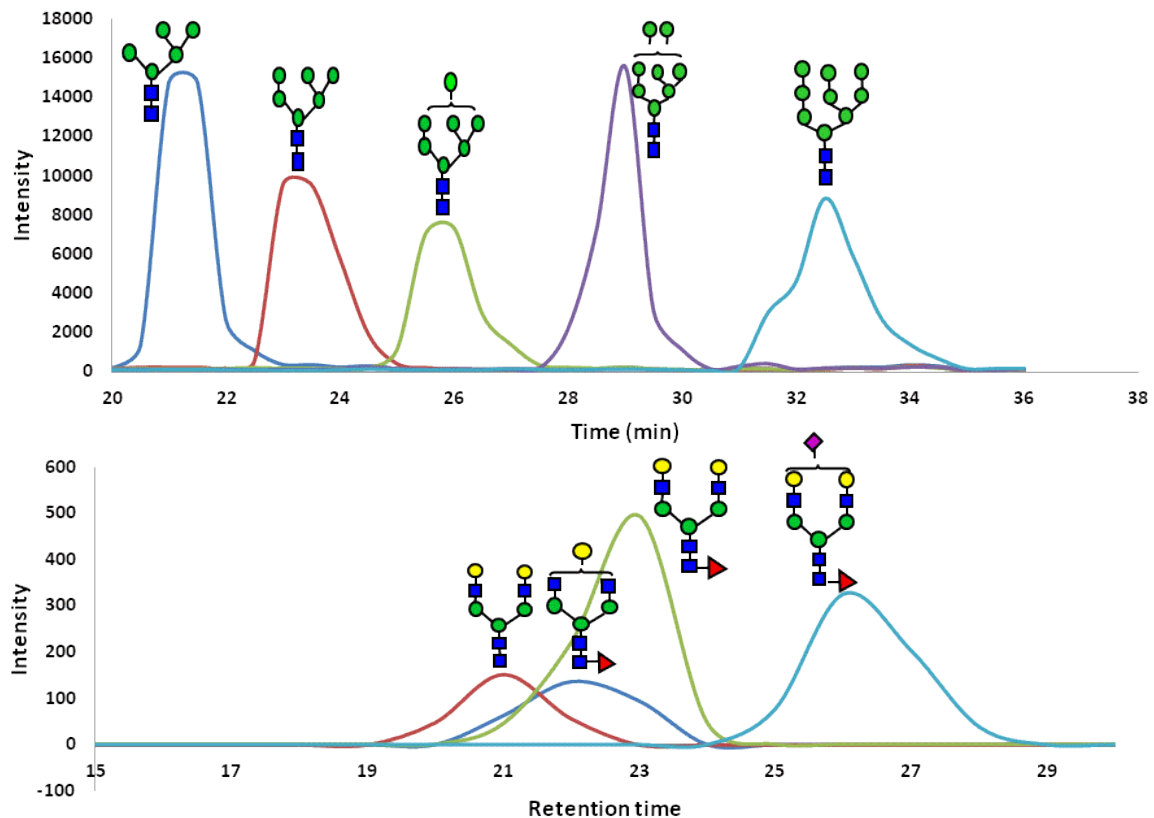


Figure 2.4 LC-MALDI-MS extract ion chromatograms of reduced and permethylated N-glycans derived from 100 ng PTG. Symbols: as in **Figure 2.1**.

Table 2.2 Relative intensities of the N-glycan structures commonly associated with PTG acquired using different analytical techniques

Structures	Relative Abundance				
	MALDI ^a	LC ^b	LC-ESI	LC-MALDI	MALDI
	16	8	34.6	20.1	25
	10	6	19.8	19	15
	7	3	9.7	16.4	11
	3	ND	1.4	0.4	0.5
	2	ND	0.3	0.5	1
	10	11	12.9	19.5	15
	13	2	5.8	1.6	7
	9	15	13.8	20.5	10
	4	ND	0.4	0.5	1
	20	18	0.8	1	10
	4	14	0.3	0.4	3
	3	13	0.04	ND	1
	ND	6	0.1	0.06	0.5
	ND	ND	0.06	0.04	ND

a) Data is obtained from reference ¹³⁹b) Data is obtained from reference ¹³⁵

allow quantitative profiling of PTG N-glycans. Although there is no absolute agreement between the different studies listed in **Table 2.2**, the overall results appear to be comparable with LC-ESI-MS permitting the detection of more structures than any of the other methods. All of the structures listed in **Table 2.2** were detected only through RPLC-ESI-MS.

According to the above results, LC-ESI-MS analyses offer higher sensitivity as the heterogeneity of the glycomic profile increases. This increase in sensitivity is seen through an increase in the number of glycan structures that are detected with S/N ratios better than 3. Additionally, LC of permethylated glycan enhanced the MALDI analysis by reducing competitive ionization and minimizing saturation of detectors. This was further supported by the glycomic profile of human blood serum sample.

Alley *et al.* have recently reported the separation of reduced and permethylated N glycans derived from HBS on a reversed-phase chip interfaced to an ion trap mass spectrometer.¹⁹ Only 20 N-glycan structures were confidently detected. This limited number of glycan structures might be due to the limited loading capacity of the chip as well as to the mass spectrometer employed. The 2D overlaid base peak intensity plot of LC-ESI-MS analysis of 35 reduced and permethylated N-glycans derived from the equivalence of 250 nL of blood serum is depicted in **Figure 2.5**, while the EIC of ten of these structures observed in the LC-MALDI-MS analysis is shown in **Figure 2.6**. In total, 73 glycan structures were confidently detected in the LC-ESI-MS analysis of 250 nL of blood serum, while 53 structures were detected in the LC-MALDI-MS analysis of the same amount of blood serum (Data not show). All of the detected glycan structures exhibited an S/N ratio better than 3. On the other hand, only 42 glycans structures were

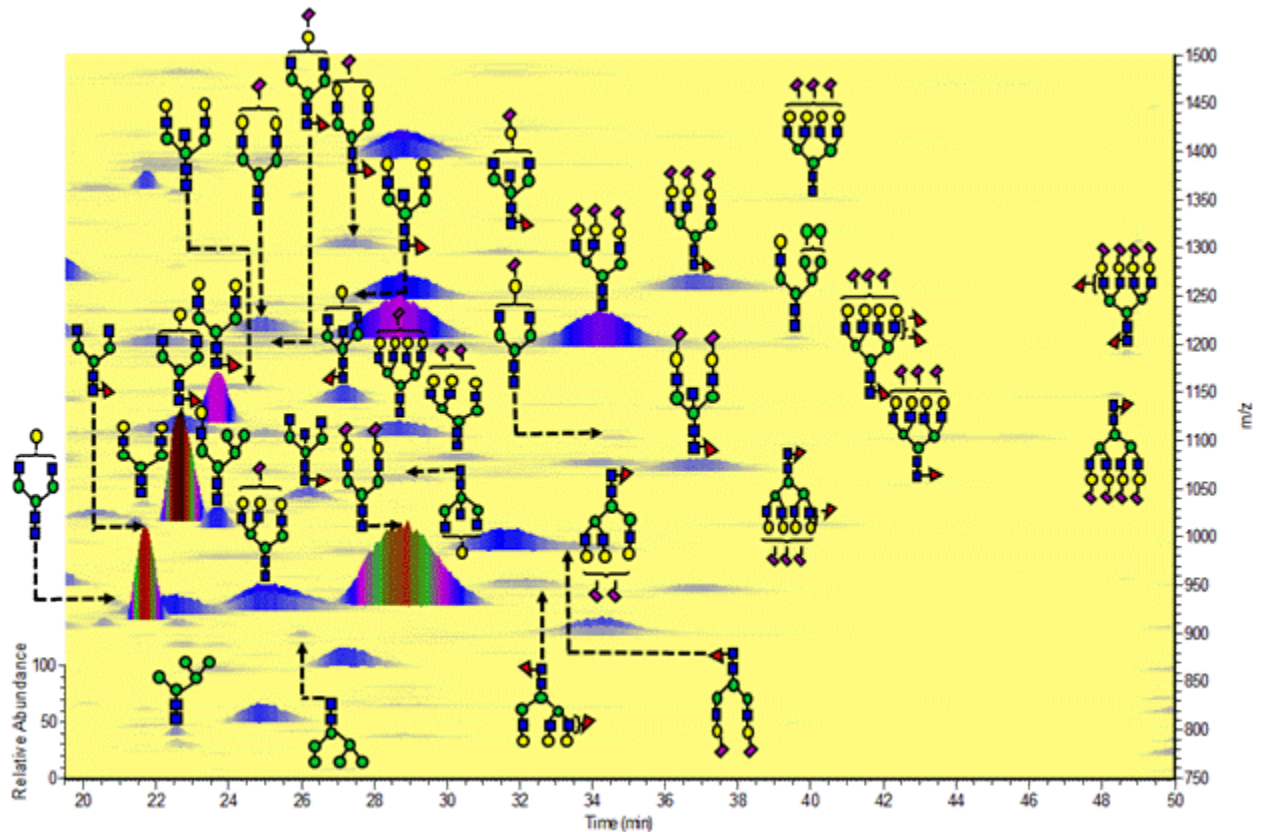


Figure 2.5 LC-ESI-MS 2-D overlaid BPI plot of reduced and permethylated N-glycans derived from 250nL HBS. Symbols: as in **Figure 2.1**.

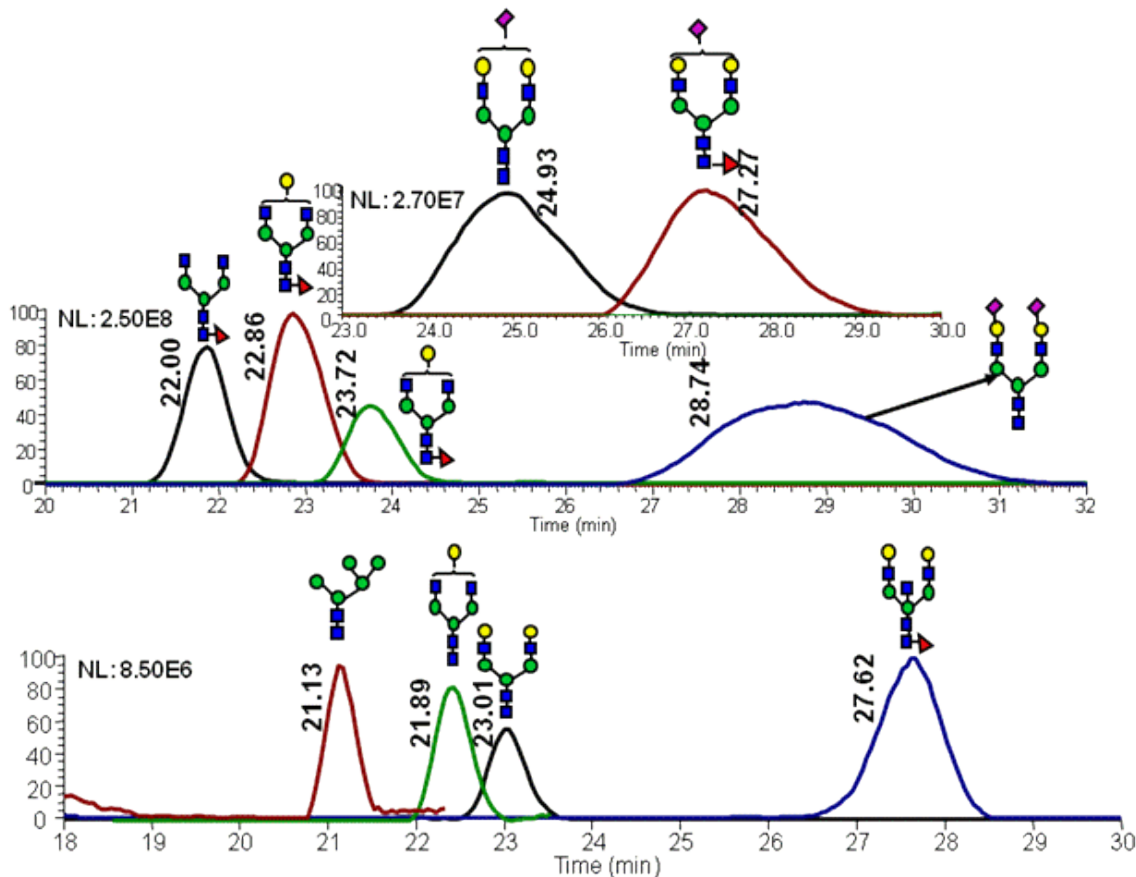


Figure 2.6 LC-MALDI-MS extract ion chromatograms of reduced and permethylated N-glycans derived from 250nL HBS. Symbols: as in **Figure 2.1**.

reported in the case of the MALDI-MS analysis of the same amount of sample with S/N ratio of 4.7 or better (Data not show). The chromatographic separation substantially enhanced the S/N ratios observed in MALDI-MS analyses as shown in **Figure 2.7** for three representative glycan structures. The S/N ratio increased between 13- and 16-folds as a result of the chromatographic separation. This substantial increase is expected, and is mainly originating from the reduction in both competitive ionization and saturation of detectors.

Of the structures detected in the three analyses, 40 were common among all. 40 structures and 52 structures were common among the MALDI-MS, RP-LC-MALDI-MS analyses and RP-LC-ESI-MS analyses, respectively. A single structure was unique for the MALDI-MS, while a different one was unique to the RP-LC-MALDI-MS analyses. Twenty N-glycan structures were only observed in the RP-LC-ESI-MS analysis, which is equal to the total number of structures reported by Alley *et al.*¹⁹ The confident detection of more structures in this study, relative to the previous study (ca. 4-fold), might be attributed to sample purification (liquid–liquid extraction versus online purification in this study), loading capacities of the traps, and the mass accuracy and resolution of mass spectrometers (ion trap versus Orbitrap this study). The N-glycan structures that were detected only as a result of LC-separation prior to MS were at low abundance (Data not show). The inability to see these structures in MALDI spectrum might be attributed to competitive ionization and in some cases might be a combination of both competitive ionization and saturation of detectors (structures with low *m/z* values).

The RP chromatographic separation of the permethylated N-glycans derived from model glycoproteins or HBS did not only allow the detection of low abundant structures,

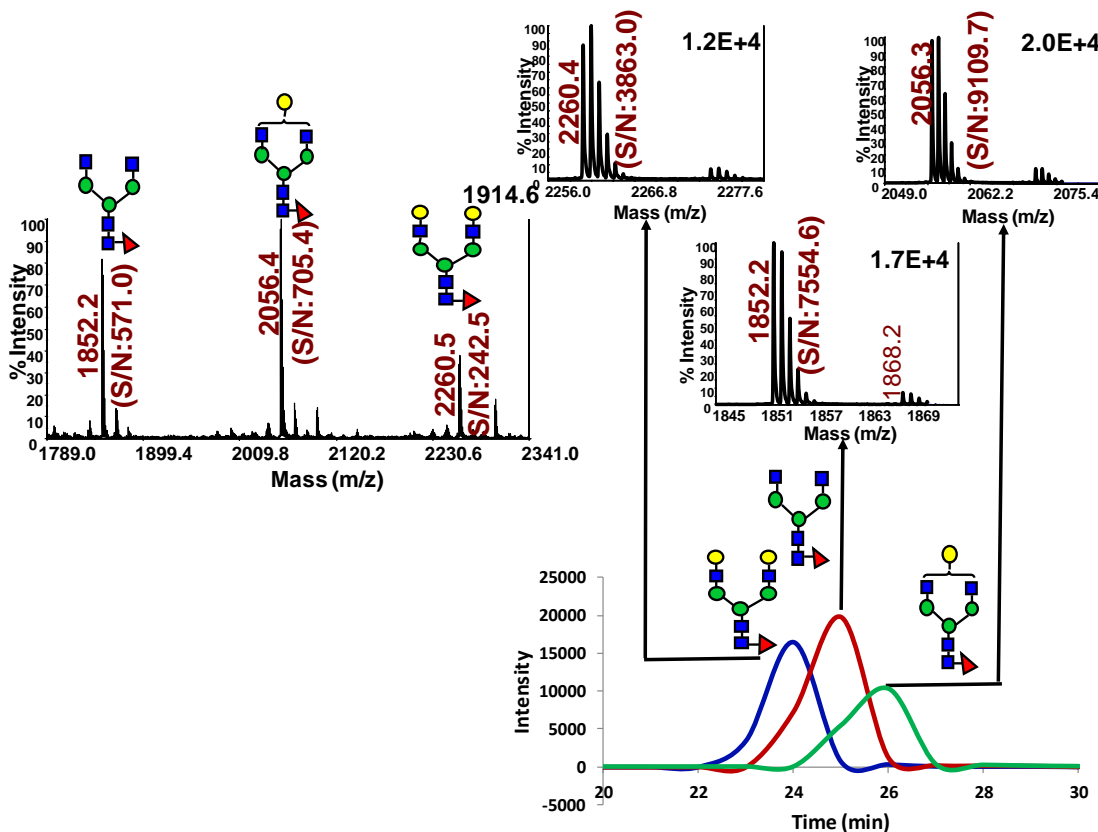


Figure 2.7 MALDI mass spectra and LC-MALDI-MS extracted ion chromatograms of N-glycans derived from blood serum. The inset depicting the mass spectra associated with the LC analysis. Symbols: as in **Figure 2.1**.

but also resolved some structural isomers as shown in **Figure 2.8**. The reversed-phase separation permitted the separation of permethylated glycans with the same molecular weight but different structures. The separation is based on the overall hydrophobicity of the permethylated structures; however, the branching of the glycan structures also dictates their overall hydrophobicity. The latter explains the higher retention of hybrid glycans on a reversed-phase media relative to that of complex-type glycans (**Figure 2.8a**). Complex glycans are more compact with intramolecular interactions between the different methoxy groups on the different antenna. This intramolecular interaction reduces the overall hydrophobicity of the molecule and subsequently reduces interactions with the chromatographic media. On the other hand, the hybrid structure shown in **Figure 2.8b** appears to have less intramolecular interaction between the different methoxy groups. This limited intramolecular interaction is prompted by the bisecting GlcNAc. Accordingly, this hybrid glycan structure has more methoxy groups available for interaction with the chromatographic media and subsequently is retained more on the reversed-phase column. The separation of the two structures shown in **Figure 2.8b** could be also explained in the same way. Tandem MS data was essential to unequivocally assign the different structures (data not shown). Glycans that did not have tandem MS data are listed in **Table 2.3** only in term of composition.

2.4 Conclusion

To our knowledge, this is the first study that highlights the advantages and disadvantages of LC-ESI-MS analysis of permethylated N-glycans. Reduced and permethylated N-glycans derived from both model glycoproteins and HBS were analyzed by different analytical techniques, including MALDI-MS and LC-MS with MALDI and

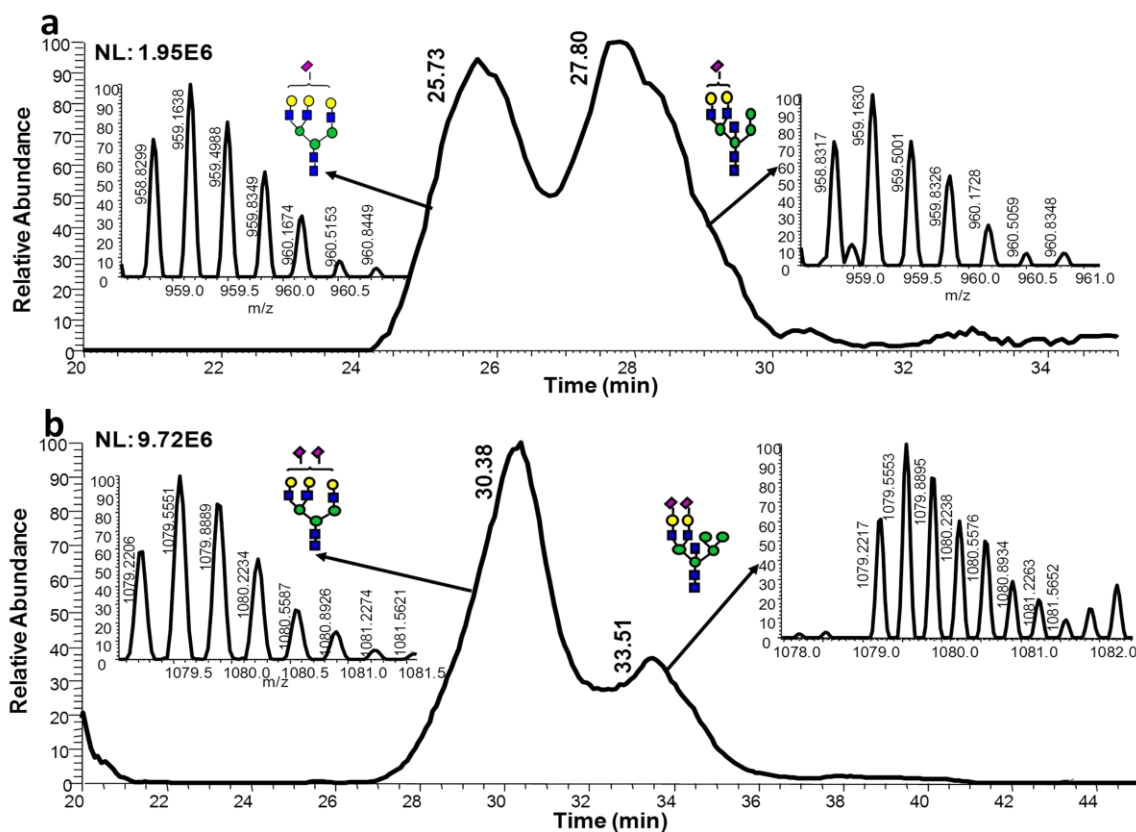


Figure 2.8 LC-ESI-MS extracted ion chromatograms of some N-glycan isomers derived from HBS. Symbols: as in **Figure 2.1**.

Table 2.3 Signal-to-Noise ratios and relative intensities of HBS permethylated N-glycans analyzed by LC-ESI-MS, LC-MALDI-MS and MALDI-MS.

Structures	S/N			Intensity	
	LC-ESI	LC-MALDI	MALDI	LC-ESI	LC-MALDI
	871.9	2020.8	24.0	0.8	5.1
	7.7	57.4	ND	0.04	0.1
	3.4	33.9	ND	0.04	0.2
	42.8	62.2	ND	0.4	0.3
	58.0	708.2	17.2	0.3	1.7
	29.9	119.1	9.7	0.2	0.4
	1510.0	7554.6	172.8	14.1	18.2
	140.8	198.0	12.8	0.9	2.6
	15.4	49.8	ND	0.1	0.2
	9.1	84.0	6.7	0.1	0.2
	12.1	346.7	11.0	0.08	0.9
	30.0	53.3	ND	0.2	0.1
	1482.6	9109.7	478.5	16.4	21.9
	92.7	129.5	30.4	0.9	1.0
	394.6	963.3	56.6	2.2	2.6
	51.0	220.6	8.7	0.4	0.4
	32.3	70.4	8.0	0.2	0.2
	27.7	228.7	ND	0.1	0.5
	32.2	162.9	10.5	0.2	0.5
	9.72	ND	ND	0.08	ND
	1012.1	3863.0	199.5	8.5	11.4

Table 2.3 Continued

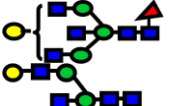
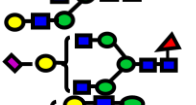
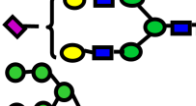
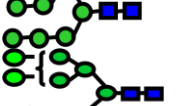
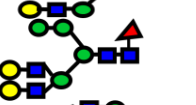
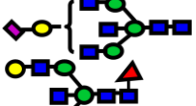
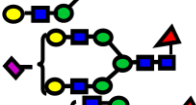
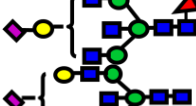
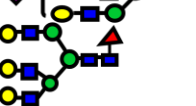
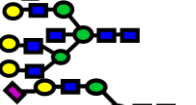
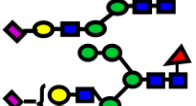
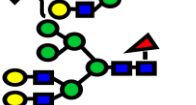
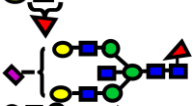
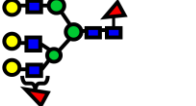
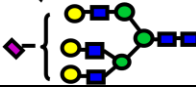
Structures	S/N			Intensity	
	LC-ESI	LC-MALDI	MALDI	LC-ESI	LC-MALDI
	391.8	643.1	97.4	2.9	1.7
	28.5	34.3	11.9	0.2	0.07
	114.2	276.8	27.0	0.7	0.8
	297.8	1904.9	194.2	2.5	4.1
	120.3	ND	ND	0.2	ND
	181.5	ND	14.3	1.5	ND
	126.0	187.3	ND	1.0	0.5
	ND	28.0	ND	ND	0.07
	126.8	321.2	35.3	1.0	0.7
	217.3	1006.4	165.2	1.8	2.7
	21.5	ND	ND	0.1	ND
	10.9	70.7	15.4	0.1	0.2
	3.7	15.2	ND	0.04	0.05
	ND	ND	31.3	ND	ND
	1292.5	5243.7	1493.3	14.2	12.2
	555.0	365.0	ND	6.1	1.2
	224.5	ND	ND	2.5	ND
	355.3	703.9	163.6	1.5	1.2
	79.7	ND	ND	0.3	ND
	12.7	99.2	29.5	0.2	0.3

Table 2.3 Continued

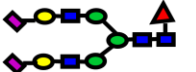
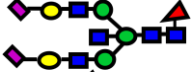
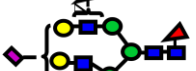
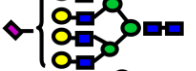
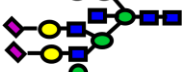
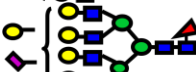
Structures	S/N		Intensity		
	LC-ESI	LC-MALDI	MALDI	LC-ESI	LC-MALDI
	832.8	1141.1	212.8	3.9	2.0
	26.8	38.5	13.2	0.09	0.08
	39.1	37.6	15.5	0.2	0.07
	34.8	ND	ND	0.2	ND
	639.1	356.6	100	2.00	0.6
	273.2	41.5	24.5	1.5	0.1
	248.5	164.2	57.3	1.3	0.3
	16.8	ND	ND	0.1	ND
	9.1	ND	ND	0.1	ND
	64.8	31.5	21.0	0.3	0.07
	248.47	ND	ND	1.3	ND
	43.1	ND	ND	0.3	ND
	6.6	ND	ND	0.04	ND
	110.8	757.9	233.6	0.6	1.3
	66.4	46.4	18.7	0.4	0.08
	27.4	ND	ND	0.2	ND
	707.2	310.7	89.0	2.6	0.5

Table 2.3 Continued

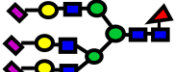
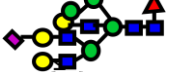
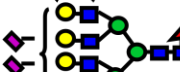
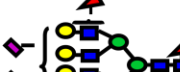
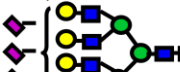
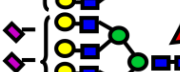
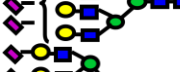
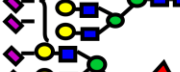
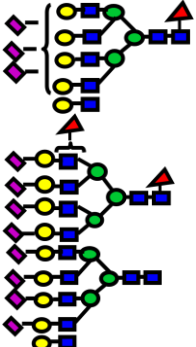
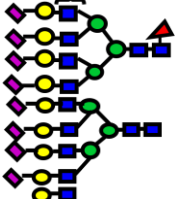
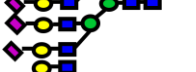
Structures	S/N		Intensity		
	LC-ESI	LC-MALDI	MALDI	LC-ESI	LC-MALDI
	707.2	310.7	89.0	2.6	0.5
	51.8	ND	ND	0.2	ND
	27.2	13.2	4.7	0.1	0.02
	71.1	14.1	10.9	0.1	0.03
	4.5	ND	ND	0.03	ND
	4.5	ND	ND	0.05	ND
	217.7	62.7	17.2	0.3	0.1
	13.3	ND	ND	0.01	ND
	5.4	22.8	ND	0.01	0.02
	22.4	ND	ND	0.04	ND
	14.7	7.9	6.8	0.01	0.05
	530.5	182.8	20.5	0.5	0.3
	50.9	29.3	ND	0.05	0.02
	204.7	29	9.4	0.2	0.07

Table 2.3 Continued

Structures	S/N		Intensity		
	LC-ESI	LC-MALDI	MALDI	LC-ESI	LC-MALDI
	9.1	ND	ND	0.01	ND
	72.4	ND	ND	0.1	ND
	56.4	ND	ND	0.08	ND

ESI sources. Permetylation of glycans made these structures hydrophobic enough to be retained and separated by RP nanocolumn. The chromatographic separation helped reduce the competitive ionization and saturation of detector in the case of MALDI-MS. The results of the analyses of N-glycans derived from model glycoproteins using three methods compared here were very comparable with a slight edge for LC-ESI-MS. However, the analysis of N-glycans derived from HBS demonstrated the major advantage of LC-ESI-MS over the other methods. In conjunction with our recent online purification of permethylated glycans, LC-ESI-MS of permethylated N-glycans derived from HBS allowed the confident detection of 73 glycan structures through tandem MS and the high mass accuracy offered by the mass spectrometer used. Although tandem MS can be acquired in the case of LC-MALDI-MS, it is more automated and requires a lot less sample in the case of an ion trap mass spectrometer. Although multiple ions and adducts are formed in LC-ESI-MS, this technique offers unmatched simplicity, convenience, high sensitivity, and better tandem MS data. Currently, we are routinely utilizing LC-ESI-MS for the analyses of permethylated glycans derived from biological specimens, including human blood serum, fluids, and tissues.

CHAPTER IV

COMPARATIVE GLYCOMIC PROFILING OF ISOTOPICALLY PERMETHYLATED N-GLYCANS BY LC-ESI-MS

Y. Hu, J. L. Desantos-Garcia, Y. Mechref, *Rapid Communication in Mass Spectrometry*,
2012, 33, 1768–1777

3.1 Introduction

Glycosylation is one of the most common and structurally diverse post-translation modifications of proteins and lipids. More than 50% of proteins are N- and O-glycosylated.¹⁴⁰ This does not include O-GlcNAc modification or sulfation and acetylation of glycans attached to polypeptides.¹⁴¹ Glycosylation of proteins plays essential roles in many integral biological functions.⁴ Moreover, the functions of many glycoconjugates are modulated by glycosylation. Additionally, aberrant glycosylation of proteins has been implicated in many diseases,^{5,108} including cancer.¹⁴²⁻¹⁴⁷ Therefore, reliable quantification of glycans is currently considered being of considerable importance for biomarker discovery and early stage disease diagnosis.

Recently, several studies have demonstrated the utility of glycomic profiling to assess cancer development and progression.^{13,18,20,21,28,29,33,46,78,110,148-151} Developing a robust quantification method is essential for investigating the changes of glycosylation in biological systems. Typically, there are two types of quantification strategies: one is label-free and the other involves the use of stable isotopic reagents. Label-free quantification method is limited by the need for normalization to account for the different ionization efficiencies of analytes and instrument response instabilities. Using relative quantification strategies with stable isotopic reagents can reduce the influence of

instrument response and ionization variation prompted by experimental variation. Meanwhile, stable isotope labeling could be employed to simultaneously analyze samples representing different biological conditions such as disease states. The most widely applied isotopic reagent in quantification methods include metabolic (*in vivo*) stable isotopic labeling¹⁰² or incorporating an isotopic label in common glycan derivatization strategies such as reductive amination^{64,92,94,152} and permethylation.^{96,97}

Metabolic labeling of glycans with isotopic amino acid or sugar is an example of isotopic labeling strategies. Orland and co-workers¹⁰² have introduced isotopic labeling in cell culture. This strategy involves the incorporation of ¹⁵N into N-linked glycans by using amide-¹⁵N-Gln media. This strategy minimizes variations associated with sample preparation. However, incorporating the isotopic reagent is limited to living organisms.

Reductive amination reagents suitable for stable-isotopic labeling have been developed to modify the reduced end of N-glycans and allows for relative quantification. Several reductive amination reagents for the quantification of glycans have been developed, including PA (*d*₀-PA, *d*₄-PA),⁹⁰ AA (*d*₀-AA, *d*₄-AA)⁹¹ and aniline([¹²C₆], [¹³C₆]).¹⁵² Bowman and Zaia⁹⁴ synthesized a stable isotope-labeled tag in four forms (+0,+4,+8,+12) and labeled the reduced end of glycans. Direct comparison of four samples was achieved through this method. However, one disadvantage of this method is a need for theoretical simulations to extract ion abundance to account for the overlap of isotopic distributions.

Stable isotopic labeling of N-glycans through permethylation is an alternative to reductive amination and offers many advantages, including enhanced ionization efficiency, enhanced hydrophobicity, and simplified tandem MS interpretation. The

enhanced hydrophobicity as a result of permethylation allows separation on a C₁₈ column. Also, permethylation permits the simultaneous analysis of both neutral and acidic glycans to be detected in positive ion mode mass spectrometry. Orlando and coworkers⁹⁷ utilized ¹³CH₃I and ¹²CH₂DI to generate a pair of isobaric derivatives with a mass difference of 0.002922 Da for each methylation site. High resolution mass spectrometry ($m/\Delta m > 30000$) is required to distinguish such minute *m/z* differences. Another isotopic reagent pairs for permethylation is CH₃I and CD₃I, which was recently reported by Mechref and Novotny.⁹⁶ This differential permethylation permits relative quantification of different samples to be achieved in a single MALDI-MS analysis.

We here used different permethylation reagents (iodomethane and iodomethane-*d*₁ or -*d*₃) to permethylate N-glycans derived from model glycoproteins (RNase B, fetuin) prior to their LC-ESI-MS analyses using RP chromatographic media as we have recently described.^{131,153} Also, HBS was permethylated with “heavy” (CH₂DI or CD₃I) and “light” (CH₃I) reagents and mixed at 1:1 ratio to evaluate the quantification aspects of N-glycan pairs. The method was then applied to determine glycomic differences among different esophageal diseases. High grade dysplasia (HGD), Barrett’s disease and esophageal adenocarcinoma samples were derivatized with CD₃I reagent while samples collected from disease-free (DF) subjects were labeled with CH₃I reagent. Disease samples and DF sample were then mixed at 1:1 volume ratios and subjected to LC-ESI-MS analysis. This comparative glycomic profiling by LC-ESI-MS is effective in depicting the N-glycan differences among esophageal disease samples and DF samples.

3.2 Experiment

3.2.1 Material

Ammonia borane complex, sodium hydroxide beads, DMSO, iodomethane, iodomethane-*d*₁, iodomethane-*d*₃, trifluoroacetic acid, MS-grade formic acid, RNase B, fetuin, and pooled HBS were obtained from Sigma-Aldrich (St. Louis, MO). Empty microspin columns and graphitized carbon and C₁₈ microspin columns were purchased from Harvard Apparatus (Holliston, MA). Acetic acid and HPLC-grade solvents, including methanol and isopropanol were procured from Fisher Scientific (Pittsburgh, PA) while ACN was obtained from JT Baker (Phillipsburg, NJ). HPLC grade water was acquired from Mallinckrodt Chemicals (Phillipsburg, NJ). PNGase F was obtained from New England Biolabs Inc. (Ipswich, MA).

3.2.2 N-Glycans Released from Model Glycoproteins

PNGase F was used for enzymatic release of N-glycans from RNase B, fetuin. The process was performed according to a previously published procedure.^{66,67,96} Briefly, a 9-μL aliquot of 10x diluted G7 solution (50 mM sodium phosphate buffer, pH 7.5) was added into a 1-μL aliquot of glycoproteins (1 μg/μL). The samples were then mixed prior to the addition of a 1.2-μL aliquot of PNGase F. Next, samples were incubated at 37°C in a water bath for 18h.

3.2.3 N-Glycans Released from HBS, Esophageal Disease and DF samples

HBS samples were provided by Dr. Zane Hammoud of Henry Ford Medical Systems, Detroit, MI. Samples were collected under Institutional Review Board (IRB) approved protocols with consents of donors. Barrett's esophagus serum samples (N=7),

high-grade dysplasia (HGD, N=11) and esophageal adenocarcinoma (N=59) serum samples were individually pooled. Serum samples from 61 DF volunteers were also pooled and used as control. A 1- μ L aliquot of each disease and DF samples were pipetted into four separate vials. A 90- μ L aliquot of PBS was added into each disease and DF vials containing 10 μ L of pooled blood serum. Then, a 1.2- μ L aliquot of PNGase F was added, and reaction mixtures were placed in a 37°C water bath overnight.

3.2.4 Purification of N-Glycans Released from Pooled HBS

Graphitized carbon microspin columns were used for the purification of released N-glycans from pooled HBS, disease and DF samples as previously described.^{29,110,151} Briefly, the graphitized carbon spin column was washed with a 400- μ L aliquot 100% ACN and two 400- μ L aliquot of 85% ACN aqueous solution (0.1 % TFA) were applied twice. The column was then conditioned with a 400- μ L aliquot of 5% ACN aqueous solution (0.1% TFA). This step was repeated twice. A 690- μ L aliquot of 5% ACN aqueous solution (0.1% TFA) was added to the enzymatically released glycans and centrifuged at 10k rpm for 30 min prior to loading on the conditioned activated charcoal microspin columns. Then, 5% ACN aqueous solution (0.1% TFA) was used to wash nonspecifically bound material. This step was repeated five times. Finally, glycans were eluted using a 200- μ L aliquot of 40% aqueous ACN (0.1% TFA). This elution step was repeated one more time, prior to drying the eluants under vacuum.

3.2.5 Reduction of N-Glycans

Fresh ammonia borane complex solution (10 μ g/ μ L) was prepared in 29% ammonium hydroxide solution. A 10- μ L aliquot of this solution was added to the purified N-glycans enzymatically released from model glycoproteins and HBS samples to reduce

all glycans. The samples were then placed at 65°C in a water bath for 1h before adding a 100- μ L aliquot of acetic acid (10%). Then, the reaction mixtures were dried under vacuum. Next, methanol was added to evaporate borate salt. A volume 100 μ L of methanol was added to each sample and dried. This step was repeated several times to remove all borate salt.

3.2.6 Permetylation of N-Glycans

Iodomethane (ICH_3), iodomethane- d_1 (ICH_2D) and iodomethane- d_3 (ICD_3) were used to permethylate N-glycans enzymatically released from model glycoproteins and HBS. N-glycans enzymatically released from DF HBS was permethylated with ICH_3 while those released from Barrett's disease, HGD and esophageal adenocarcinoma HBS samples were methylated with ICD_3 . Permetylation was performed following the previous reported procedure.^{48,66,67} First, empty microspin columns were filled to a 3-cm depth with sodium hydroxide beads and washed twice with a 50- μ L aliquot of DMSO. Samples were prepared in 30 μ L DMSO and 1.2 μ L water. A 20- μ L aliquot of ICH_3 or ICD_3 was applied to purified and reduced N-glycans from RNase B, fetuin and HBS. ICH_3 (20 μ L) was added to the DF HBS samples while ICD_3 (20 μ L) was added to the disease samples. The reaction mixtures were then applied to microspin columns packed with sodium hydroxide beads and allowed to sit for 25 min. Another 20- μ L aliquot of ICH_3 or ICD_3 was added into each sample. The reaction was allowed to proceed for another 15 min. Next, a 50- μ L aliquot of ACN was added to the column and centrifuged at low speed (1000 rpm). This step was repeated twice to ensure quantitative elution of all permethylated N-glycans.

3.2.7 Solid-phase purification of N-Glycans

C₁₈ microspin column was used for the purification of permethylated N-glycans. C₁₈ column was washed with 100% ACN and 85% ACN aqueous solution (0.1% TFA). The columns were then conditioned with 5% ACN aqueous solution (0.1% TFA). A 690- μ L aliquot of 5% ACN aqueous solution (0.1% TFA) was added to the sample prior to loading on the column. Next, the column was washed with 5% ACN aqueous solution (0.1% TFA) three times and then 80% ACN aqueous solution (0.1% TFA) was applied to elute the N-glycans from the column. The samples were dried under vacuum and resuspended in 20% ACN for LC-ESI-MS analysis.

3.2.8 LC-ESI-MS

Reduced and isotopically permethylated N-glycans were separated by nano-LC (Dionex, Sunnyvale, CA) on a reverse phase Acclaim[®] PepMap capillary column (150 mm x 75 μ m i.d) packed with 100 Å C₁₈ bounded phase (Dionex). Separation was attained using a two solvent system; solvent A consisted of 2% acetonitrile and 98% water with 0.1% formic acid while solvent B consisted of acetonitrile and 0.1% formic acid. Separation was attained using gradient conditions (38%-45% solvent B over 32 min, followed by 10 min wash with 80% B, and conditioned for 10 min with 20% B). The LC system was operated at a flow rate of 350 nL/min. The Nano-LC system was interfaced to a Velos LTQ Orbitrap hybrid mass spectrometer (Thermo Scientific, San Jose, CA). The mass spectrometer was operated in an automated data-dependent acquisition mode in which the scan mode switched between MS full scan (*m/z* from 500-2000) and CID MS/MS scan which was conducted on the 8 most abundant ions with a 0.250 Q-value, 20 ms activation time, and 35% normalized collision energy.

3.2.9 Data Evaluation

LC/ESI-MS data acquired were processed using Xcarlibur Qual Browser (Thermo Fisher Scientific). The isotopic masses of glycans were used to generate extracted ion chromatograms with 10 ppm mass tolerance. A seven-point boxcar smoothing was enabled to improve peak quality. The integrated peak areas of ion adducts representing the same glycan structure were summed. This value is used to represent the abundance of a glycan structure. MS spectra of glycans were obtained by averaging over the LC profile. Tandem mass spectra of glycans were within the elution profile representative of each glycan structure. B-, C-, X-, Y-ion series were the common fragment ions observed in tandem MS.

3.3 Results and Discussion

Comparative glycomic mapping (C-GlycoMAP) was introduced by Mechref and Novotny⁹⁶ for MALDI-MS analysis of N-glycans permethylated using iodomethane and iodomethane-*d*₃. This strategy was effective in comparing the glycomic profiles derived from blood serum for samples representing different stages of breast cancer. We here extend MC-GlycoMAP to LC-ESI-MS analysis of glycans permethylated using multiple stable isotopic iodomethane reagents, thus enabling MC-GlycoMAP of glycans derived from different biological samples.

Figure 3.1 illustrates the overall workflow for LC/ESI-MS MC-GlycoMAP. N-Glycans were enzymatically released from equal amounts of proteins, or equal volumes of HBS samples, using PNGase F. Released N-glycans were then reduced and isotopically permethylated using ICH₃, ICH₂D or ICD₃. Equal amounts of differentially permethylated N-glycans were subsequently mixed prior to LC/ESI-MS analyses.

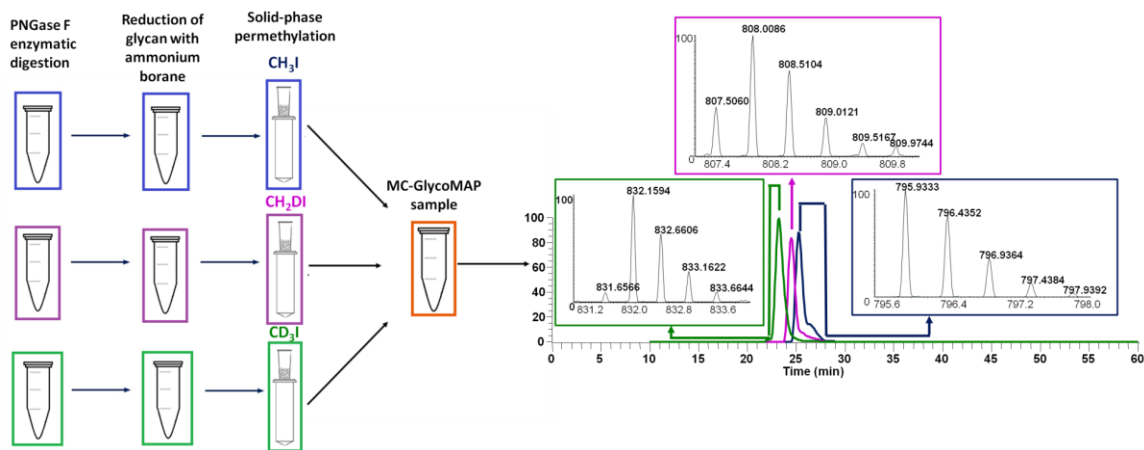


Figure 3.1 Schematic of sample preparation process

Chromatographic separation on reversed-phase column prompts the efficient separation of “light” and “heavy” permethylated glycans.

3.3.1 Comparative quantification of permethylated N-glycans derived from model glycoproteins

N-Glycans derived from RNase B and fetuin were employed to explore the potential of isotopic permethylation for comparative glycan quantification. The same glycans were also employed to assess the repeatability and permethylation efficiency of the three stable isotopic iodomethane reagents. Equal aliquots of RNase B N-glycans were simultaneously released and differentially labeled with stable isotopic iodomethane reagents (“light” ICH_3 , and “heavy” ICH_2D or ICD_3). The chromatographic retention times of isotopically permethylated N-glycans derived from RNase B were different, thus prompting the efficient separation of all species (**Figure 3.2**). Equal amounts of ICH_3 , ICH_2D and ICD_3 permethylated RNase B N-glycans were mixed and subjected to LC-ESI-MS. The peaks areas of all isotopically permethylated N-glycans were representative of their natural distribution. Each permethylated N-glycan structure formed multiple adducts in the ESI source. The most intense ions were representative of protonated and ammoniated ($[\text{M}+\text{H}+\text{NH}_4]^{2+}$) ions. Moreover, the intensities of singly protonated and ammoniated ions were representative of the intensities of all adducts. The retention times decreased with deuterium substitution increase, which is due to the decrease in the hydrophobicity of N-glycans as a result of this type of derivatization. The retention time difference between Man 5 counterparts was 3.19 min while there was 6.52 min difference between “heavy” and “light” permethylated Man 8. This is due to the higher number of permethylation sites. The retention time difference decreased for Man 9 counterparts,

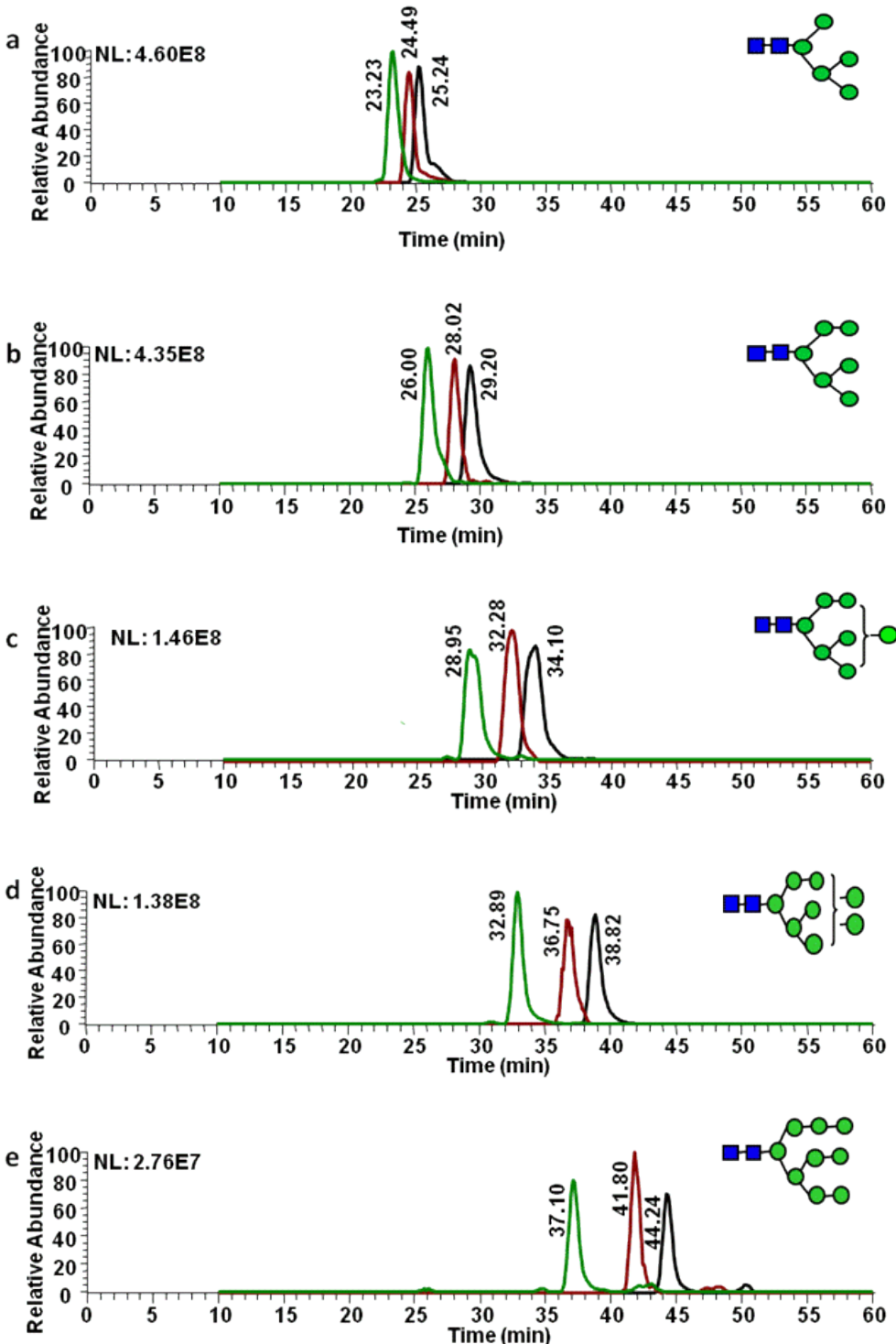


Figure 3.2 Extracted ion chromatograms (EIC) and MS spectra of Man 5 (a), Man 6 (b), Man 7 (c), Man 8 (d), and Man 9 (e) glycans derived from RNase B. Equal amounts of N-glycans released from RNase B were permethylated with iodomethane (ICH_3), iodomethane- d_1 (ICH_2D) and iodomethane- d_3 (ICD_3) reagents and mixed prior to LC-ESI-MS analysis. Symbols: as in **Figure 2.1**.

which is due to solvent B being increased to 80% at 43 min to 48 min. The hydrophobic differences among all pairs prevented the isotopic peak overlap while the isotopic mass difference provides sufficient *m/z* value dispersion. Therefore, each isotopically labeled species were distinguished and quantified without interference from the isotopic distribution of its counterparts. The peak area ratios ($\text{ICD}_3:\text{ICH}_2\text{D}:\text{ICH}_3$) were 1.10:0.87:1, 1.11:0.86:1, 0.89:1.02:1, 1.01:0.90:1, and 1.12:1.27:1 for Man 5 (**Figure 3.2a**), Man 6 (**Figure 3.2b**), Man 7 (**Figure 3.2c**), Man 8 (**Figure 3.2d**), and Man 9 (**Figure 3.2e**), respectively. Peak area differences were attributed to ionization efficiencies dictated by the mobile phase composition as well as the isotopic purity of iodomethane reagents.

The comparative glycomic quantification strategy was also evaluated using the six sialylated N-glycans derived from fetuin. N-glycans were released from fetuin and “light” and “heavy” permethylated using ICH_3 and ICD_3 reagents, respectively. The samples were mixed together after purification using C_{18} cartridges (see Experimental section). The purified and mixed samples were then subjected to LC-ESI-MS analysis. Extracted ion chromatograms of the four most abundant N-glycans of fetuin are depicted in **Figure 3.3**. The most intense ions of these glycan structures were $[\text{M}+3\text{H}]^{3+}$ or $[\text{M}+2\text{H}+\text{NH}_4]^{3+}$. Extracted ion chromatogram and mass spectrum of H4N5S1 glycan with 809.0916 *m/z* values (“light” permethylated) and 844.3113 (“heavy” permethylated) are depicted in **Figure 3.3a**. The peak heights of the “heavy” permethylated glycans relative to that of “light” permethylated ones (H/L) for H4N5S1 (**Figure 3.3a**), N4H5S2 (**Figure 3.3b**), N5H6S3 (**Figure 3.3c**), and N5H6S4 (**Figure 3.3d**) were 1.07, 1.11, 0.99, and 1.10, respectively. The peak area ratios (H/L) for the same structures were 1.05, 1.14, 0.99, and

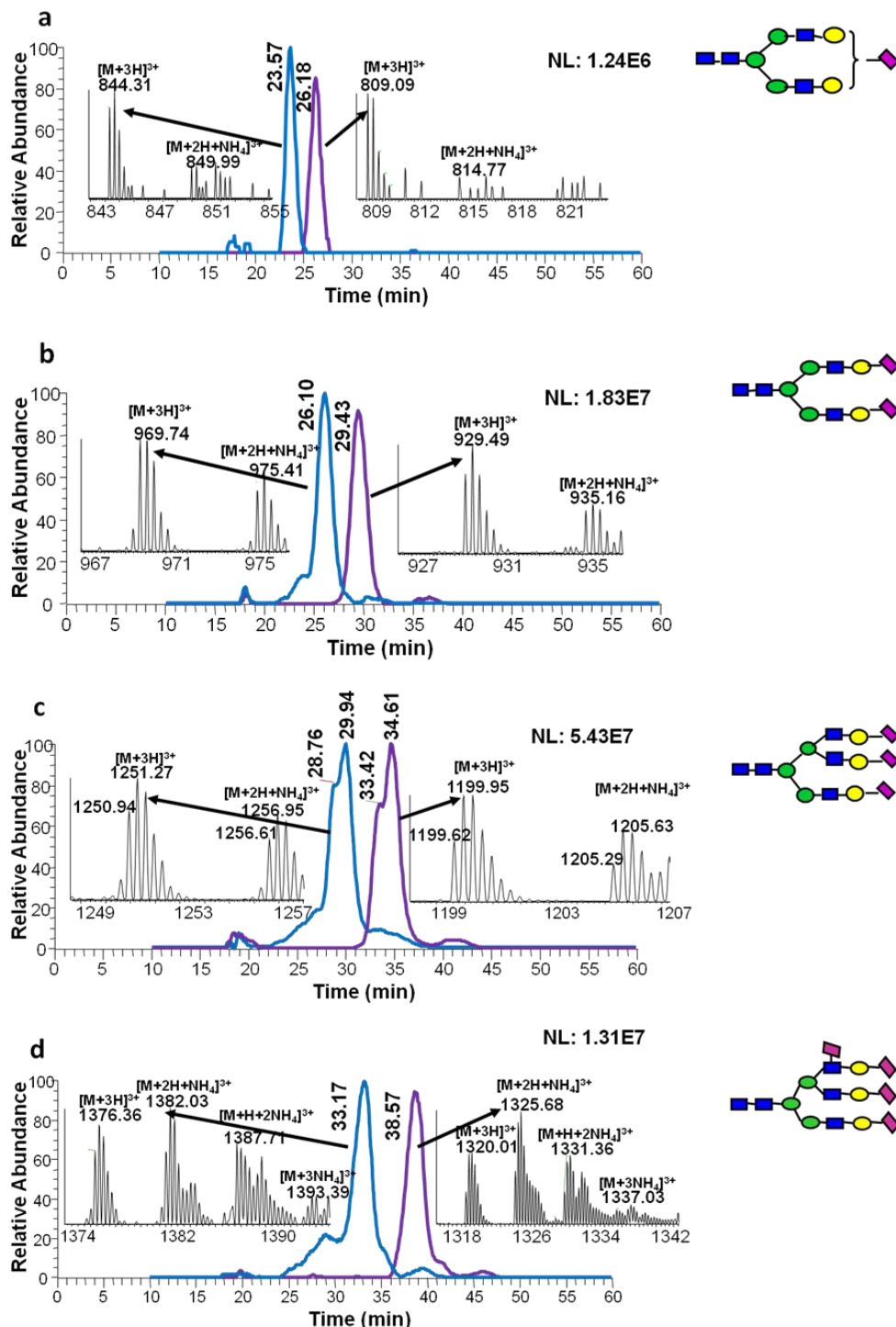


Figure 3.3 EIC and MS spectra of biantennary monosialylated (a) biantennary disialylated (b), triantennary trisialylated (c), and triantennary tetrasialylated (d) N-glycans derived from fetuin. Equal amounts of N-glycans released from fetuin were “heavy” and “light” permethylated using ICH_3 , and ICD_3 reagents, respectively. Symbols: as in **Figure 2.1**.

1.12, respectively. Similar to N-glycans derived from RNase B, intensity of “heavy” permethylated N-glycans and “light” N-glycans are not identical. However, the intensity varies within $\pm 11.4\%$ of the theoretical values. Again this difference is lower than the variation routinely observed in label-free ESI-based quantification methods and can be partially attributed to the purity of isotopic iodomethane reagents.

3.3.2 Comparative quantification of permethylated N-glycans derived from HBS

Serum glycomics profiling is important for the discovery of human disease biomarkers as has been demonstrated by several studies.^{13,21,28,29,33,148,151} To explore the potential of employing comparative quantification of glycans using isotopic permethylation reagents in conjunction with LC-ESI-MS for complex biological samples, two equal volumes of blood serum samples were subjected to PNGase F treatment prior to “heavy” and “light” permethylation and LC-ESI-MS analysis. This analysis permitted the detection of 73 glycan structures. The ratios of their peak height or areas were also within $\pm 11.4\%$ of the theoretical values.

The comparative glycomic quantification strategy was employed to investigate differences in glycosylation patterns between esophageal disease samples and DF sample. Serum samples collected from different patients diagnosed with different esophageal diseases, (Barrett’s disease, HGD and esophageal adenocarcinoma) and sex- and age-matching DF samples were separately pooled. N-Glycans derived from the pooled esophageal disease samples were permethylated with “heavy” reagent while those from DF sample were “light” permethylated. Comparative glycomic LC-ESI-MS profiling was acquired with equal volume mixtures of disease sample and DF sample. The extracted ion chromatograms of three representative human blood serum N-glycans are depicted in

Figures 3.4-3.6. The H/L ratios of N-glycan pairs for the same samples, but “light” and “heavy” permethylated were 1.05, 0.858 and 1.11 for H5N2 (**Figure 3.4a**), F1H3N5 (**Figure 3.4b**) and F1H4N5 (**Figure 3.4c**), respectively. These glycans should have depicted ratios of 1. The slight variation from the theoretical ratios may be due to the same above discussed reasons. Despite this fact, all pairs had an H/L ratio almost equal 1, indicating that a complex biological system does not influence comparative LC-ESI-MS glycomic analysis. Meanwhile, the same structures derived from esophageal adenocarcinoma and DF samples depicted different peak ratios. The peak area ratios of H/L for the same glycans derived from disease samples (“heavy” permethylated) and DF samples (“light” permethylated) were 1.52, 0.85, and 0.70 for H5N2 (**Figure 3.4d**), F1H3N5 (**Figure 3.4e**), and F1H4N5 (**Figure 3.4f**), respectively. In cancer samples, the intensity of Man 5 is significantly higher than that in DF HBS while that of bisecting fucosylated N-glycan is lower than that in DF HBS. The same N-glycans derived from Barrett’s samples were also compared to DF samples (**Figure 3.5**). The peak area ratios for Barrett’s samples are shown in **Figures 3.5 a-c**. The ratios were 4.14 for H5N2 (**Figure 3.5a**), 0.63 for F1H3N5 (**Figure 3.5b**) and 0.80 for F1H4N5 (**Figure 3.5c**). The H/L peak area ratios of the same peaks derived from HGD and DF were 3.25 for H5N2 (**Figure 3.6a**), 0.63 for F1H3N5 (**Figure 3.6b**) and 0.69 for F1H4N5 (**Figure 3.6c**). These results were in agreement with recently reported results.¹¹⁰ **Table 3.1** summarizes the changes of N-glycans in the cancer samples as well as other esophageal disease samples. Only the peaks with significant changes (H/L ratio higher than 1.2 or lower than 0.8) were listed in the table. For cancer samples, there were 40 compositions that were significantly different from the DF sample. 8 N-glycan compositions were over expressed.

Table 3.1 Intensities and Ratios of N-glycans derived from cancer, Barrett's, HGD and DF HBS samples.

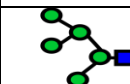
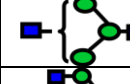
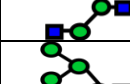
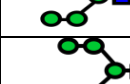
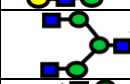
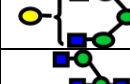
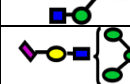
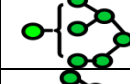
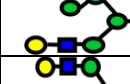
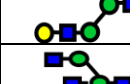
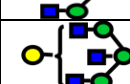
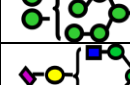
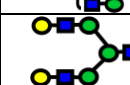
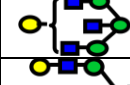
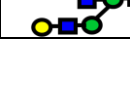
Structures	Disease free(L)	Cancer (H)	Ratio (H/L)	Disease free(L)	Barrett's (H)	Ratio (H/L)	Disease free(L)	HGD (H)	Ratio (H/L)
	4.57E+08	6.94E+08	1.52	1.25E+09	5.18E+09	4.14	1.33E+09	4.33E+09	3.25
	-----	-----	-----	1.01E+08	6.91E+07	0.68	1.26E+08	6.63E+07	0.53
	4.78E+08	3.78E+08	0.79	5.25E+08	2.84E+08	0.54	5.61E+08	7.99E+08	1.42
	-----	-----	-----	3.56E+08	2.28E+09	0.64	3.63E+08	1.91E+09	5.26
	1.81E+08	4.79E+07	0.26	-----	-----	-----	4.93E+08	6.30E+08	1.28
	-----	-----	-----	1.14E+10	1.49E+10	1.30	2.20E+10	3.13E+10	1.42
	-----	-----	-----	6.32E+08	7.91E+08	1.25	9.38E+08	1.15E+09	1.23
	1.18E+08	1.57E+08	1.33	6.77E+07	1.05E+09	15.5	7.72E+07	1.46E+09	18.9
	-----	-----	-----	2.75E+08	8.35E+08	3.03	2.22E+08	8.23E+08	3.70
	9.79E+08	1.88E+08	0.19	6.22E+08	4.68E+08	0.75	8.23E+08	5.56E+08	0.68
	1.72E+08	2.89E+07	1.68	2.12E+08	2.82E+08	1.33	-----	-----	-----
	4.92E+08	3.43E+08	0.69	4.21E+08	8.95E+08	2.12	4.35E+08	8.81E+08	2.02
	-----	-----	-----	5.75E+09	3.64E+09	0.63	5.92E+09	4.14E+09	0.69
	-----	-----	-----	3.42E+08	1.51E+09	4.44	3.23E+08	1.43E+09	4.43
	7.14E+08	3.71E+08	0.52	5.95E+08	1.44E+09	2.42	5.32E+08	9.81E+08	1.84
	4.26E+09	6.80E+08	1.60	4.14E+09	1.50E+09	0.36	4.12E+09	5.87E+09	1.42
	5.35E+08	2.22E+09	0.41	3.58E+08	3.36E+09	9.39	3.35E+08	3.39E+09	0.10
	9.44E+09	7.13E+09	0.76	6.77E+09	9.88E+09	1.46	7.04E+09	7.43E+09	1.06
	8.99E+09	6.25E+09	0.70	-----	-----	-----	7.87E+09	5.44E+09	0.69
	1.77E+08	5.38E+07	0.30	1.31E+08	6.60E+08	5.03	1.55E+08	5.16E+08	3.32

Table 3.1 Continued

Structures	Disease free(L)	Cancer (H)	Ratio (H/L)	Disease free(L)	Barrett's (H)	Ratio (H/L)	Disease free(L)	HGD (H)	Ratio (H/L)
	1.31E+10	7.39E+09	0.56	1.21E+10	1.53E+10	1.26	-----	-----	-----
	1.81E+10	1.43E+10	0.79	1.35E+10	3.39E+10	2.51	1.40E+10	2.95E+10	2.10
	4.82E+09	3.44E+09	0.71	3.17E+09	8.20E+09	2.59	3.21E+09	8.01E+09	2.50
	-----	-----	-----	-----	-----	-----	5.92E+07	4.28E+08	7.23
	2.07E+09	1.24E+09	0.60	1.89E+09	3.48E+09	1.84	1.89E+09	2.34E+09	1.23
	1.52E+10	8.88E+09	0.58	-----	-----	-----	1.29E+09	4.96E+09	3.84
	-----	-----	-----	1.26E+09	3.48E+09	2.76	1.24E+09	3.67E+09	2.96
	9.38E+08	3.64E+08	0.39	7.84E+08	4.69E+09	0.60	7.93E+08	3.18E+09	4.01
	-----	-----	-----	-----	-----	-----	9.79E+07	4.07E+08	4.16
	-----	-----	-----	1.28E+11	1.62E+11	1.27	1.40E+11	1.98E+11	1.41
	3.15E+10	2.12E+10	0.67	-----	-----	-----	2.99E+10	3.69E+10	1.23
	-----	-----	-----	6.85E+09	1.04E+10	1.52	8.37E+09	1.11E+10	1.33
	1.27E+10	5.23E+09	0.41	1.20E+10	2.06E+10	1.72	1.30E+10	1.53E+10	1.18
	4.77E+09	1.29E+09	0.27	4.52E+09	1.95E+09	0.43	5.21E+09	2.51E+09	0.48
	-----	-----	-----	1.03E+09	2.30E+09	2.23	8.33E+08	2.32E+09	2.79
	4.72E+10	2.48E+10	0.53	3.51E+10	4.30E+10	1.23	-----	-----	-----
	9.09E+08	4.60E+08	0.51	7.07E+08	9.78E+08	1.38	8.27E+08	1.15E+09	1.39
	1.12E+09	1.56E+08	0.14	8.72E+08	3.97E+08	0.46	-----	-----	-----
	2.97E+10	2.36E+10	0.79	2.39E+10	4.13E+10	1.73	3.04E+10	3.93E+10	1.29
	-----	-----	-----	8.10E+09	1.17E+10	1.44	1.01E+10	1.32E+10	1.31

Table 3.1 Continued

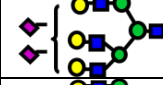
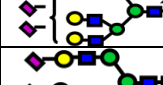
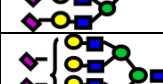
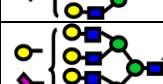
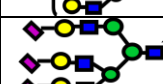
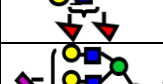
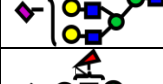
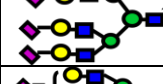
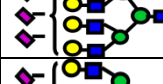
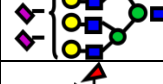
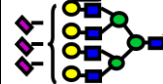
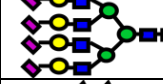
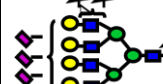
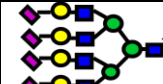
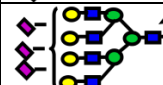
Structures	Disease free(L)	Cancer (H)	Ratio (H/L)	Disease free(L)	Barrett's (H)	Ratio (H/L)	Disease free(L)	HGD (H)	Ratio (H/L)
	5.86E+09	4.30E+09	0.73	4.26E+10	4.65E+09	0.10	-----	-----	-----
	1.81E+09	8.55E+07	0.05	1.34E+09	6.48E+08	0.48	1.67E+09	4.24E+08	0.25
	6.32E+10	1.84E+10	0.29	3.39E+10	4.58E+10	1.35	-----	-----	-----
	2.12E+09	1.05E+08	0.05	1.78E+09	5.27E+08	0.30	1.65E+09	1.68E+09	1.01
	-----	-----	-----	-----	-----	-----	4.51E+08	2.77E+08	0.61
	-----	-----	-----	3.39E+10	4.58E+10	1.35	2.31E+10	5.64E+10	2.44
	3.03E+09	3.88E+09	1.28	2.33E+09	7.19E+09	3.09	2.68E+09	8.08E+09	3.01
	-----	-----	-----	1.73E+09	8.17E+08	0.47	4.47E+08	9.41E+08	2.10
	-----	-----	-----	1.39E+09	4.00E+09	2.88	1.71E+09	4.34E+09	2.53
	5.64E+09	2.91E+09	0.51	4.53E+09	2.92E+09	0.64	5.58E+09	7.23E+09	1.29
	2.20E+10	2.30E+09	0.10	-----	-----	-----	1.16E+10	5.93E+09	0.51
	2.02E+09	1.54E+09	0.76	1.05E+09	2.32E+09	2.20	2.73E+08	5.80E+09	21.2
	1.07E+10	6.47E+09	0.60	-----	-----	-----	6.44E+09	2.31E+10	3.58
	8.55E+08	6.89E+07	0.81	-----	-----	-----	-----	-----	-----
	5.40E+09	7.17E+09	1.32	4.56E+09	2.18E+10	4.78	5.13E+09	2.14E+10	4.17
	-----	-----	-----	-----	-----	-----	4.62E+08	1.87E+08	0.40

Table 3.1 Continued

Structures	Disease free(L)	Cancer (H)	Ratio (H/L)	Disease free(L)	Barrett's (H)	Ratio (H/L)	Disease free(L)	HGD (H)	Ratio (H/L)
	9.33E+08	2.96E+09	3.17	1.30E+09	4.16E+09	3.20	9.26E+08	3.09E+09	3.34
	1.10E+08	5.71E+08	5.42	1.66E+08	3.07E+09	18.49	1.94E+08	1.79E+09	9.22
	4.95E+07	1.14E+07	0.23	5.37E+07	7.90E+08	14.70	9.02E+07	8.44E+08	9.35

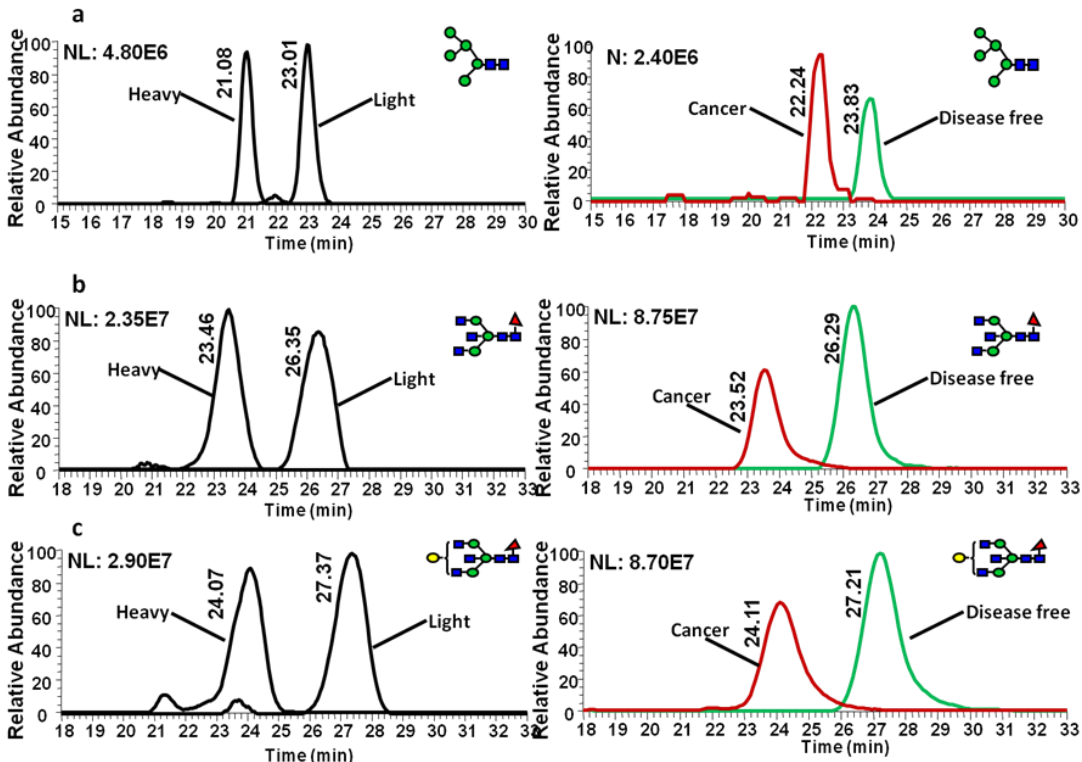


Figure 3.4 EIC of equal amounts of “heavy” and “light” permethylated (a) H5N2, (b) F1H3N5, and (c) F1H4N5 N-glycans derived from DF samples. EIC of equal amounts of “heavy” and “light” permethylated (d) H5N2, (e) F1H3N5, and (f) F1H4N5 N-glycans derived from cancer and DF samples, respectively. Symbols: as in **Figure 2.1**.

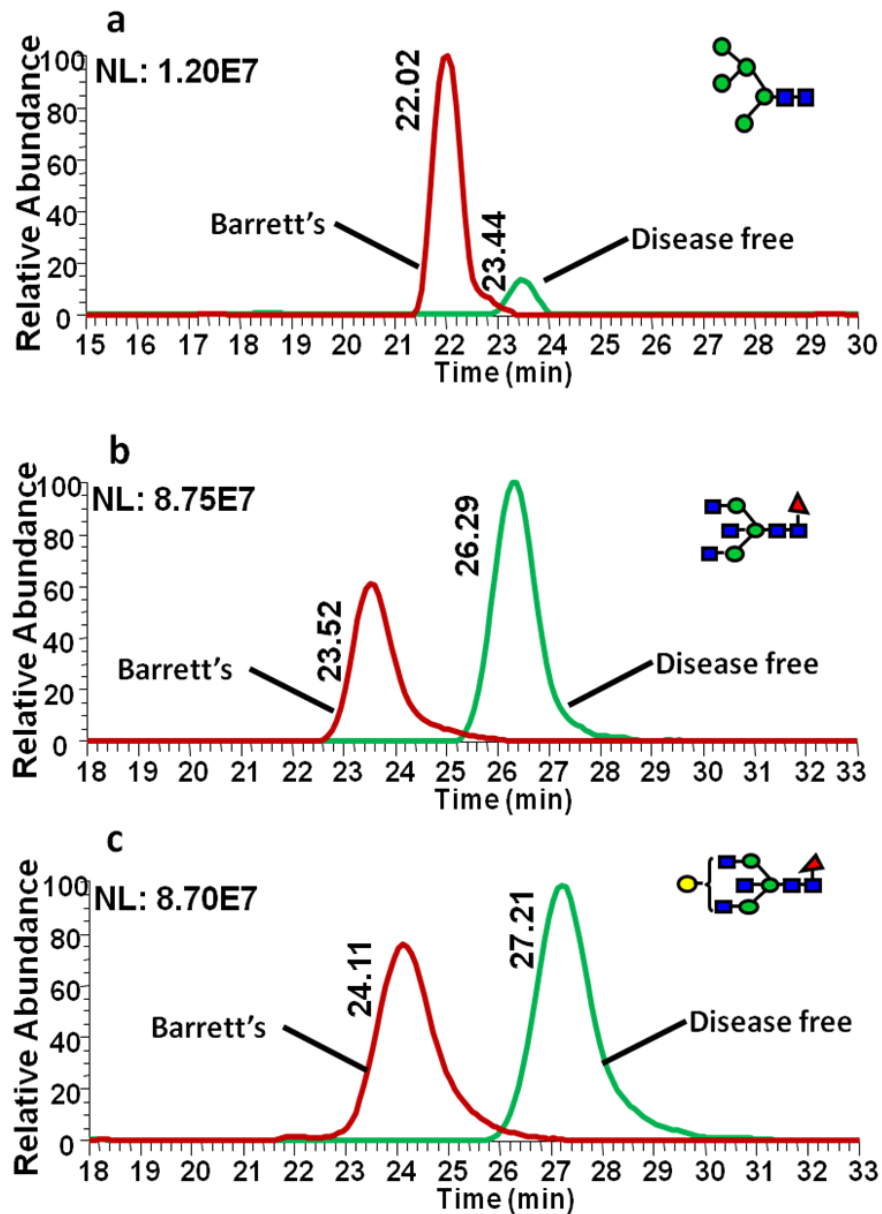


Figure 3.5 EIC of equal amounts of “heavy” and “light” permethylated (d) H5N2, (e) F1H3N5, and (f) F1H4N5 N-glycans derived from Barrett’s disease and DF samples, respectively. Symbols: as in **Figure 2.1**.

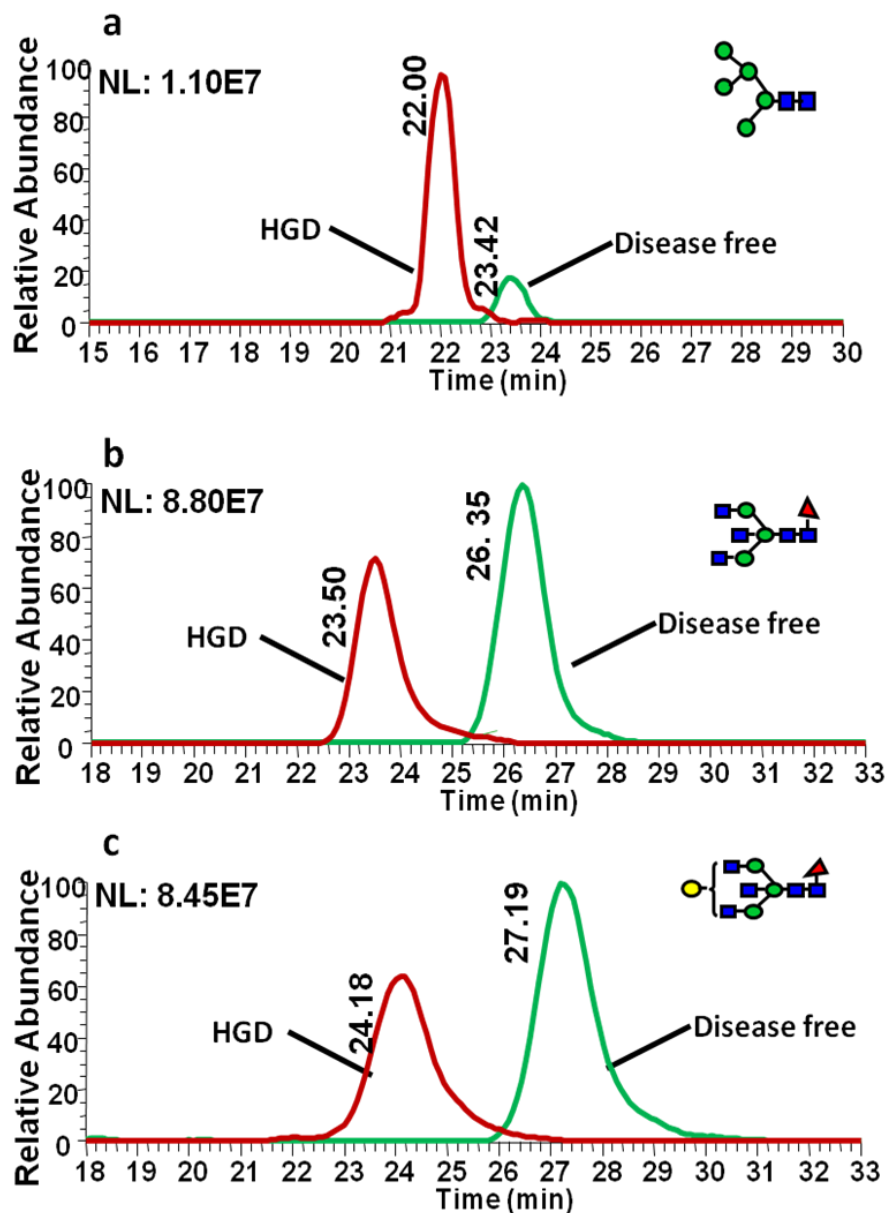


Figure 3.6 EIC of equal amounts of “heavy” and “light” permethylated (d) H5N2, (e) F1H3N5, and (f) F1H4N5 N-glycans derived from HGD and DF samples, respectively. Symbols: as in **Figure 2.1**.

As for the Barrett's sample, there were 32 compositions that were largely increased and 14 compositions were decreased. In the case of HGD, 39 compositions were increased while 10 others were decreased. Accordingly, it appears that C-GlycoMAP of HBS by LC-ESI-MS is adequate to distinguish esophageal diseases from each other and from DF control.

3.4 Conclusion

Combining the permethylation and isotopic labeling, allows simultaneously quantification of N-glycans in comparative glycomics studies. N-Glycans derived from model glycoproteins and human blood serum demonstrated the effective glycan quantification using "heavy" and "light" permethylation of glycans. LC-ESI MS results indicated that this strategy is reliable for quantitative glycomics analysis of glycans derived from different samples. Comparative glycomics profiling of N-glycans derived from esophageal disease and DF samples illustrated the potential of using this strategy. The comparative glycomics profiling strategy described here may be utilized to monitor glycomics changes associated with the development and progression of diseases. The strategy could also be employed to monitor any glycomics changes resulting from drug treatment.

CHAPTER IV

LC-MSMS OF PERMETHYLATED N-GLYCANS DERIVED FROM MODEL AND HUMAN BLOOD SERUM GLYCOPROTEINS

Y. Hu, T. Shihab, Y. Mechref, in preparation

4.1 Introduction

Glycosylation is one of the most common posttranslational modifications of proteins, since protein glycosylation attributes to many biological processes such as protein folding, transport, and targeting.³ Moreover, aberrant glycosylation has been linked to the development of many human diseases, including cancer, inflammation and many immune diseases.^{5,108} Therefore, glycans could be potentially utilized as biomarkers for disease diagnosis and prognosis. As such, characterization of glycosylation is a research area that has recently attracted a lot of attention.

Among the various analytical methods routinely employed for glycomics analysis, MS has proven to be one of the most powerful tools because of its ability to produce a wealth of reliable data, allowing the analysis of glycans associated with complex biological samples. MS has been recently employed to elucidate glycan structures and their roles in disease progression.^{18,109-111} However, structural elucidation remains a challenge in glycomics studies. Currently, the most reliable analytical tool for structural elucidation is tandem MS (MS^2 and MS^n) analysis, which provides structural information, thus allowing unequivocal glycan structural assignment.^{41,154} Despite the wealth of information provided by MS^2 analysis, it is still challenging to identify some glycan structures, as there are not enough fragments produced to prompt effective identification. This ambiguity can be somewhat resolved through MS^3 , or in some cases

through MSⁿ analysis. However, MSⁿ analysis is not attainable in cases where the abundances of glycans are very low. Additionally, glycan concentration dynamic range within one sample can extend over several orders of magnitude, prompting detector bias which severely limits tandem MS capabilities. For glycans existing at low concentrations, chromatographic or electrophoretic separations overcome such limitations and generate reliable MSⁿ acquisitions.

Glycans of complex samples are effectively identified and characterized by combining LC and MS. Recently, an LC method employing amide based columns was devised to analyze heterogeneous glycan mixtures.¹⁵⁵ The retention times of fluorescently labeled glycans were initially correlated to the retention times of dextran linear oligosaccharides to determine GU values. Such values were subsequently employed to deduce the structures of unknown glycans. Amide-modified nanocolumns have also been used to separate underivatized N-glycans for MS analysis⁷⁷. Additionally, porous graphitic carbon columns interfaced to MS have been applied to separate and identify N-glycan isomeric structures.^{84,156,157} Most of the recent studies employing this chromatography medium focused on structural identification of native glycans. However, one issue encountered when using mass spectrometry for the analysis of native glycans is the low ionization efficiency of such structures, especially in the case of sialylated glycans. The simultaneous detection of both acidic and neutral glycans in positive-mode MS is analytically challenging. This problem is easily addressed through the permethylation of N-glycans.^{48,66,67} Not only can all of the permethylated glycans be observed in positive mode, but the ionization efficiency and stability of sialylated glycans is substantially improved as a result of permethylation.

In this study, we attained the separation of permethylated N-glycans using a C₁₈ nanocolumn that is interfaced to an Orbitrap mass spectrometer to investigate the relationship between retention time and glycan structure. The chromatographic separation allowed the identification of glycan structures by their specific retention times. Also, the chromatographic separation allowed the confirmation of the majority of glycan structures commonly observed in HBS. A comprehensive 2-D map was generated and subsequently employed to determine the glycan structures associated with different samples. The above described LC-MS method permitted a simplified characterization and unequivocal structural assignments of glycan structures associated with complex biological samples such as HBS.

4.2 Experiment

4.2.1 Material

Dextran, dextrin, model glycoprotein (including RNase B, fetuin) and HBS were obtained from Sigma-Aldrich (St. Louis, MO). Other chemicals such as ammonia borane complex, sodium hydroxide beads, DMSO, methyl iodide, TFA, chloroform, and MS-grade FA were also purchased from Sigma-Aldrich. Microspin columns and graphitized carbon and C₁₈ microspin columns were purchased from Harvard Apparatus (Holliston, MA). Acetic acid and HPLC-grade solvents, including methanol and isopropanol, were procured from Fisher Scientific (Pittsburgh, PA), while acetonitrile was obtained from JT Baker (Phillipsburg, NJ). HPLC grade water was acquired from Mallinckrodt Chemicals (Phillipsburg, NJ). PNGase F purified from *Flavobacterium meningosepticum* (500,000 units/mL) was obtained from New England Biolabs Inc. (Ipswich, MA). Neuraminidase from clostridium perfringens was purchased from Sigma-Aldrich.

4.2.2 N-glycans Released from Model Glycoproteins

Stock solutions of model glycoproteins (10 µg/µL concentrations), including RNase B and fetuin were prepared. A 1-µL aliquot of each of the model glycoprotein stock solutions was mixed with a 9-µL aliquot of G7 buffer (50 mM sodium phosphate buffer, pH 7.5) provided by the vendor. Next, a 1-µL aliquot of a diluted PNGase F solution (prepared by diluting the vendor stock solution 10-times with G7 buffer) was added to each of the model glycoprotein solutions. The unit concentration of the diluted PNGase F solution is 50 units/µL. The reaction mixtures were then incubated for 18 hours at 37°C in a water bath (Thermo Scientific, Pittsburgh, PA). Upon the completion of the enzymatic digestion, samples were dried under vacuum (Labconco, Kansas City, MO).

4.2.3 N-glycans Released from HBS Glycoproteins

A 90-µL aliquot of denaturation phosphate buffer saline (PBS, consisting of 10mM sodium phosphate, 10 mM sodium chloride, 4 mM dithiothritol (DTT), 0.5% sodium dodecyl sulfate (SDS), pH 7.5) was added to a 10-µL aliquot of HBS. The sample was then incubated at 60°C for 45 minutes and allowed to reach room temperature. This is employed to prompt partial denaturation of glycoproteins which permits efficient enzymatic release of N-glycans. A 5-µL aliquot of 10% aqueous NP-40 solution was added to consume free SDS. Next, a 2.4-µL aliquot of PNGase F (120 units) was then added prior to placing the sample in a 37°C water bath for 18h. Next, a 690-µL aliquot of 5% acetonitrile (0.1% trifluoroacetic acid) was added to the enzymatically released glycans and centrifuged at 10K rpm for 30 min. The samples were then purified with charcoal microspin columns. First, the charcoal spin columns were washed with 100%

ACN. Then, the column was washed with a 400- μ L aliquot of 85% aqueous ACN solution. This step was repeated twice. Next, columns were conditioned with 400 μ L of 5% aqueous ACN solution twice. The samples were then applied to the columns and the columns were washed five times with 5% aqueous ACN solution. Finally, glycans were eluted from the column using 200 μ L of 40% aqueous ACN solution. This elution step was repeated twice, prior to mixing all eluants in a clean vial and drying under vacuum.

4.2.4 Desialylation of N-glycans from Fetuin

N-glycans released from fetuin were also desialylated as described here. A 5- μ L aliquot of enzymatically released fetuin was adjusted to pH 6.5 with 0.1 M hydrochloric acid. Next, a 1- μ L aliquot of neuraminidase (1 μ g/ μ L concentration, 0.01 unit) was added to the sample and incubated at 37°C for 4h. This was performed to generate non-sialylated biantennary and triantennary complex glycan compositions.

4.2.5 Reduction of N-glycans

A 10- μ L aliquot of aqueous borane-ammonium complex (10 μ g/ μ L concentration) was added to dextran, dextrin and the N-glycans enzymatically released from fetuin, RNase B, HBS, and neuraminidased treated fetuin. Each sample was then incubated in a 60°C water bath for 1 hour prior to the addition of 10 μ L of 5% acetic acid. Samples were then dried under vacuum. Next, a 100- μ L aliquot of HPLC-grade methanol was added to form volatile methyl borate. The samples were then dried under vacuum. The last two steps were repeated several times to ensure effective elimination of excess borate introduced through the reduction reaction.

4.2.6 Solid-Phase Permetylation of N-glycans

Reduced glycans were permethylated using solid-phase permethylation according to the previously published method.^{48,66,67} First, microspin columns were filled to 3 cm depth with sodium hydroxide beads and washed twice with 50- μ L aliquots of DMSO. The dried and reduced glycan samples were resuspended in 1.2 μ L water and 30 μ L DMSO. A 20- μ L aliquot of methyl iodide was then added to the sample prior to the application of the sample to the sodium hydroxide packed microspin column. The samples were allowed to sit for 30 minutes before the addition of another 20- μ L aliquot of methyl iodide. The samples were then allowed to sit for an additional 20 minutes before centrifuged at 1.6K rpm. Finally, the sodium hydroxide columns were washed with 50 μ L ACN twice to elute all permethylated glycans.

4.2.7 Solid-Phase Purification of N-glycans

Solid-phase C₁₈ cartridges (Harvard Apparatus, Holliston, MA) were used for purification of permethylated N-glycans prior to LC-MS/MS analyses. A 400- μ L aliquot of 80% aqueous ACN solution were applied to C₁₈ columns and centrifuged. This was repeated twice. The cartridges were then washed with 400 μ L of 100% ACN. Next, the cartridges were washed with 5% aqueous ACN solution. Permethylated samples were suspended in 690- μ L aliquots of 5% aqueous ACN solution prior to loading to the cartridges. The columns were then washed three times with 400- μ L aliquots of 5% aqueous ACN solutions. The cartridges were placed in clean eppendorf tubes prior to elution with 200- μ L aliquot of 80% aqueous ACN solution. This step was repeated twice and the eluants were then collected in one vial and dried under vacuum. The dried

samples were resuspended in 20% aqueous ACN solution containing 0.1% formic acid prior to MS analyses.

4.2.8 LC-MS and LC-MSMS

A Dionex 3000 Ultimate nano-LC system (Dionex, Sunnyvale, CA) was used for LC-MS analysis. The LC separation was attained under gradient conditions from 38%-45% solvent B over 32 min at flow rate of 350 nL/min. Solvent A consisted of 2% acetonitrile and 98% water with 0.1% formic acid, while solvent B consisted of acetonitrile and 0.1% formic acid. Acclaim® PepMap capillary column (150 mm x 75 μ m i.d) packed with 100 \AA C₁₈ bounded phase (Dionex) was used for sample separation. Velos LTQ Orbitrap hybrid mass spectrometer (Thermo Scientific, San Jose, CA) was used for detection. The mass spectrometer was operated in an automated data-dependent acquisition mode in which the scan mode switched between MS full scan (*m/z* from 500-2000) and CID MS/MS scan which was conducted on the 8 most abundant ions with a 0.250 Q-value, 20 ms activation time, and 35% normalized collision energy.

4.2.9 Data Evaluation

Xcarlibur Qual Browser (Thermo Fisher Scientific) was used for LC/ESI-MS data processing. Retention times of glycans were read from extracted ion chromatograms, which were generated using the isotopic masses of glycans with 10 ppm mass tolerance. A seven-point boxcar smoothing was enabled to improve peak quality. Peak height was used to represent the abundance of a glycan structure.

4.3 Results and Discussion

The nonpolar surface area (NPSA) is the surface sum over all nonpolar atoms, primary carbon and hydrogen. Nonpolar driving forces of proteins were well studied for fundamental insights of protein folding and protein binding reactions.^{158,159} Due to the hydrophilic property of native glycans, the nonpolar surface area is not well investigated. Hydrophobic tagging of glycans, including hydrazone formation, permethylation and peracetylation, has shown enhanced mass spectrometric ionization and detection.^{64,85} Permethylation serves to render hydrophobicity to glycans, thus allowing separation on the C₁₈ column. In this study, we correlated NPSA value to experimental retention time to better understand the chromatographic behavior of permethylated N-glycan. NPSA values of glycans were calculated to determine the optimal condition of chromatography and applied to estimate the retention time of unknown glycans as well as identify structural isomers. Dextran is a branched glucan composed of chains of varying lengths while dextrin is a linear low-molecular-weight carbohydrate. Here, we use dextran and dextrin as model glucan to study the relationship between molecular weight and retention time as well as glucose unit with retention time. To further study how the branching of N-glycans influence the retention time, we mixed the reduced permethylated fetuin and desialylated fetuin and evaluated the chromatographic behavior of the different glycans present in such a mixture. **Figure 4.1** illustrates the relationship between retention time and glucose unit as well as the relationship between estimated NPSA and glucose unit for dextrin and N-glycans derived from fetuin. The estimated NPSA of a glycan is calculated using the assumption that the additional intermolecular forces that arise with glycan branching cause the loss of availability of functional groups that would otherwise be

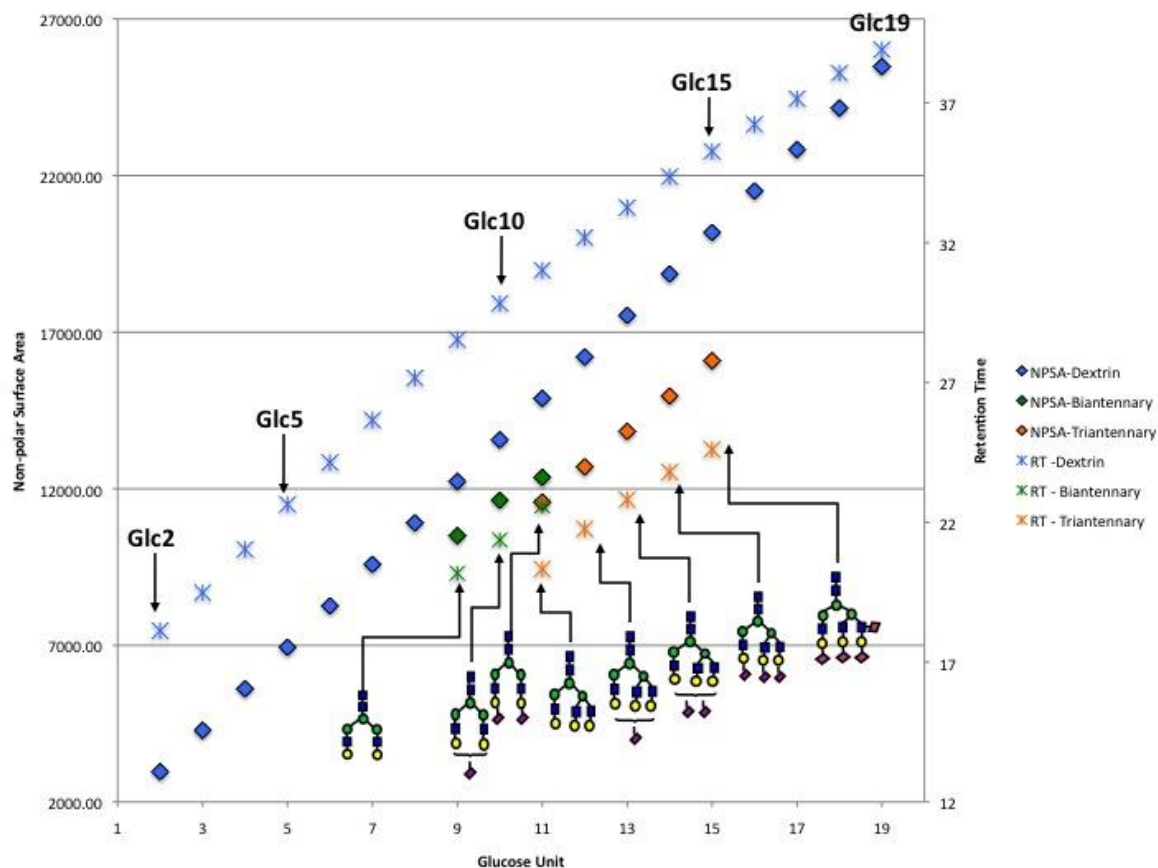


Figure 4.1 Comparison of retention time vs. glucose unit and NPSA vs. glucose unit of dextrin and N-glycans derived from fetuin. Symbols: as in **Figure 2.1**

available to interact with the C₁₈ column.⁶⁴ With the increase of glucose unit, the retention time as well as NPSA was increased. And the trends of retention time and NPSA were similar; both of them show linear increasing. Moreover, retention time and NPSA value also related to the branch of glycans. With the increase of branch, the retention time and NPSA value decreased. **Table 4.1** summarizes the intensity and retention time of dextran, dextrin, and the mixed fetuin. When retention time *vs.* molecular weight (**Figure 4.2a**) or the retention time *vs.* glucose unit (**Figure 4.2b**) was plotted, a linear like relationship can be observed. As shown in **Figure 4.2** and **Table 4.1**, the retention times of linear glucans are lower than those of branched glucans for the same molecular weights. This might be due to the chain conformation of dextrin and dextran, both of which can be regarded as helical in various states of extension. Thus, for linear carbohydrates such as dextrin, the methyl groups inside the helix are not available for hydrophobic interaction with C₁₈ column. However, the hydrophobicity of dextran increased with the increase in the number of branch glucose units outside and inside the helix. For fetuin, the retention times of triantennary glycans are lower than those of biantennary glycans for the same glucose unit or molecular weight. The interaction between branched glucose units resulted in the decrease of the glycan hydrophobicity. Moreover, the retention times of fetuin glycans appear to be substantially lower than their dextrin or dextran counterpart, even when the molecular weight is the same. The methyl groups associated with the permethylated fetuin N-glycans are not completely available for interacting with chromatographic media, which caused lower retention on the C₁₈ column, whereas the methyl groups on the linear and partially linear structures appeared to be more available for interaction.

Table 4.1 Intensity and retention time of dextran, dextrin and N-glycans derived from fetuin

Dextran			Dextrin		Fetuin	
GU	Intensity	Retention time	Intensity	Retention time	Intensity	Retention time ^a
2	(8.39±0.4)e5	18.38±0.03	(3.98±0.5)e6	18.13±0.01		
3	(5.55±0.8)e7	20.27±0.05	(5.98±1)e7	19.48±0.08	(2.72±0.4)e7 (8.58±1)e7	20.18±0.07(9) ^a 20.33±0.04(11) ^a
4	(1.05±0.2)e8	22.52±0.02	(4.65±0.4)e7	21.04±0.06	(5.20±0.5)e6 (9.05±2)e6 (8.94±1)e5 (7.00±1)e6	21.37±0.2(10) ^a 21.77±0.03(12) ^a 22.60±0.1(11) ^a 22.82±0.2(13) ^a
5	(1.09±0.1)e8	24.72±0.08	(3.46±0.8)e7	22.64±0.05	(1.67±0.08)e4 (1.70±0.3)e6	23.81±0.06(14) ^a 24.61±0.04(15) ^a
6	(3.90±2)e7	26.91±0.10	(2.44±0.3)e6	24.14±0.06		
7	(1.76±0.5)e7	28.96±0.05	(1.43±0.1)e6	25.66±0.09		
8	(1.41±0.4)e7	30.83±0.07	(3.51±0.5)e6	27.17±0.05		
9	(1.73±0.07)e7	32.66±0.03	(7.49±0.9)e6	28.53±0.06		
10	(1.33±0.09)e7	34.30±0.08	(3.69±0.1)e6	29.83±0.05		
11	(1.05±0.3)e7	35.83±0.08	(4.36±0.9)e6	31.02±0.1		
12	(5.46±0.4)e6	37.32±0.1	(3.26±0.4)e6	32.19±0.03		
13	(2.64±0.2)e6	38.75±0.1	(2.14±0.5)e6	33.26±0.07		
14	(1.31±0.3)e6	40.08±0.05	(8.73±0.9)e5	34.36±0.08		
15	(7.01±0.8)e5	41.29±0.05	(5.36±1)e5	35.27±0.02		
16	(2.58±0.2)e5	42.44±0.2	(2.60±0.3)e5	36.23±0.08		
17	(1.16±0.2)e5	43.67±0.2	(1.27±0.2)e5	37.15±0.05		
18	(3.87±0.3)e4	44.65±0.08	(6.83±1)e4	38.06±0.04		
19	(1.77±0.3)e4	45.89±0.1	(3.10±0.1)e4	38.90±0.05		

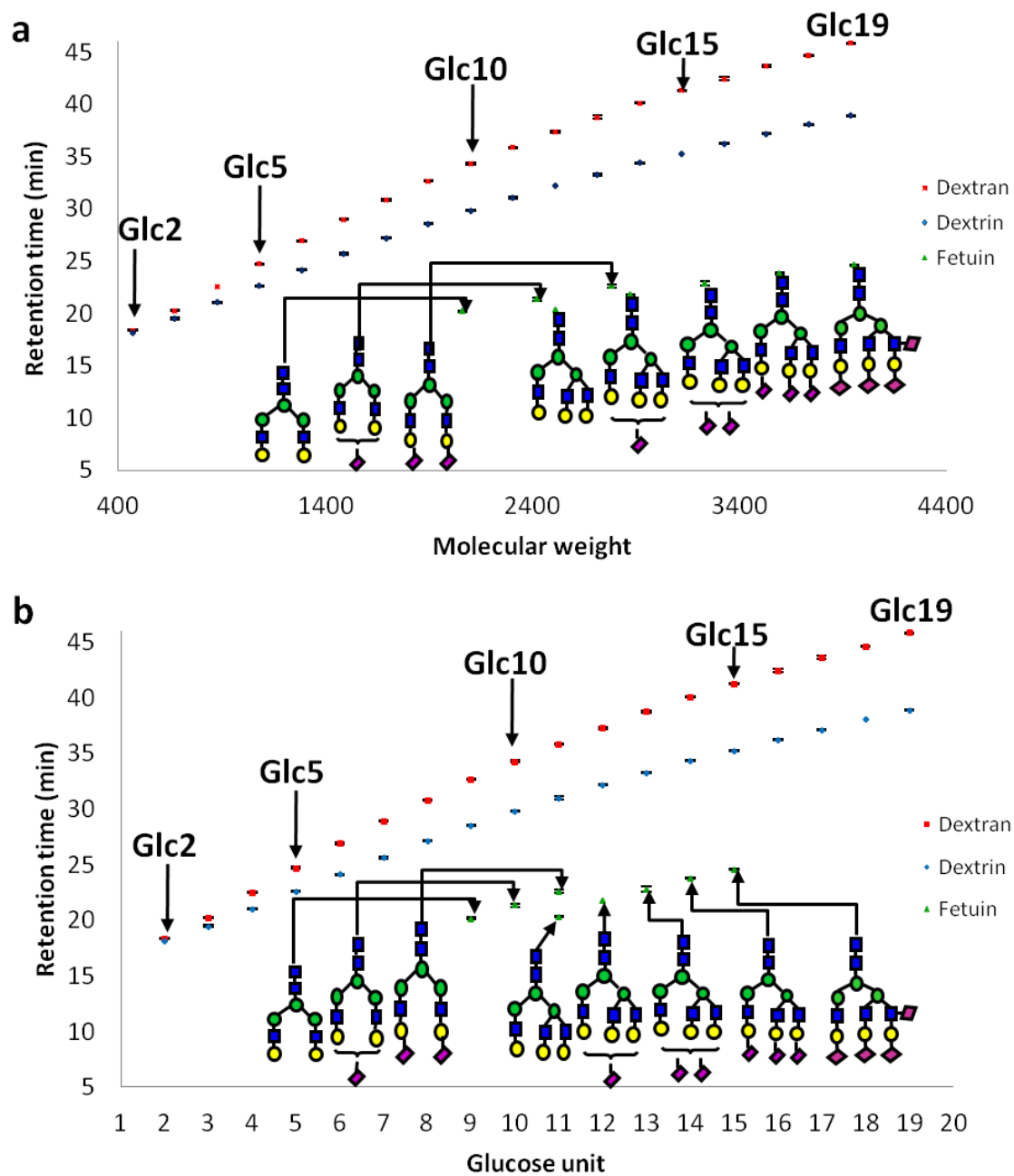


Figure 4.2 Retention time of dextran, dextrin and N-glycans extracted from Fetauin vs molecular weight (a); and glucose unit (b). The standard deviations are very small as depicted by the error bars of each structure ($N=3$). Symbols: as in **Figure 2.1**

N-glycans derived from RNase B were further used as N-glycan models to demonstrate the possibility of using retention time as a structural indicator. **Figure 4.3** compared the retention time and glucose unit as well as the relationship between estimated NPSA and glucose unit for dextrin and high mannose glycans. The retention time as well as NPSA increased with the increase of glucose unit. **Figure 4.4** depicts the extracted ion chromatograms of RNase B. Five unique compositions of RNase B (Man5, Man6, Man7, Man8, Man9) were observed and their intensities varied from Man5 to Man9. The retention time and the molecular weight have a great linear relationship, as evidenced by an R^2 value of 0.998. The similar trend was discussed in the previous publication with R^2 value of 0.993.¹⁹

We applied the N-glycans analysis model, which is based on the use of high mass accuracy and retention time to confirm serum N-glycans. First, MS full scan was analyzed and all possible N-glycans were extracted based on accurate mass (**Figure 4.5**). The total compositions determined by mass accuracy (less than 2 ppm) were 70 (**Table 4.2**). We compared our results to those previously published by several groups,^{117,121,160-162} more compositions especially unique compositions are confirmed by our work (**Table 4.3**). N-glycan structures in this study were also confirmed through MS/MS. Among the total detected glycans, 52 had sufficient MS/MS data for structural confirmation. Thus, identifying other compositions based on retention time and accurate mass is of great importance. Based on the results obtained from dextrin, dextran and N-glycans extracted from model glycoproteins, molecular weight, glycan structure and branching plays an important role in the retention time. Total N-glycans confirmed in serum were then divided into several groups based on glycan types and antennary. The relationship

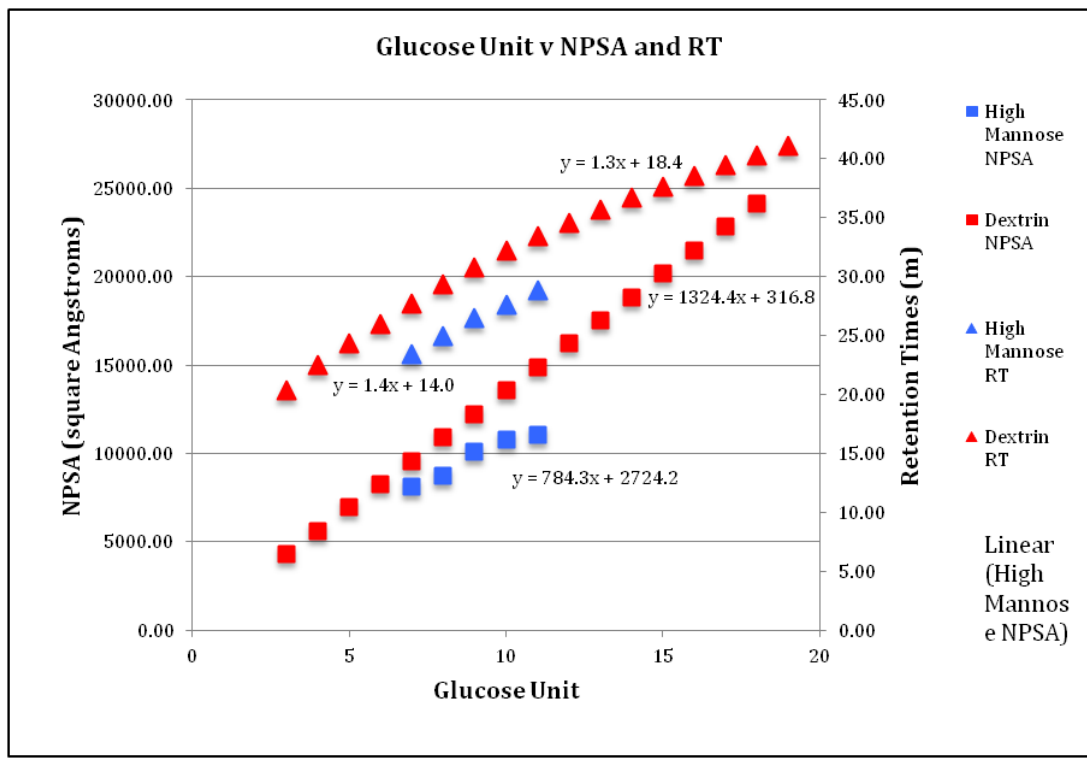


Figure 4.3 Comparison of retention time vs glucose unit and NPSA vs glucose unit of dextrin and high mannose structures derived from RNase B.

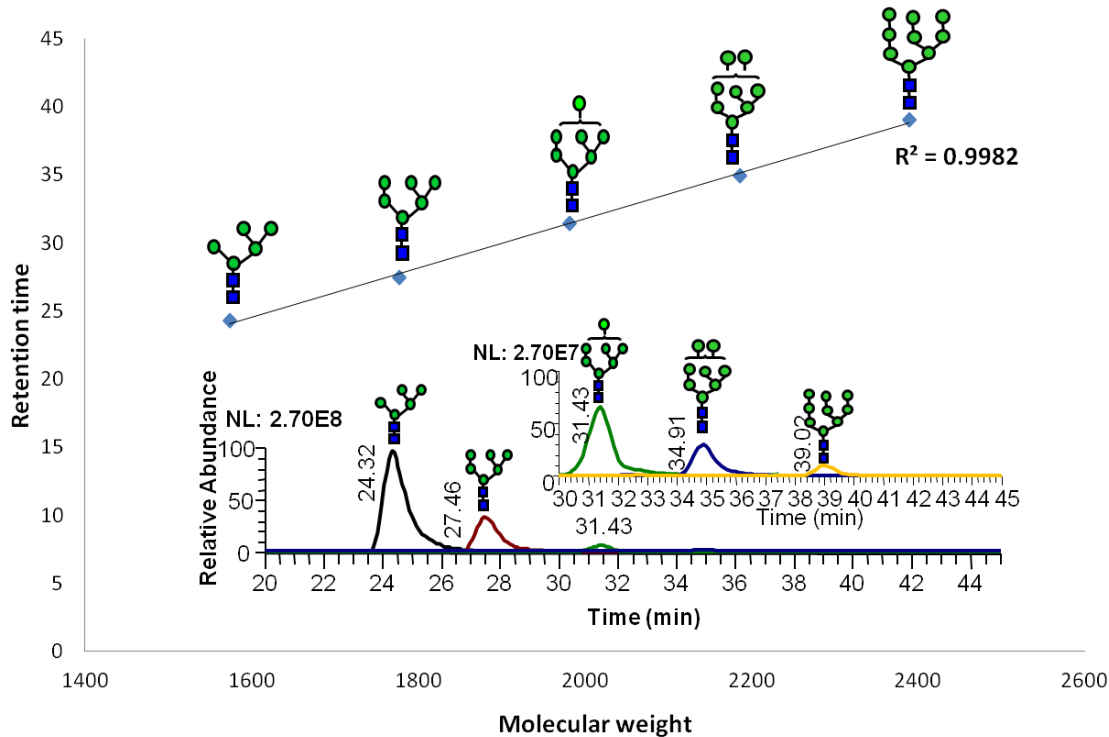
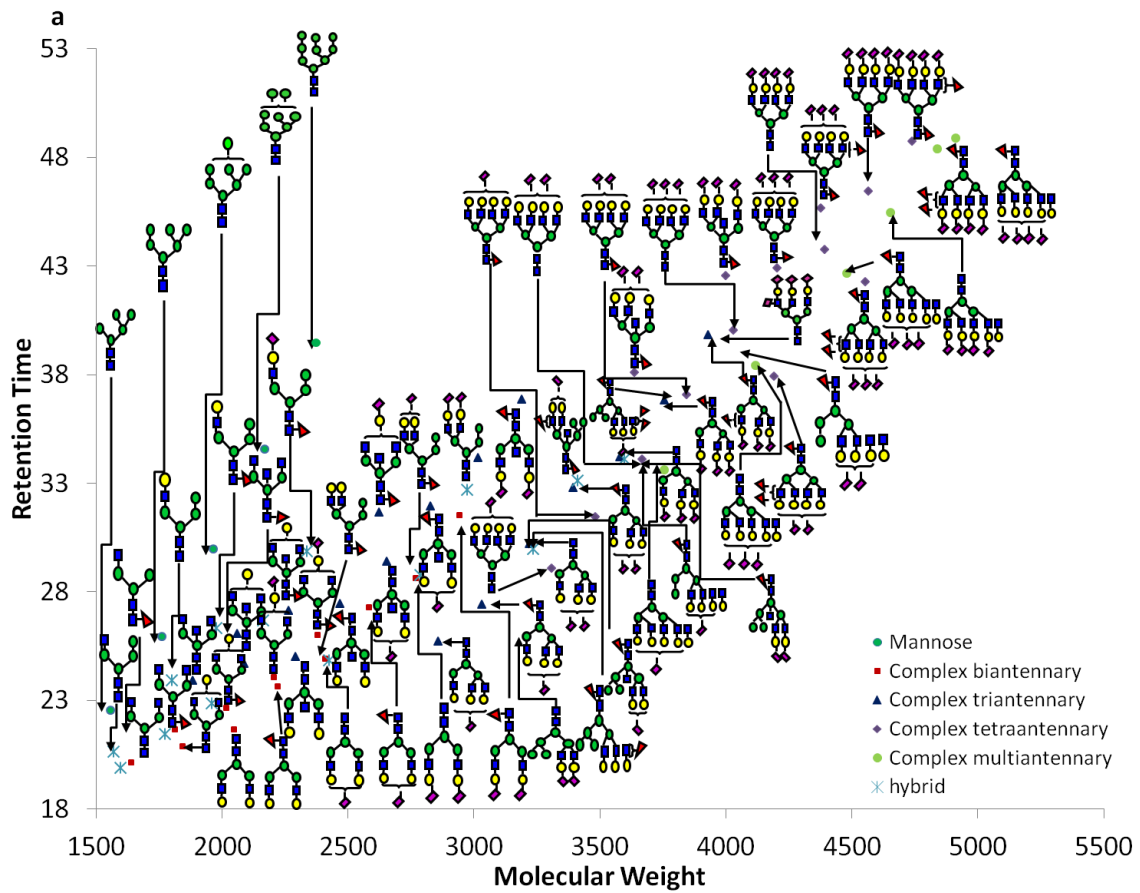


Figure 4.4 Retention time of N-glycans extracted from RNase B vs molecular weight. The inset depicts extract ion chromatograms of reduced and permethylated N-glycans derived from RNase B. Symbols: as in **Figure 2.1**



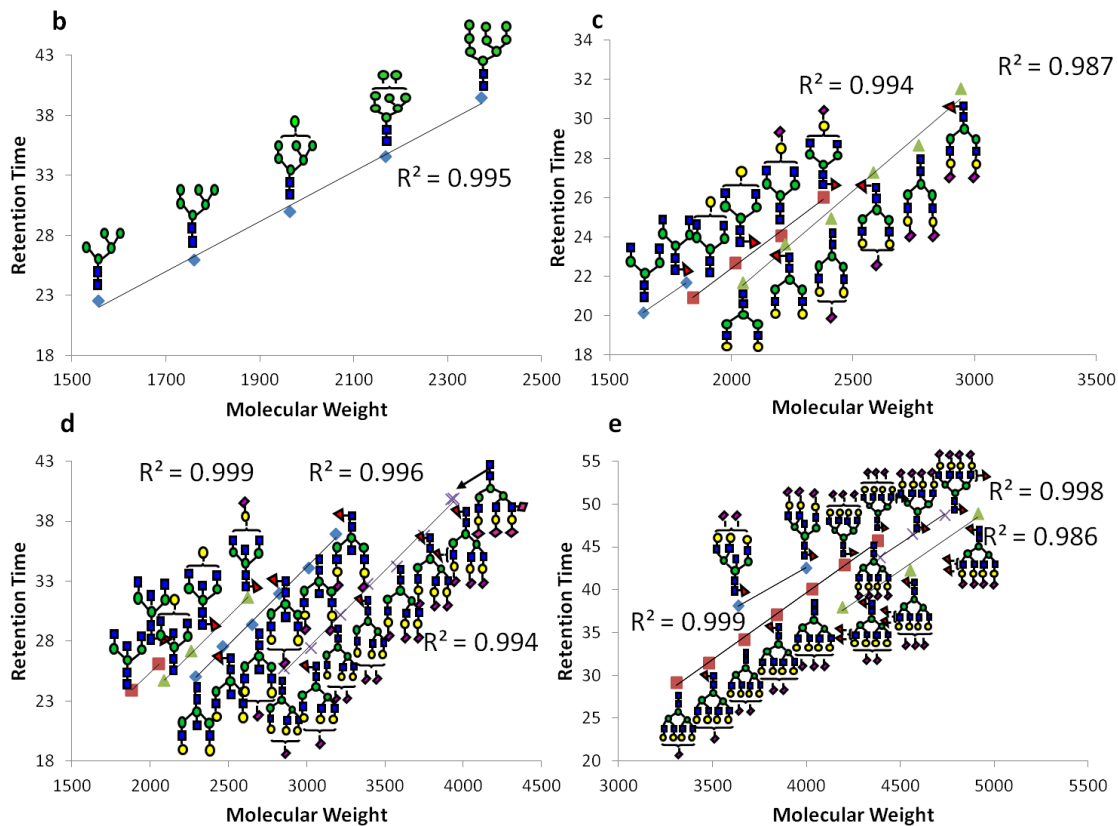


Figure 4.5 Glycomics mapping of N-glycans derived from HBS (a). Linear fitting of the retention times of (b) high mannose; (c) complex-type biantennary; (d) complex-type triantennary; and (e) complex-type tetraantennary. Symbols: as in **Figure 2.1**

Table 4.2 Total N-glycans extracted from blood serum and linear equation of each subtype

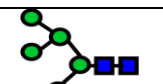
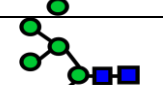
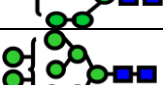
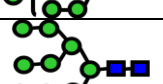
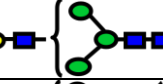
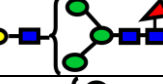
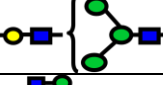
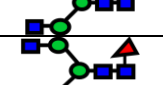
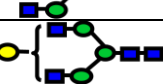
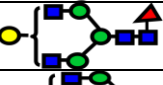
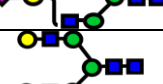
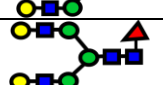
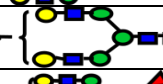
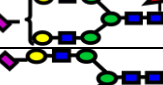
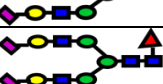
Subtype	Structure	Structure confirmation	Retention time	Linear equation (R^2)
Mannose		<2 ppm (MSMS)	22.547±0.006	$y = 0.0208x - 10.365$ (0.995)
		<2 ppm (MSMS)	25.950±0.05	
		<2 ppm (MSMS)	29.967±0.1	
		<2 ppm (MSMS)	34.560±0.1	
		<2 ppm	39.463±0.2	
Complex (monoantennary)		<2 ppm	19.897±0.006	$y = 0.0082x + 6.8389$ (0.998)
		<2 ppm	21.440±0.090	
		<2 ppm	22.860±0.1	
Complex (biantennary)		<2 ppm (MSMS)	20.143±0.006	$y = 0.0088x + 5.8029$ (1)
		<2 ppm (MSMS)	21.667±0.06	
		<2 ppm (MSMS)	20.893±0.06	
		<2 ppm (MSMS)	22.673±0.1	
		<2 ppm (MSMS)	24.057±0.06	
		<2 ppm	26.013±0.1	
		<2 ppm (MSMS)	21.667±0.06	$y = 0.0106x - 0.1504$ (0.987)
		<2 ppm (MSMS)	23.633±0.06	
		<2 ppm (MSMS)	24.923±0.1	
		<2 ppm (MSMS)	27.277±0.09	
		<2 ppm (MSMS)	28.647±0.2	
		<2 ppm (MSMS)	31.550±0.2	

Table 4.2.Continued

Subtype	Structure	Structure confirmation	Retention time	Linear equation (R^2)
Complex (triantennary)		<2 ppm (MSMS)	23.917±0.090	$y=0.0125x+0.2889$ (1)
		<2 ppm (MSMS)	26.100±0.05	
		<2 ppm (MSMS)	24.693±0.09	
		<2 ppm (MSMS)	27.163±0.06	
		<2 ppm (MSMS)	31.663±0.1	
		<2 ppm (MSMS)	25.033±0.09	$y=0.0130x-4.7245$ (0.996)
		<2 ppm (MSMS)	27.480±0.1	
		<2 ppm (MSMS)	29.420±0.08	
		<2 ppm (MSMS)	31.953±0.1	
		<2 ppm	34.183±0.08	
		<2 ppm (MSMS)	36.880±0.2	
		<2 ppm (MSMS)	25.750±0.05	$y=0.0131x-12.063$ (0.994)
		<2 ppm (MSMS)	27.420±0.2	
		<2 ppm (MSMS)	30.223±0.2	
		<2 ppm (MSMS)	32.797±0.08	
		<2 ppm (MSMS)	34.213±0.2	
		<2 ppm (MSMS)	36.820±0.2	
		<2 ppm (MSMS)	39.857±0.2	
		<2 ppm	39.89±0.4	

Table 4.2.Continued

Subtype	Structure	Structure confirmation	Retention time	Linear equation (R^2)
Complex (Tetraantennary)		<2 ppm (MSMS)	38.127±0.3	$y=0.0123x-6.527$ (0.996)
		<2 ppm (MSMS)	42.560±0.2	
		<2 ppm (MSMS)	29.109±0.2	
		<2 ppm (MSMS)	31.463±0.1	
		<2 ppm (MSMS)	34.127±0.2	
		<2 ppm (MSMS)	37.083±0.09	
		<2 ppm (MSMS)	40.070±0.1	
		<2 ppm (MSMS)	42.930±0.3	
		<2 ppm	45.673±0.2	
Complex (Tetraantennary, multi-sialylated)		<2 ppm (MSMS)	43.783±0.2	$y=0.0143x-18.731$ (0.998)
		<2 ppm (MSMS)	46.470±0.2	
		<2 ppm	48.747±0.04	
Complex (Tetraantennary, multi-fucosylated)		<2 ppm	37.917±0.3	$y=0.0152x-26.189$ (0.986)
		<2 ppm	42.283±0.3	
		<2 ppm	48.903±0.06	

Table 4.2.Continued

Subtype	Structure	Structure confirmation	Retention time	Linear equation (R^2)
Complex (Multiantennary)		<2 ppm	33.613±0.2	$y=0.0125x-13.194$ (0.987)
		<2 ppm	38.415±0.08	
		<2 ppm	42.680±0.2	
		<2 ppm	45.460±0.3	
		<2 ppm	48.383±0.03	
		<2 ppm	48.527±0.1	
		<2 ppm	48.553±0.07	
Hybrid (Biantennary)		<2 ppm	20.637±0.05	$y=0.0119x+2.2485$ (0.990)
		<2 ppm	23.917±0.006	
		<2 ppm	26.330±0.1	
		<2 ppm	29.840±0.05	
		<2 ppm	24.863±0.01	$y=0.0138x-8.9812$ (0.968)
Hybrid (Triantennary)		<2 ppm	28.790±0.06	
		<2 ppm	32.707±0.2	
		<2 ppm	24.890±0.02	

Table 4.2.Continued

Subtype	Structure	Structure confirmation	Retention time	Linear equation (R^2)
Hybrid (Tetraantennary)		<2 ppm	26.560±0.8	

Table 4.3 Comparison of the total detected N-glycans of previous published work with this work

Technique	Total glycans detectd	Structures common with this study	Structures that were not observed in this study	Structures that were only observed in this study
NanoLC-FTICR ^a	42	37	5	33
nanoLC LTQ Orbitrap ^b	12	9	3	61
microfluidic chip and time-of-flight ^c	20	19	1	51
HILIC HPLC-FL, MALDI-TOF-MS and CE-ESI-MS ^d	47	43	4	27
Direct infusion nanoESI and ITMS ^e (no IgG depletion) ^e	50	31	19	39
Direct infusion nanoESI and ITMS ^f (IgG depletion) ^f	106	54	52	16

^a structures listed in ref.¹²¹^b structures listed in ref.¹¹⁷^c structures listed in ref¹⁶⁰^d structures listed in ref¹⁶¹^{e,f} structures listed in ref¹⁶²

between retention time and molecular weight was investigated (**Figure 4.5**). In the case of mannose type glycans derived from HBS, the linear fit of the retention time demonstrated an R^2 value of 0.996 (**Figure 4.5b**), which is comparable to that obtained for RNase B glycans. Although Man 9 derived from HBS has no MSMS for structure confirmation, we can determine the structure based on the retention time and mass accuracy. Complex N-glycans were classified into biantennary, triantennary tetraantennary and multiantennary subclasses. Also, for each subclass, they can be divided into several subgroups based on the Gal moieties. As the increase of Gal moieties, the intermolecular interaction increased, thus the interaction of methyl group with C₁₈ column decreased. From the equation, the slope remains the similar and the intercept decreased with the increase of the Gal moieties. This matches our assumption, intermolecular interaction contributes to the retention time. This phenomenon can be observed from biantennary, triantennary and tetraantennary complex type N-glycans. Generally, the retention time increases as molecular weight increases, and there is a good linear relationship with each subclass. For example, the R^2 values of biantennary glycans with one and two Gal moieties are 0.987 and 0.994 (**Figure 4.5c**). The triantennary glycans with one, two and three Gal moieties have an R^2 value of 0.999, 0.998 and 0.994, respectively (**Figure 4.5d**). On the other hand, the influence of fucosylation to the retention time is subtle when the fucosylated sites are less than two. However, the multifocusylated glycans have lower retention time compared to their own antennary group (**Figure 4.5e**). This can be explained with the stereo-hindrance effect, less methyl groups were available for interaction with C₁₈ column. When it comes to sialic acid N-glycans, the similar phenomenon were observed. When the sialic acid unites increased to

four, the retention times of them were decreased (**Figure 4.5e**). The hybrid type N-glycans can be also divided into groups based on the antennary, too. Biantennary hybrid glycans has the R^2 of 0.990, when the compositions with multiantennary show a linear relationship with R^2 of 0.953. The relatively low R^2 partially due to the detected number is low for each subtype to study the relationship of molecular weight and retention time (**Table 4.2**). Also, in one subgroup, there are different branches. For example, both H6N3 and H6N4F1 could be triantennary hybrid glycans. H6N3 has two mannose branch when H6N4F1 has two complex branch, thus, they are not fit in a same line.

According to the above discussion, retention time can be used to predict N-glycans structure. For example, at the composition of H6N5S1 and H6N5S2, there are two peaks with equal masses extracted from chromatography. The H6N5S1 of chromatography peak at 25.93 min fit the line of triantennary subgroup, which indicates the structure type (**Figure 4.6**). And for peak of retention time at 27.5 min, the elution position fell consistent with other hybrid glycans. Similar to H6N5S1, H6N5S2 has two peaks from extracted chromatogram. The one with lower retention time fit the line of triantennary subgroup. MSMS data was interpreted for structural elucidation (**Figure 4.7**). The intensity of MSMS peaks varies from each other, there are few diagnostic peak for us to confirm the structure. This difference in conformation can be elucidated based on it's expected relationship between estimated NPSA and retention time, whose standard is developed from the glucan models. The N-glycans with the composition of H6N5F1S1 and H6N5F1S2 have three total peaks each. This is attributes to multiple positional attachment and linkage attachment. However, the specific structures cannot be discerned

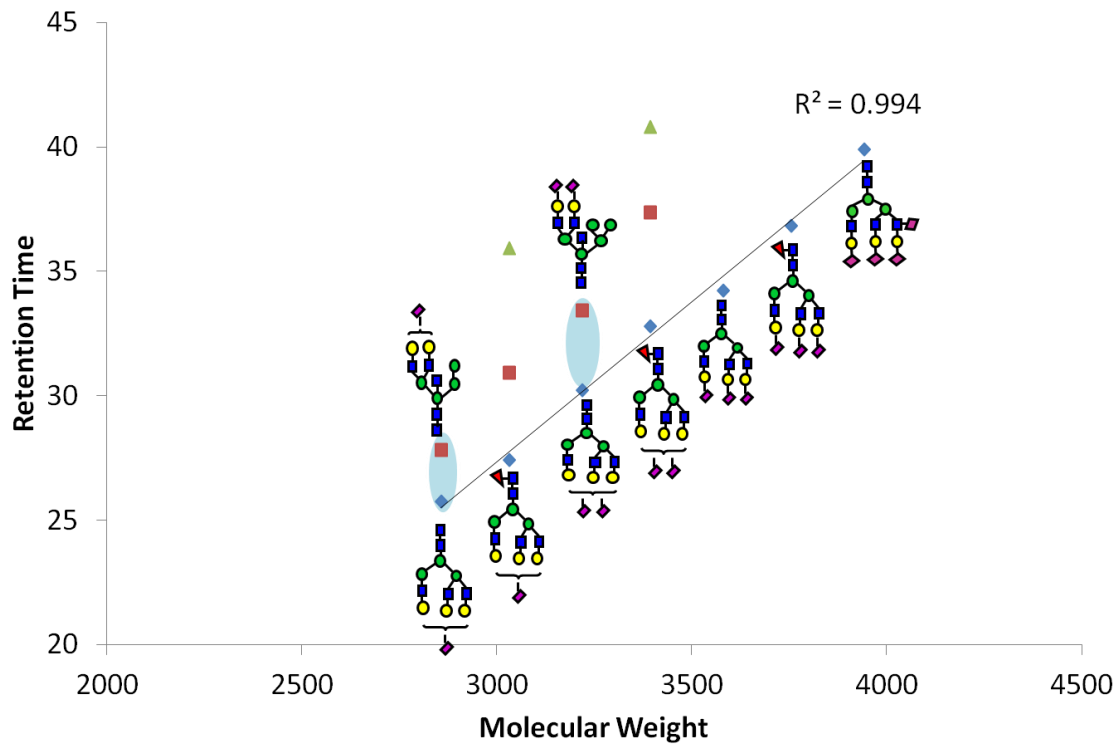


Figure 4.6 Linear plot of different glycan structures with each of the m/z values detected at two different retention times suggesting structural differences. Symbols: as in **Figure 2.1**

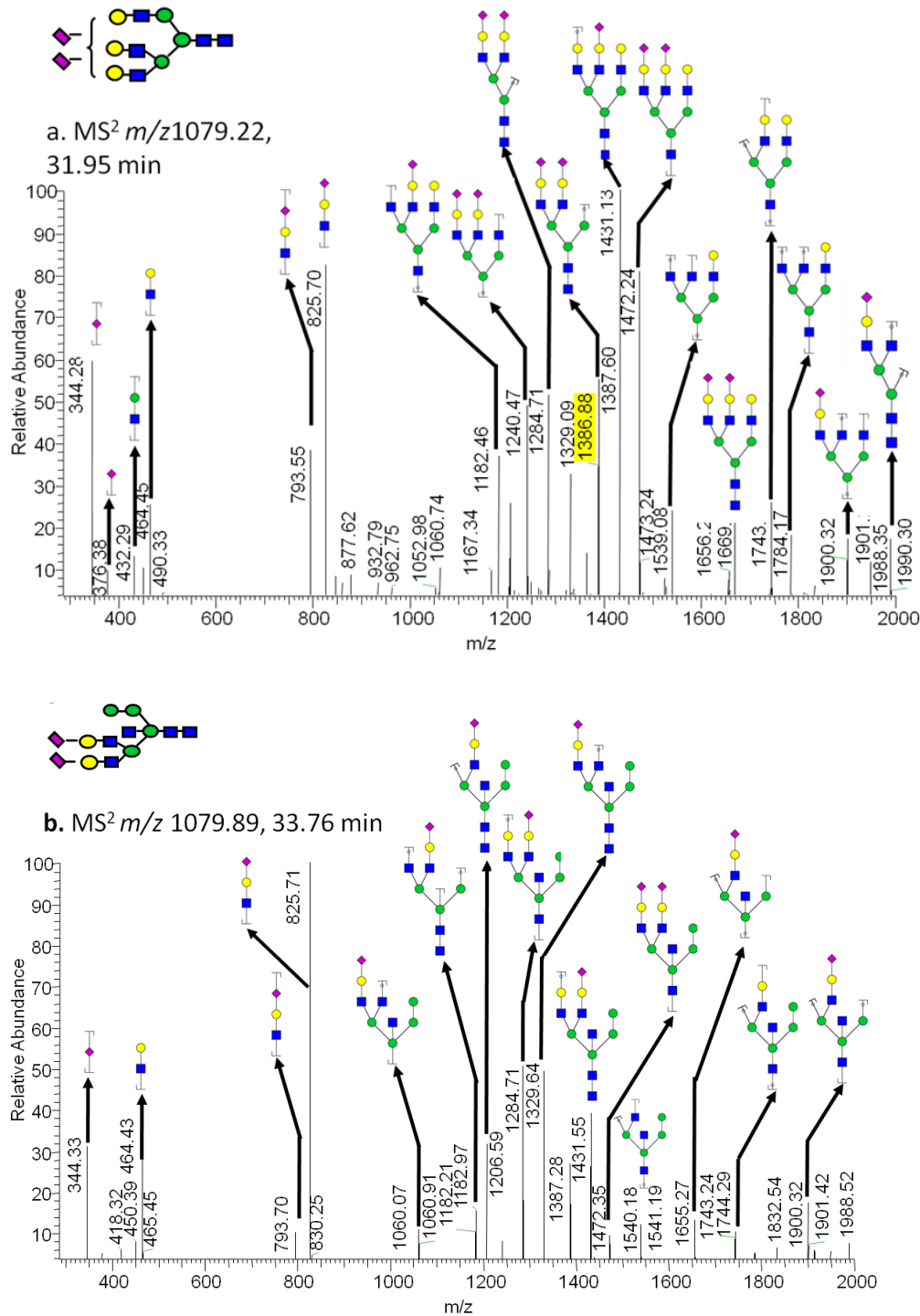


Figure 4.7 Tandem mass spectra of the ion observed at m/z value of 1079.225 at retention times of (a) 31.95 min, and (b) 33.76 min. Symbols: as in **Figure 2.1**

from tandem MSMS due to the lack of high collision energy to prompt cross ring fragments.

4.4 Conclusions

In this study, a new method was developed for confirming the compositions of reduced permethylated N-glycans based on retention time and molecular weight. Previous studies were mostly based on MS/MS, but as a result of the variability of glycan structure, MS/MS data must be explicated manually, increasing the complexity of glycomic studies. In this new developed method, no MS/MS data interpretation is required for structure identification, and all structural identification is based on mass, retention time, and estimated NPSA. Dextrin, dextran and model glycans extracted from RNase B and Fetuin were used to investigate chromatographic behavior. Next, the glycans from HBS, a complex biological sample, were enzymatically released, reduced, permethylated, and purified by LC-MS. In total, 78 compositions were identified with mass accuracy less than 2 ppm. Most of the identified N-glycans from HBS fits the linear line of their own group. Also, when compared to estimated NPSAs, retention time can be used to predict N-glycan compositions, which can be used to differentiate between groups of structures with identical molecular weights. As these LC-MS procedures are further applied to glycomics studies, biomarker discovery will become largely simplified.

CHAPTER V

GLYCOMIC PROFILING OF TISSUE SECTIONS BY LC-MS

Y. Hu, S. Zhou, S. Khalil, K. Renteria, Y. Mechref, *Analytical Chemistry*, **2013**, 85, 4074–4079

5.1 Introduction

Glycosylation is one of the most common posttranslational modifications of proteins and is widely involved in many biological processes.^{141,163} Aberrant glycosylation occurs in many human diseases, including cancer,^{13,164} autoimmune disease¹⁶⁵ and inflammation.¹⁶⁶ Thus, glycans are potentially useful as biomarkers for disease diagnosis and prognosis. Development of reliable quantitative methods is essential for biomarker discovery.

Various glycan analysis methods have been developed on cell lines,^{18,27,32,35,46} blood serum^{19–21,29,33,78,110,151,167} and large tissue samples.¹⁶⁸ Label free quantification strategies and isotopic labeling strategies are the most widely used quantitative methods. Many current preparation methods require relatively large fresh or frozen samples. Bulk tissue samples yield no detailed molecular spatial information and require special care to maintain proper storage and shipping conditions. Glycan analysis on tissue sections offers several advantages over bulk material, including smaller sample size, easier storage and shipping conditions, and it provides histological scale information on pathology. Moreover, when several adjacent tissue sections are used, it is possible to correlate N-glycan characterization and immunofluorescence imaging.

Although there are obvious advantages of N-glycan profiling of tissue sections, approaches for extracting N-glycans from tissue histological slices await development.

Current sample preparation methods first release glycans from glycoproteins in solution with PNGase F. To remove proteins and salts that might interfere with derivatization and detection, porous graphitized carbon,^{151,169-171} Nafion® membrane,¹⁷² cellulose membrane⁷⁶ were utilized. Various derivatization methods, such as hydrazone formation,^{64,85} permethylation^{48,66,67} and peracetylation^{173,174} are commonly applied for enhanced mass spectrometric (MS) ionization and detection. A clean up step, such as liquid-liquid extraction or solid-phase extraction, is then required to remove excess salts, which can interfere with MS analysis. Although these routine strategies have been shown to increase glycans recovery, they are labor-intensive and time-consuming. They are additionally not suitable for glycomic profiling of tissue sections since they might prompt sample loss and subsequently reduce sensitivity. Glycan analysis on-tissue sections can eliminate sample preparation steps, thus permitting efficient sample preparation method with a minimal number of steps.

Here, we describe a protocol that enables glycomic profiling of the surface of a section of tissue. This protocol optimizes glycan sample preparation steps to minimize sample loss and analytical variability. On-plate digestion has previously been reported to yield analytically sufficient quantities of glycans for profiling.^{132,175} Enzymatic cleavage of N-linked glycans from glycoproteins is performed on the glass or tissue surface, which is more efficient than digestion in solution. The crude digestion mixtures are then reduced and permethylated without prior purification. Lastly, permethylated N-glycans are on-line purified as we have previously described, thus allowing efficient and sensitive analysis of low abundance materials.¹³¹

5.2 Experiment

5.2.1 Material

Model glycoproteins (including ribonuclease B (RNase B), porcine thyroglobulin (PTG), Fetuin) and pooled human blood serum (HBS) were purchased from Sigma-Aldrich (St. Louis, MO). Other chemicals such as ammonia borane complex, sodium hydroxide beads, dimethyl sulfoxide (DMSO), iodomethane, trifluoroacetic acid, chloroform, and MS-grade formic acid were also obtained from Sigma-Aldrich. Microspin columns were purchased from Harvard Apparatus (Holliston, MA). Endoglycosidase purified from *Flavobacterium meningosepticum* (PNGase F, 500,000 units/mL) was obtained from New England Biolabs Inc. (Ipswich, MA). Acetic acid was procured from Fisher Scientific (Pittsburgh, PA) while acetonitrile (ACN) was obtained from Fisher Scientific (Fair Lawn, NJ). HPLC-grade water was acquired from Mallinckrodt Chemicals (Phillipsburg, NJ).

5.2.2 On Surface Enzymatic Digestion of Model Glycoproteins and Human Blood Serum

Several 0.5- μ L aliquots of model glycoprotein mixtures were deposited on a glass surface while 0.5 μ L of HBS was deposited on a Teflon surface. Then, a 0.5- μ L aliquot of PNGase F was added to each spot. Enzymatic digestion was performed either at room temperature or in a 37°C water bath. For these analyses, the glass slides were covered to decrease liquid evaporation. A 0.5- μ L aliquot of water was added to each spot every 20 minutes to keep it wet. The digestion was allowed to proceed for 4 hours on the model glycoproteins and 8 hours on the HBS.

5.2.3 On-Tissue Enzymatic Digestion of Mouse Brain Section

A 0.5- μ L aliquot of PNGase F (50 units) was deposited on the surface of each mouse brain section, spreading to form a spot *ca.* 1.5 mm in diameter. The enzymatic digestion was conducted in a 37 °C water bath for 4 hours. Water was added to each spot every 20 minutes.

5.2.4 Reduction of N-glycan

Released N-glycans were initially collected from the surfaces, and the spots washed with 1 μ L of water five times. The collected liquids were added to the same vial and dried under vacuum. Next, a 10- μ l aliquot of an aqueous ammonia borane complex solution (1 μ g/ μ L) was added to each sample vial and incubated at 65°C for one hour. The incubated mixtures were then dried under vacuum. Methanol was then added into the sample and dried under vacuum. This process was repeated several times to ensure efficient removal of borate salts.

5.2.5 Permetylation of N-glycan

Permetylation was performed according to the previously reported procedure.^{48,66,67} Briefly, an empty column was filled with sodium hydroxide beads. DMSO was added to the column to wash the sodium hydroxide beads. Then, dried sample was resuspended into a solution of 7.5 μ L DMSO, 0.3 μ L water and 20 μ L iodomethane. The sample solution was then applied to the sodium hydroxide column and incubated at room temperature for 30 minutes. Another 20- μ L aliquot of iodomethane was then added to the column and allowed to incubate for another 20 minutes. Next, the sodium hydroxide column was first centrifuged and then washed with a 100- μ L aliquot of

ACN to elute all permethylated glycans. The collected solution was then dried under vacuum.

5.2.6 LC-MS/MS Analysis

Permethylated N-glycans were purified and separated using an ultimate 3000 nano-LC system (Dionex, Sunnyvale, CA) which consisted of a loading pump and a separation pump, autosampler, and a switching valve. Sample injection was performed in the microliter pick-up mode. Permethylated samples without additional purification were resuspended in a 20% ACN solution containing 0.1% formic acid and loaded onto an Acclaim[®] PepMap100 C₁₈ nano-trap column (Dionex, Sunnyvale, CA) for on-line purification. Mobile-phase A, which consisted of 98% acetonitrile, 2% water, and 0.1% formic acid, was used to wash the nano-trap for 10 minutes at a flow rate of 3 µL/min. After sample loading, the 10-port valve was switched to separate the samples on an Acclaim[®] PepMap100 RSLC column (75cm x 15cm, C₁₈, 2µm, 100Å, Dionex, Sunnyvale, CA). The separation was attained using a gradient program starting at 20% mobile-phase B, which consisted of 98% ACN, 2% water, and 0.1% FA. Next, mobile-phase B was then increased to 38% over 11 min followed by an increase to 45% over 32 min. The column was then washed with 90% mobile-phase B for 5 min prior to preconditioning with 20% mobile-phase B for 5 min. The Dionex nanoLC system was interfaced to an LTQ Orbitrap Velos hybrid mass spectrometer (Thermo Scientific, San Jose, CA). MS was acquired in positive-ion mode alternating between an MS scan (mass range m/z 400-2000) and a data-dependent MS/MS scan of the 8 most abundant ions. For the MS/MS scan, the normalized collision energy was set to 30 with a 0.250 Q-value, 15

ms activation time and an isolation width of 3 Da. The dynamic exclusion was set at a repeat count of 2 and exclusion duration of 60 s.

5.2.7 Data Evaluation

Xcarlibur Qual Browser (Thermo Fisher Scientific) was used to generate extracted-ion chromatograms from the full MS scans using glycan isotopic masses with mass tolerance of 10 ppm. A seven-point boxcar smoothing was enabled to improve the peak quality. Peak areas of different charge states and ion adducts were added for quantification evaluation. Tandem mass spectra corresponding to glycan ions were manually annotated and diagnostic fragment ions were utilized to confirm the glycan structures.

5.3 Results and Discussion

N-glycan profiling of model glycoproteins and mouse brain tissue sections was performed according to the abovementioned experimental procedure. The workflow was shown in **Figure 5.1**. Enzymatic digestion was performed on the glass or Teflon surface for glycoproteins and on tissue sections for mouse brain samples. To obtain efficient N-glycan releasing, on-surface enzymatic digestion parameters such as incubation time and enzyme concentration were optimized. A 100-ng aliquot of RNase B was utilized to evaluate the efficiency of N-glycan release at different incubation times. As shown in **Figure 5.2**, the intensities of permethylated N-glycans released from RNase B at 4 h incubation was comparable to that obtained at 8 h. This suggests that 4 h of enzymatic digestion is sufficient for releasing N-glycans from this relatively small glycoprotein. **Figure 5.3a** shows the comparison of intensities of N-glycans released from RNase B with PNGase F concentration of 5 U and 25 U. The intensity of low abundance N-glycan

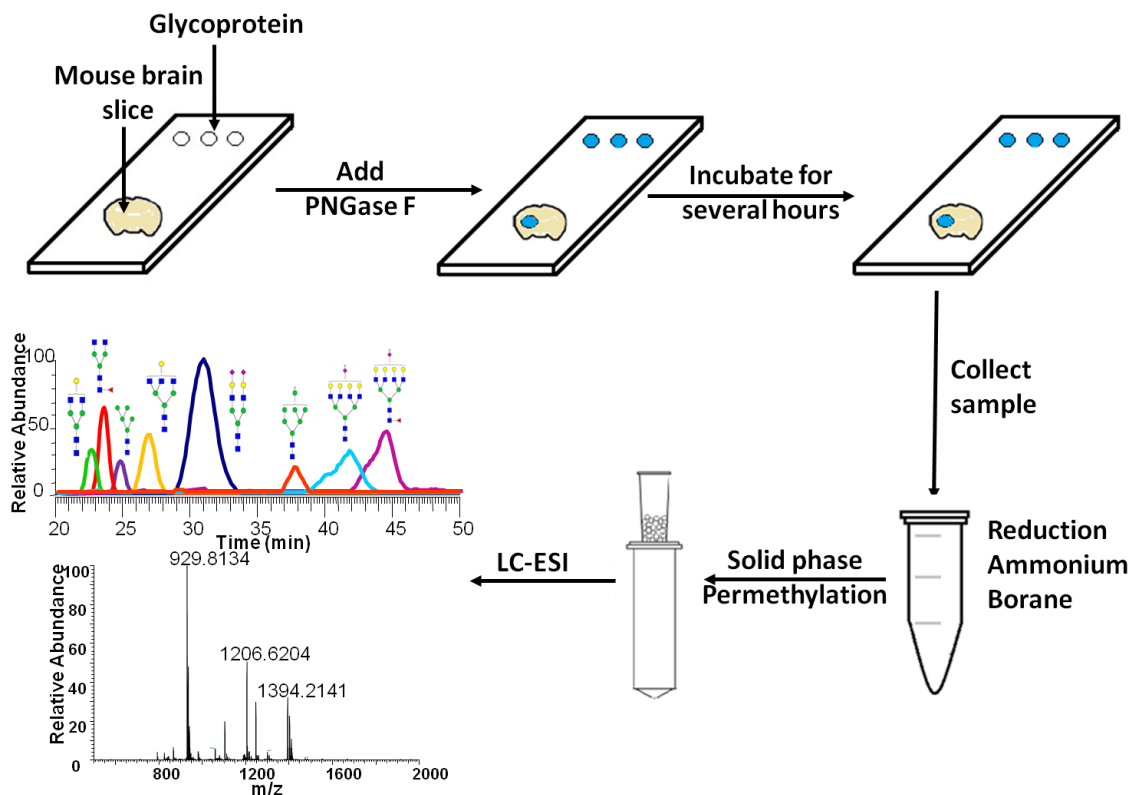


Figure 5.1 Workflow of N-glycan profiling of tissue sections and model glycoproteins.

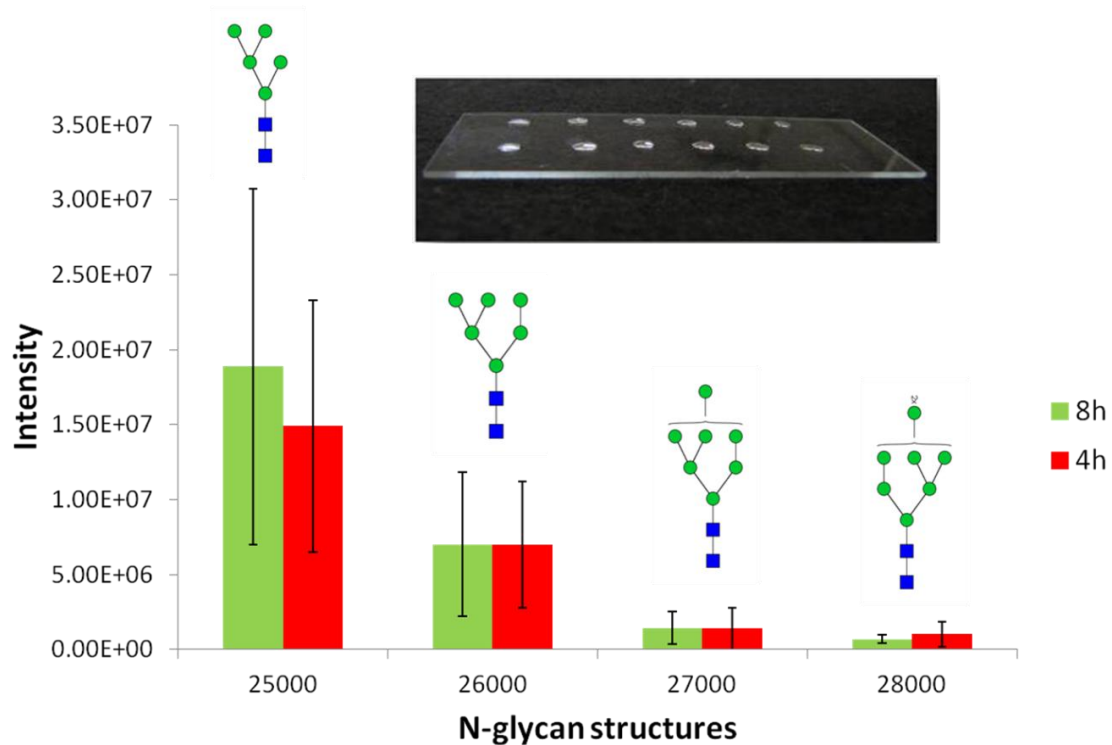


Figure 5.2 Bar graphs of LC-ESI-MS intensities of permethylated N-glycans derived from RNase B and subjected to on-glass digestion for 4 h (green) and 8 h (red). Man 5, Man 6, Man 7 and Man 8 derived from 100 ng RNase B were monitored. Error bars represent standard deviation ($N = 3$ technical replicates). Symbols as indicated in **Figure 2.1**.

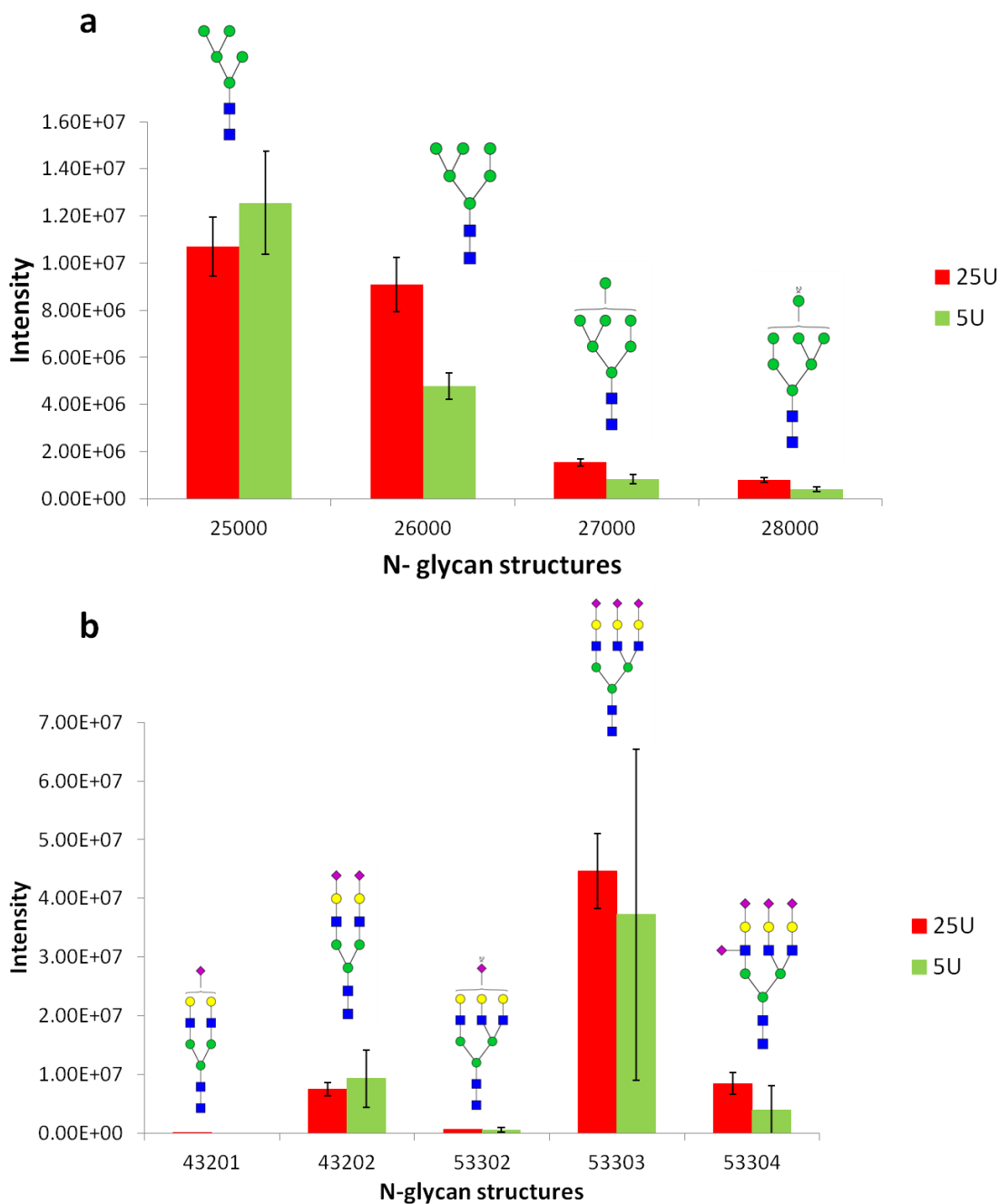


Figure 5.3 Bar graphs of LC-ESI-MS intensities of permethylated N-glycans derived from 100 ng RNase B (a) and 500 ng fetuin (b) and subjected to on-glass digestion using 5 U (green) and 25 U (red) of PNGase F. Error bars represent standard deviation (N = 3 technical replicates). Symbols: as in **Figure 2.1**.

is largely increased with the higher enzyme concentration. The intensities of Man 6, Man 7 and Man 8 increased 89.88%, 85.90% and 100%, respectively. The intensities of N-glycans released from fetuin using 25 U PNGase F were slightly higher than those observed using 5 U PNGase F (**Figure 5.3b**). More importantly, the standard deviation is much lower with the high enzyme concentration. The data suggested that an increased enzyme concentration prompted efficient N-glycan release.

5.3.1 Profiling of Permethylated Glycans Derived from Glycoprotein

Optimum on-surface N-glycan release for model glycoproteins was achieved using 4 h incubation at 37°C and an enzyme concentration of 25 U (**Figure 5.2-5.3**). Different model glycoproteins were used to evaluate the efficiency of the sample preparation strategy. Three spots of the same concentration (10 ng) of RNase B glycoprotein were deposited on a glass surface and used to investigate the efficiency and reproducibility of enzymatic digestion. Reduced and permethylated N-glycans released from an 8.5-ng aliquot of RNase B were analyzed by LC-ESI-MS and all five glycans associated with RNase B were detected (**Figure 5.4**). Previously, on-plate enzymatic digestion allowed the detection of N-glycans derived from submicrogram amounts (5 µg) of RNase B.¹³² The sensitivity of on-glass digestion is higher than that previously reported for solution digestion.^{48,176}

The relative intensities of the five identified N-glycans were also compared to previously reported results (**Table 5.1**).¹⁵³ The relative intensities of N-glycans vary slightly among the different studies, and may reflect different sources of RNase B. Nevertheless, the glycomic profiles of RNase B N-glycans, in all cases, appear to be analytically comparable. By measuring the intensity of N-glycans from different spots,

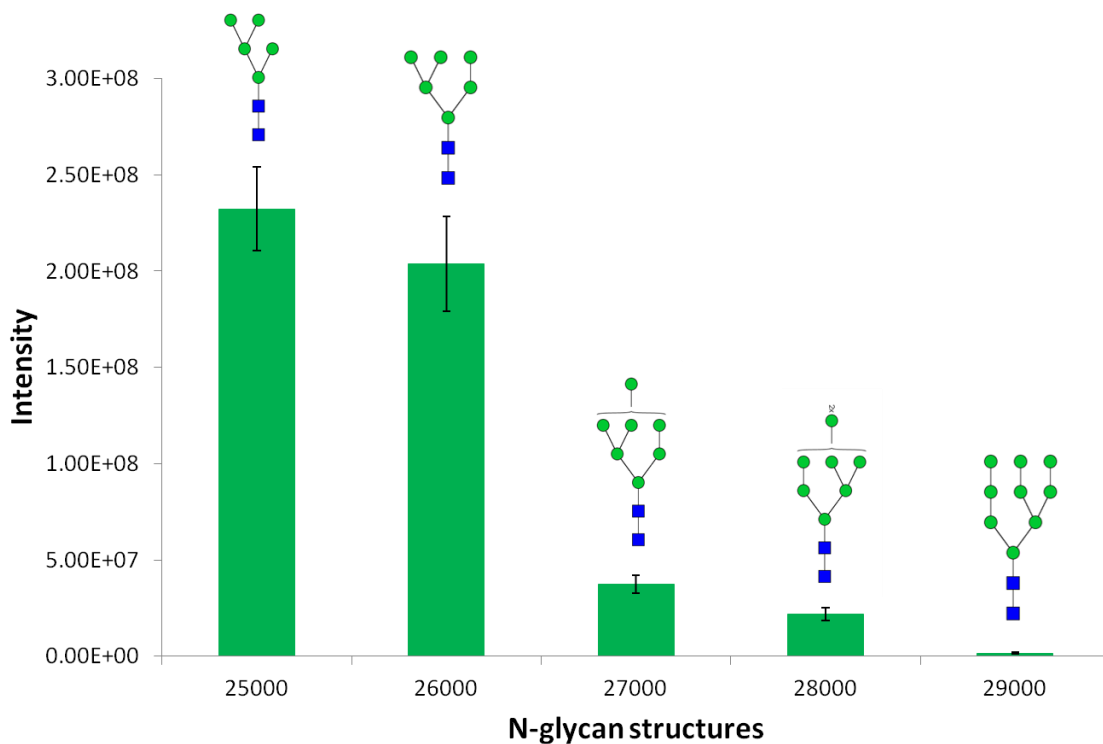


Figure 5.4 Bar graphs of LC-ESI-MS intensities of permethylated N-glycans derived from 10 ng RNase B at optimized enzymatic releasing condition. Error bars represent standard deviation ($N = 3$ technical replicates). Symbols: as in **Figure 2.1**.

Table 5.1 Relative abundances of the N-glycan structures commonly associated with RNase B acquired using different analytical techniques and methods ($n = 3$ for all methods with expressed uncertainties)

Glycan	Relative abundance							
	NMR ^a	CGE ^b	LC/MS ^c	MALDI-MS	MALDI-MS methylated ^d	LC/MS methylated ^d	LC/MALDI methylated	This study
Man 5	57	51.5	51.9±2	50.9±1	59±0.6	53.49±0.4	49.8±6	43.22±9
Man 6	31	30.3	32.1±2	27.4±0.7	29±0.7	32.46±0.6	29.77±5	39.05±4
Man 7	4	4	6.3±0.6	7.3±1	4±0.2	8.02±0.2	10.82±4	8.6±4
Man 8	7	8.5	7.2±0.8	10.9±0.6	7±0.2	5.21±0.3	7.48±4	7.52±4
Man 9	1	3.7	1.6±0.1	3.5±0.6	1±0.05	0.82±0.06	2.11±1	1.61±2

we determined that the CV% is less than 10%. The high sensitivity of this strategy and its potential utility for glycomic profiling of small amounts of glycoproteins is evident in the data.

We further explored Fetusin as another model glycoprotein to evaluate the efficiency of this protocol since fetuin N-glycans are sialylated complex-type. When 80 ng of fetuin were subjected to LC-MS/MS analysis, five peaks were successfully identified (**Figure 5.5**). The distribution of these five N-glycans was comparable to that yielded by in-solution digestion. The data demonstrated that the new strategy effectively released neutral and acidic N-glycans and can be applied to N-glycan profiling of very small samples.

On-surface PNGase F digestion was also very effective in releasing the N-glycans of a mixture of model glycoproteins, including RNase B, fetuin and PTG mixed at 1:2:5 ratios. The on-surface digestion was directly compared to in-solution digestion allowed to incubate for 4 h at 37°C. **Figure 5.6** shows the intensity of N-glycans derived from the glycoprotein mixture. In total, 14 N-glycans were detected via both methods. The relative intensities of glycans released by the different digestion methods were highly comparable. On-glass enzymatic digestion was also found to be more efficient than in-solution digestion in releasing N-glycans. The data thus far described strongly suggest the effectiveness of on-surface digestion to release N-glycans from multiple glycoproteins in a mixture.

5.3.2 Profiling of Permethylated Glycans Derived from HBS

Next, on-surface digestion was applied to 0.5 µL of HBS. To minimize sample loss from the surface, HBS solution was deposited on a Teflon surface rather than a glass

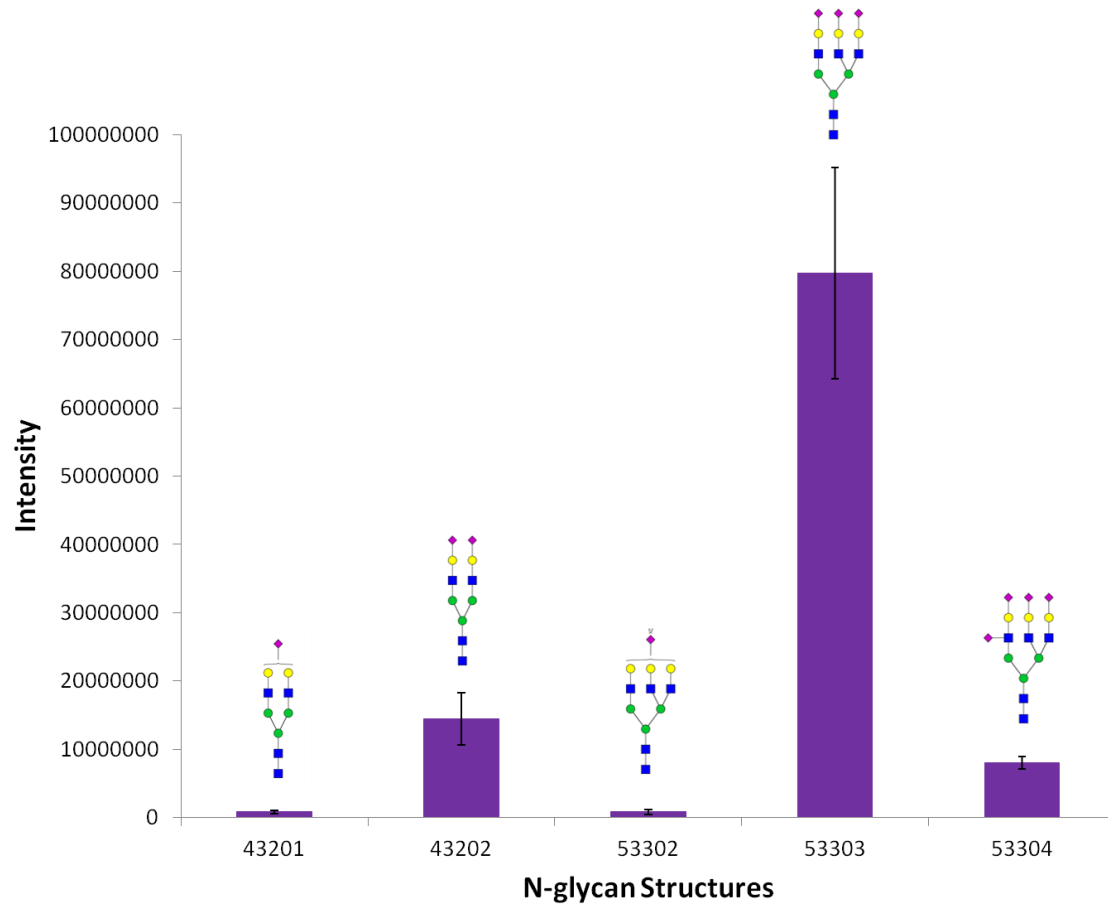


Figure 5.5 Bar graphs of LC-ESI-MS intensities of permethylated N-glycans derived from 500 ng fetuin at optimized enzymatic releasing condition. Error bars represent standard deviations ($N = 3$ technical replicates). Symbols: as in **Figure 2.1**

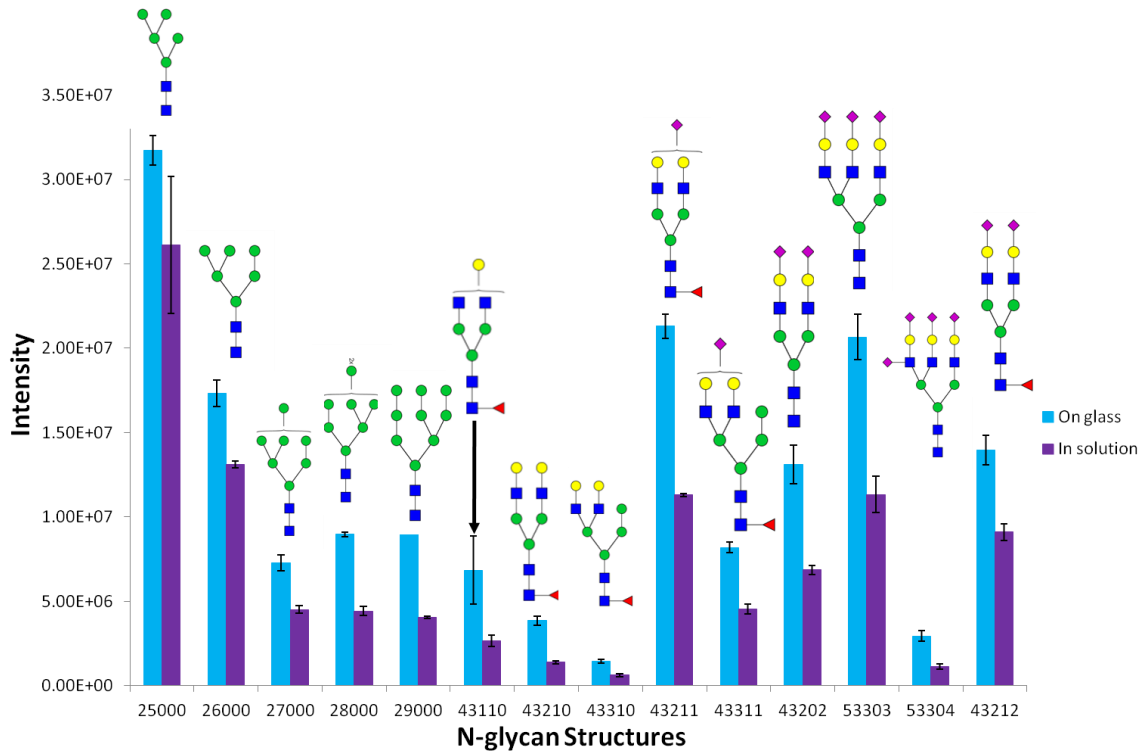


Figure 5.6 Bar graphs of the LC-ESI-MS intensities of permethylated N-glycans derived from model glycoprotein mixtures through on-glass (blue) and in-solution (purple) digestions. Error bars represent the standard deviations (N=3 technical replicated). Symbols: as in **Figure 2.1**.

surface. Using Teflon allowed the deposition of smaller sample spots, in order to limit the potential for loss of sample due to evaporation. N-glycans release was achieved at 8 hours incubation time at 37 °C and an enzyme concentration of 50 U. Incubation for 4 hrs with only 25 U of PNGase F did not produce an efficient release of HBS N-glycans. Again, released N-glycans were collected, reduced and permethylated as described above without any purification steps. To determine if a purification step was needed, the results of a sample purified with charcoal prior to reduction were compared to those of a sample not subjected to any purification. The comparison suggested that sample loss was associated with the purification step. Accordingly, the usual purification step is not required when analyzing small amounts of HBS. It may be that the salts and proteins associated with such a small sample (0.5 μL HBS) do not adversely influence permethylation. Moreover, attempts to purify such a small volume (0.5 μL) with charcoal will bring about substantial sample loss.

We believe that the efficient analysis of small sample volumes was aided by the online purification of permethylated glycans which we have recently described.¹³¹ Injecting the equivalent of 0.1 μL HBS sample subjected to PNGase F allowed the detection of 66 glycan compositions (**Figure 5.7**). A 10-μL aliquot of HBS routinely yields 73 N-glycan compositions¹³¹ and the smaller number of detected here is due to the much smaller amount of HBS analyzed (0.1 μL vs. 1 μL). The missing compositions were those of low abundances. The relative intensities of common N-glycans among all studies, however, were comparable.^{131,153}

The reproducibility of this protocol was examined by processing N-glycans from three different spots. The standard deviations of 66 glycan compositions are shown in

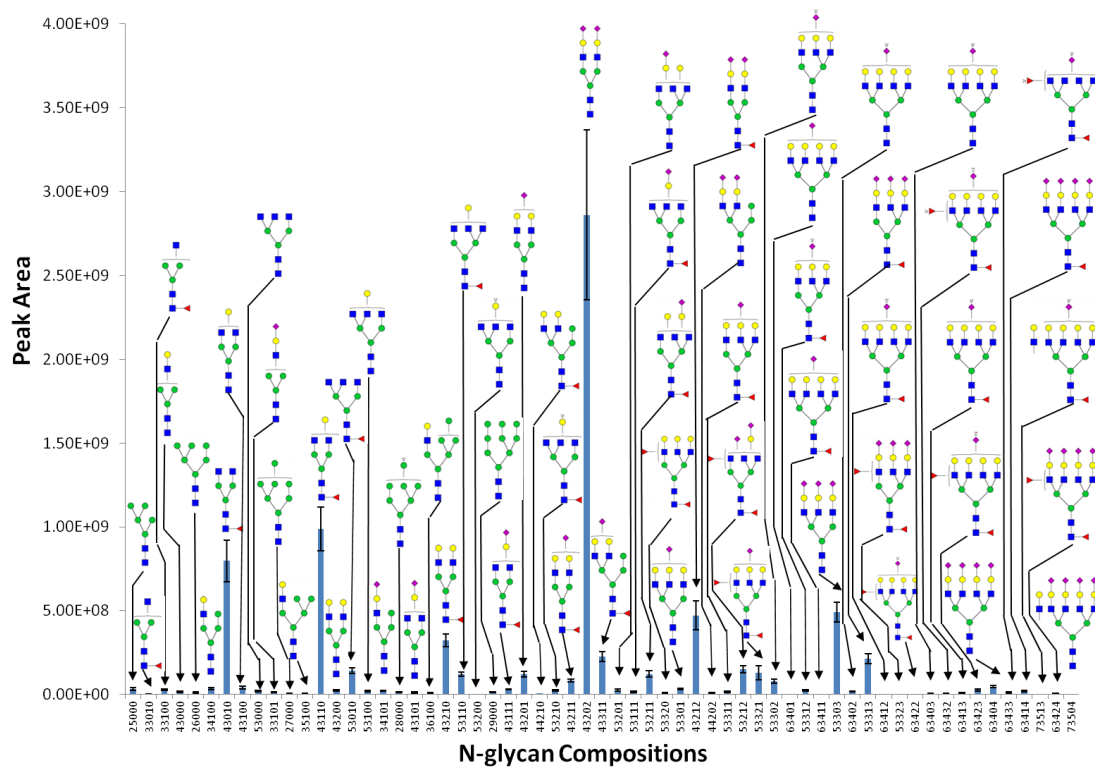


Figure 5.7 Bar graphs of the LC-ESI-MS intensities of permethylated N-glycans derived from analyzing a $0.1 \mu\text{L}$ aliquot of HBS (a $0.5 \mu\text{L}$ aliquot of HBS was subjected to sample preparation procedure as described in Methods). Error bars represent the standard deviations ($N=3$ technical replicates). Symbols: as in **Figure 2.1**.

Figure 5.7. The average %CV for the strategy was *ca.* 20%. Part of this %CV is attributed to ESI. For peptide quantification, LC-ESI-MS run-to-run CV has been reported to be 13%.¹⁷⁷ This suggests that the reproducibility of on surface N-glycan digestion and sample preparation methods prior to LC-MS/MS is better than 10%. Lebrilla and coworkers¹⁶¹ recently analyzed dried blood spots (~2 µL) and identified 44 native glycan compositions, 39 of which are detected by our new protocol. In another study, 19 native glycans were identified from 0.1 µL of HBS subjected to on-line PNGase F digestion prior to separation on an activated charcoal chip.¹⁷⁸ This relatively small number of glycans may reflect the limit of the loading capacity of charcoal chip used. The higher number we observed relative to others may be explained as a result of the permethylation of glycans prior to LC-MS/MS analysis. The addition of methyl groups increases the hydrophobicity of glycans and permits higher MS ionization efficiency. Alley *et al.*¹⁹ have reported the identification of 18 permethylated N-glycans from 0.25 µL of HBS. This low number of detected glycans might be partially attributed to the use of a chip with a limited sample loading capacity. Here, we detect more glycans from very small samples with the new protocol because enzymatic digestion on the sample surface is highly efficient, permethylation increases ionization efficiency in ESI, and eliminating charcoal purification steps conserves sample material.

5.3.3 Profiling of Permethylated Glycans Derived from Mouse Brain Sections

The data described above indicate the high efficiency of on-surface release of N-glycans from glycoproteins associated with simple and complex biological samples (i.e., HBS). The strategy was then employed to enzymatically release N-glycans from the surface of mouse brain tissue sections. A 0.5-µL aliquot of PNGase F was deposited on

the surface of tissue spreading to cover a spot approximately 1.5 mm in diameter (**Figure 5.8 insert**). N-glycan profiling of mouse brain sections utilizing this method is depicted in **Figure 5.8**. We identified a total of 43 glycan compositions, or four more than the 39 glycan compositions identified from the analysis of 100 mg to 400 mg of mouse brain tissue reported by the Consortium for Functional Glycomics (CFG) (**Table 5.2, Table 5.3 and Figure 5.9**). The relative intensities of 32 common glycan compositions in our study and CFG studies were comparable. The differences between the two set of results may be related to the use of different mouse species. CFG used C57BL/6 mice, while nude mouse brain tissue was analyzed in this study. Despite using minute amounts of sample (nanogram amounts of a tissue section) as compared to 100's of mg of brain tissue used by CFG, the number of detected N-glycans was found to be highly comparable. In a recent study, only neutral N-glycans, including high-mannose-type (M5, M6, M7, M8, and M9) and one complex-type (A2G0FB, BA-2), were detected from mouse brain tissue section using hydrazinolysis method.¹⁷⁹ The released N-glycans were purified using a graphitic carbon cartridge to remove hydrazine. The procedure also involved purification on a cellulose column after pyridylamine derivatization. These purification steps may have reduced the number of glycans detected.

To evaluate the repeatability of the sample preparation approach, twelve spots from 3 brain tissue sections were collected and analyzed. All of the 41 glycans were detected in 12 different samples, including 5 of high mannose and 36 of complex type glycans. The average %CV of the twelve samples was *ca.* 35%. We believe this high %CV indicates variation in the spatial distribution of glycans across a brain tissue section. A high %CV is common among biological replicates, which is what the separate

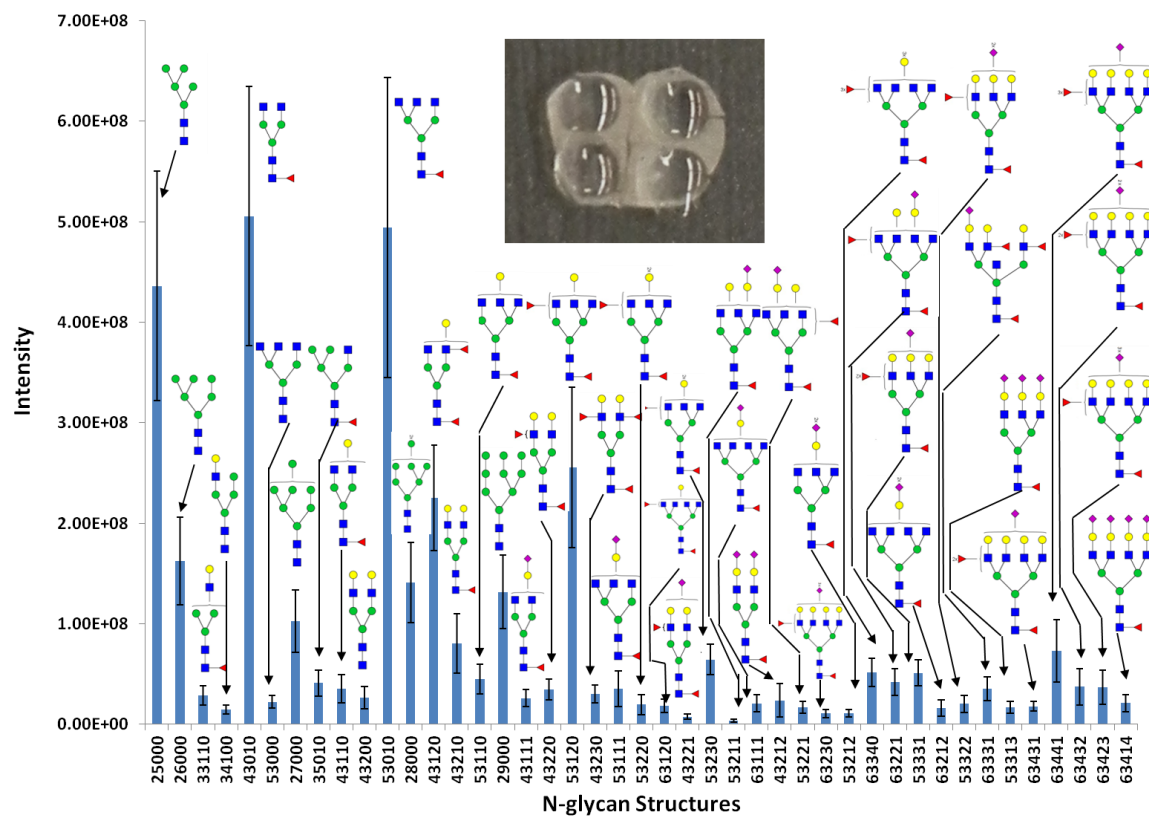


Figure 5.8 Bar graphs of the LC-ESI-MS intensities of permethylated N-glycan derived from mouse brain sections. Error bars represent the standard deviations (N=12 biological replicates). Inset depicts an image of a tissue section with 4 spots of PNGase F. Symbols as in **Figure 2.1**.

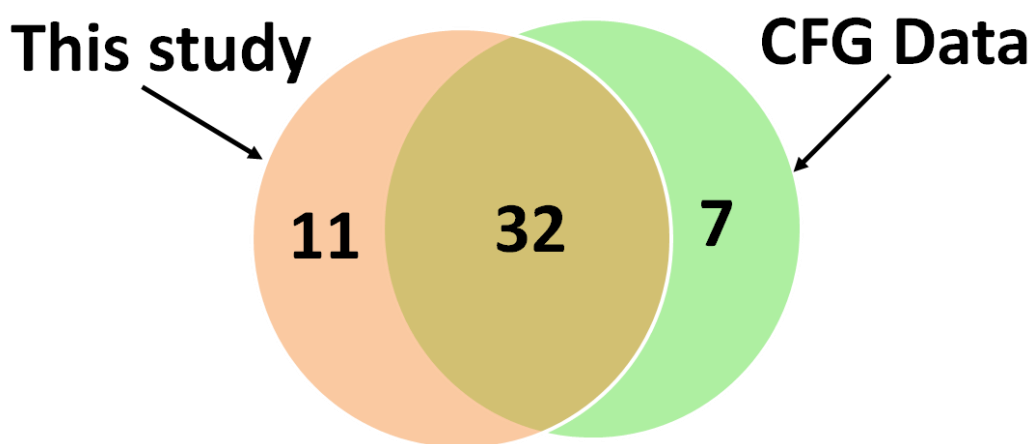


Figure 5.9 Venn plot comparing the CFG data and data of this study in term of the number of N-glycans derived from mouse brain tissues.

Table 5.2 Relative abundances of the N-glycan structures from CFG data and this study (Low mass range, mass<3250)

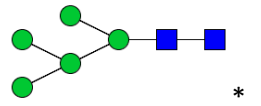
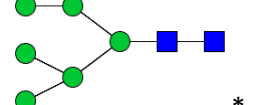
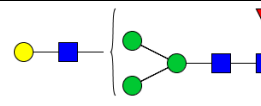
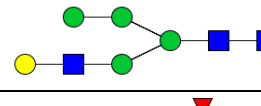
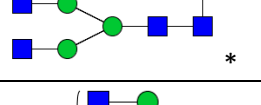
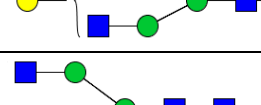
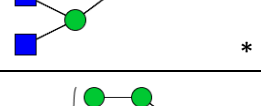
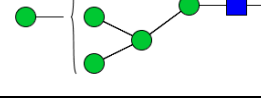
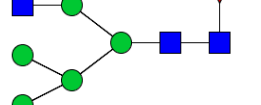
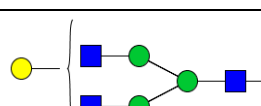
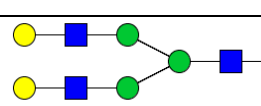
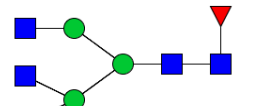
structures	This study	CFG Data
	86.27%	100.00%
	32.18%	50.80%
	5.62%	ND
	2.95%	ND
	100.00%	50.80%
	ND	2.64%
	4.41%	7.64%
	20.29%	47.64%
	8.11%	ND
	6.99%	14.11%
	5.21%	ND
	97.73%	60.00%

Table 5.2 Continued

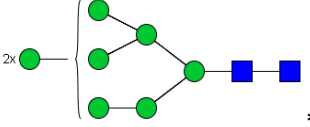
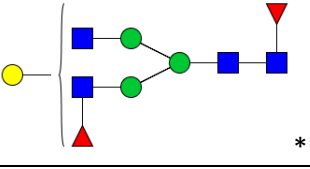
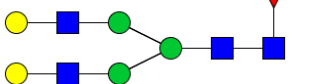
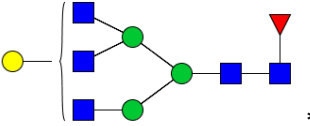
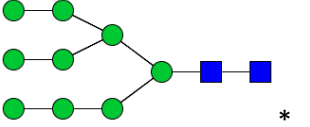
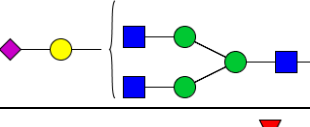
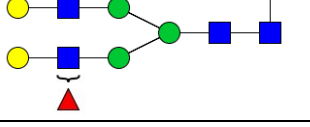
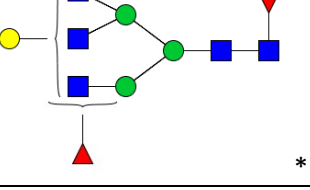
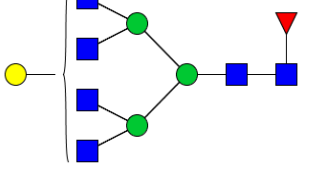
structures	This study	CFG Data
	27.85%	42.65%
	44.55%	25.29%
	15.90%	25.26%
	8.84%	15.29%
	26.03%	49.12%
	5.15%	ND
	6.89%	21.89%
	50.53%	55.50%
	ND	4.70%

Table 5.2 Continued

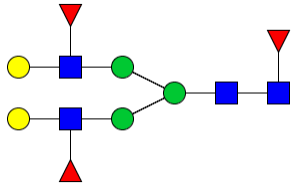
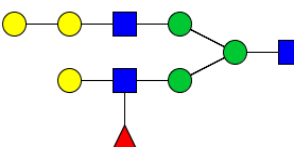
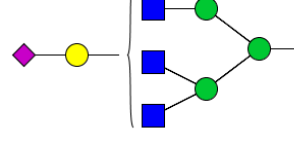
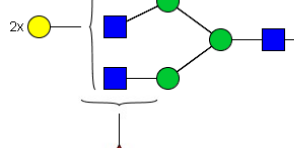
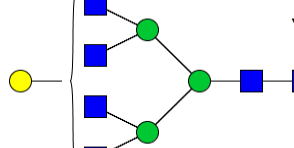
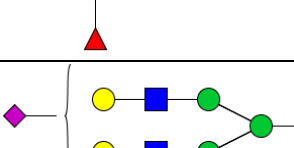
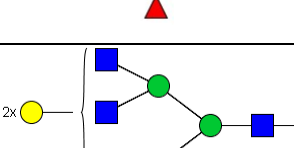
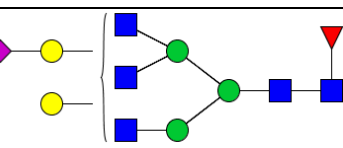
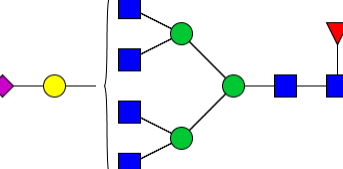
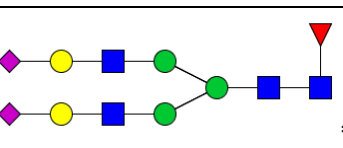
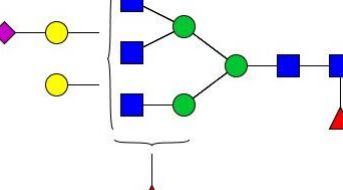
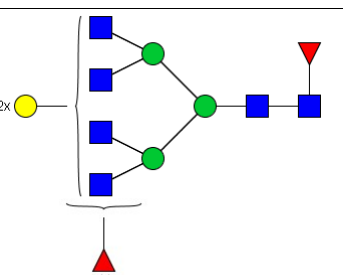
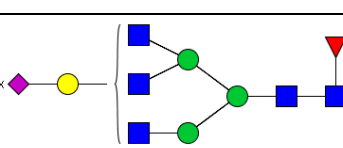
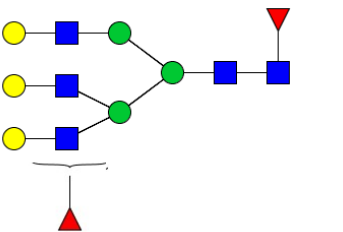
structures	This study	CFG Data
	5.96%	11.17%
*		
	ND	9.90%
*		
	6.98%	ND
*		
	3.90%	14.11%
*		
	3.61%	20.59%
*		
	1.46%	6.47%
*		
	12.74%	36.53%
*		

Table 5.2 Continued

structures	This study	CFG Data
	0.71%	5.88%
	4.14%	12.94%
	4.68%	5.88%
	3.31%	9.80%
	2.11%	9.80%
	2.19%	ND
	10.22%	21.76%

* labeled structures were identified by tandem MS, average mass accuracy<0.5 ppm.

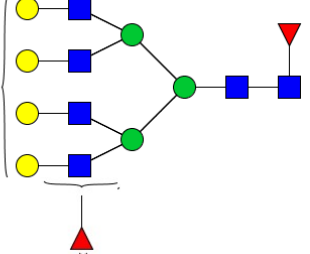
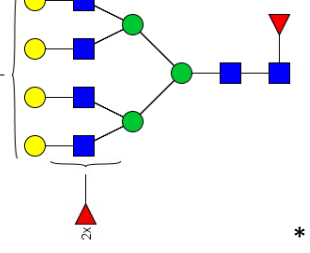
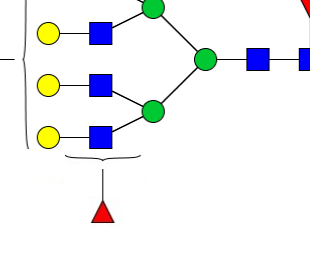
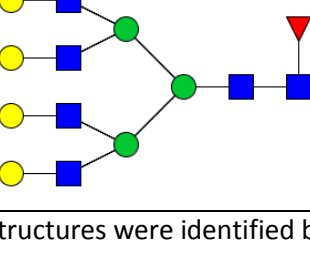
Table 5.3 Relative abundances of the N-glycan structures from CFG data and this study (High mass range, mass>3250)

structures	This study	CFG Data
 *	57.57%	91.94%
 *	69.77%	100.00%
 3x	ND	33.90%
	ND	22.50%
 *	21.92%	ND
 *	27.99%	31.60%

Table 5.3 Continued

structures	This study	CFG Data
	48.12%	58.33%
	23.32%	ND
	ND	18.00%
	ND	38.20%
	24.12%	ND

Table 5.3 Continued

structures	This study	CFG Data
	100.00%	62.61%
	50.91%	42.50%
	50.10%	20.00%
	28.79%	ND

* labeled structures were identified by tandem MS, average mass accuracy<0.5 ppm

spots represent. The much lower %CV observed on the technical replicates described in earlier sections are also worth noting in this context.

The new protocol was further compared with in solution digestion, by scratching a mouse brain tissue section from glass for analysis. Fewer N-glycans detected under this procedure, and the intensity of detected N-glycans was 2-fold weaker (data not shown). The molecular spatial information available from on-tissue digestion was lost when analyzing this homogenized tissue.

5.4 Conclusion

A highly efficient sample preparation method developed for N-glycan profiling of tissue sections, permitting the detection of 43 N-glycans from mouse brain sections. The new protocol permits the detection of more glycans from very small samples not only because enzymatic digestion on the sample surface is highly efficient, but also because eliminating charcoal purification conserves sample material and the permethylation step increases MS ionization efficiency. It also offers practical advantages in terms of nanogram scale sample size and consequent ease of sample storage and shipping and in terms of increased throughput since sample preparation time is reduced to several hours. Enzymatic digestion time is reduced to 4-8 h and the charcoal purification step is eliminated. Finally, and most promising in terms of discovering glycan biomarkers of human disease, this new protocol for N-glycans analysis can obtain molecular spatial information of tissue pathology.

CHAPTER VI

AUTOMATED ANNOTATION AND QUANTITATION OF GLYCAN BY LC-ESI-MS ANALYSIS USING MULTIGLYCAN-ESI COMPUTATIONAL TOOL

Y. Hu, S. Zhou, C.-Y. Yu, H. Tang, Y. Mechref, submitted to *Rapid communication in mass spectrometry*, 2014

6.1 Introduction

Glycosylation of proteins is one of the most common post-translational modifications. Developing qualitative and quantitative glycomics profiling strategy is of great importance to understand the biological roles of glycans in the development and progression of human diseases. With the development of MALDI and ESI, mass spectrometry is currently considered to be one of the most powerful tools for glycomics quantitation studies. LC-ESI-MS permits liquid chromatographic separation prior to mass spectrometry detection, thus minimizing ion suppression and resulting in increased glycan detection.

Quantitative glycomics methods can be classified into two categories: label free and isotopic labeling strategies. Label free quantitation method involves no labeling step. Thus, no additional derivatization and cleaning steps are required in the case of this strategy. Glycan derivatization provides advantages that outweigh the additional preparation steps, including increasing MS ionization efficiency,^{48,94,180,181} providing more structural information,^{78,182,183} allowing the glycan detection by fluorescence or UV detectors.⁴⁹⁻⁵¹ Also, isotopic labels can be incorporated into N-glycan through derivatization strategy. Isotopic labeling methods allow simultaneous analysis of several samples, which may overcome the variation that might be contributed to instrument

instability, injection variation and different ionization environment. Incorporating stable isotopes through metabolic^{97,98,102} and introducing isotopic label via reductive amination^{85,92,95,152} and permethylation^{96,184} are the commonly utilized isotopic labeling methods.

Regardless of the different quantitation approaches applied for glycomics study, manual evaluation of large sets of data files is still a challenge. Thus, developing software tools for automated glycan annotation and quantitation is required for high-throughput glycomics analysis. Cartoonist¹⁰⁴ and GlycoWorkBench¹⁰⁵ are two of the early developed glycan annotation tools, which assign the glycan peaks by matching the experimental mass to the theoretical mass in MALDI-MS. The annotation of glycan peaks only depends on the glycan mass without considering the isotopic distribution. GlycReSoft¹⁰⁷ is a recently developed software tool that enables glycan annotation and quantitation of LC-ESI-MS data. The de-isotoped LC-ESI-MS data generated by Decon2LS¹⁰⁶ was annotated by a default or a user-defined glycan library and reports the intensity of each glycan. However, GlycReSoft requires the deconvolution using Decon2LS prior to quantitation. Also, GlycReSoft enables the quantitation of only one ion adduct.

Recently, we developed an open-source LC-ESI-MS data annotation software, MultiGlycan-ESI.¹⁸⁵ The de-isotoping algorithm was incorporated in the software, thus minimizing the data processing steps. Similar to GlycReSoft, default glycan list or user-defined list can be used for automated annotation. The output of MultiGlycan-ESI is the summation of the abundances of various charges and adducts of a single glycan structure. Automated annotation of N-glycans by using this software was previously discussed.¹⁸⁵

In this study, the quantitation performance of MultiGlycan-ESI was evaluated. An updated version, MultiGlycan-ESI 1.0, was utilized to quantify the permethylated N-glycans derived from fetuin glycoproteins. The software integration results were first compared with the manual integration results to evaluate the reliability of using the software tool for quantitation. The quantitation ability of MultiGlycan-ESI is further demonstrated by the different concentration of permethylated N-glycans derived from fetuin. Different amount of fetuin samples were also spiked in samples derived from complex biological sample, HBS, to evaluate the quantitation ability of the tool.

6.2 Experimental

6.2.1 Material

The model glycoprotein fetuin and HBS were purchased from Sigma-Aldrich (St. Louis, MO). Borane-ammonia complex, sodium hydroxide beads, dimethyl sulfoxide (DMSO), iodomethane, and MS-grade formic acid were also purchased from Sigma-Aldrich (St. Louis, MO). Empty microspin columns were obtained from Harvard Apparatus (Holliston, MA). Formic acid and HPLC-grade solvents, including acetonitrile, methanol and isopropanol, were procured from Fisher Scientific (Pittsburgh, PA). HPLC grade water was acquired from Mallinckrodt Chemicals (Phillipsburg, NJ). N-Glycosidase peptide purified from *Flavobacterium meningosepticum* (PNGase F) was obtained from New England Biolabs Inc. (Ipswich, MA).

6.2.2 N-glycans Released from a Model Glycoprotein Fetuin and HBS

N-glycans were first released from model glycoprotein fetuin and HBS. Briefly, a 10- μ L aliquot of 20 mM ammonium bicarbonate was added to a 10- μ L aliquot of HBS and fetuin stock solution (1 μ g/ μ L). The glycoproteins were mixed and denatured at 80°C

for 1h. Then, 1.2 μ L of 10 times diluted PNGase F was added to glycoprotein mixture prior to incubation at 37°C in a water bath for 18h.

6.2.3 Dialysis to Remove Salts

An in-house built dialysis device was utilized to remove the salts from the digested samples. Cellulose Ester (CE) membrane with molecular weight cut off (MWCO) of 500-1000Da was used. The samples were dialyzed for 18 h to remove all impurity of molecular weight less than 1000 Da. The purified samples were then collected and dried prior to reduction and permethylation.

6.2.4 Reduction

Ammonia borane complex was used for the reduction of the purified samples. A 10- μ g/ μ L fresh borane-ammonium complex solution was prepared. A 10- μ L aliquot of this solution was then added to each sample and incubated at 65°C for 1h. A 10- μ L aliquot of aqueous acetic acid solution (5% v/v) was then added to each sample to neutralize the excess borane ammonia. Next, the samples were dried under vacuum. Methanol was applied to each dried sample to remove the borate salts. This process was repeated several times until no white solid was observed in the samples.

6.2.5 Permetylation

The reduced and cleaned samples were then permethylated. This process was performed according to our previously published protocol.^{48,66,67} Briefly, the sodium hydroxide beads-filled spin columns were first prepared. Then, DMSO was applied to the spin column to wash it. This process was repeated twice to ensure the removal of all impurities related to the beads and column. The reduced and dried samples were

resuspended in 30 μ L DMSO, 1.2 μ L water and 20 μ L iodomethane. The reaction mixture was then applied to the sodium hydroxide beads-filled spin column. The mixture was allowed to react with the beads for 25 minute and then another fresh 20- μ L aliquot of iodomethane was applied to the spin column. The reaction was allowed to proceed for another 15 minute prior to centrifugation. A 50- μ L aliquot of acetonitrile was applied to the column to wash out all the reaction mixture. Finally, the samples were dried under vacuum.

6.2.6 Nano LC-ESI-MS

The permethylated samples were resuspended into 20% ACN with 0.1% formic acid and subjected to nano-LC-ESI. Dionex nano-LC system was used for separation. Samples were on-line purified with Acclaim[®] PepMap100 C₁₈ nano-trap column (Thermo Scientific, Waltham, MA).¹³¹ The separation of glycans was performed on Acclaim[®] PepMap RSLC (75 μ m x 15 cm, 2 μ m, 100 Å) column (Thermo Scientific, Waltham, MA). The separation was attained at a flow rate of 350 nL/minute over 32 minute with a gradient from 38% solvent B to 55% solvent B. Solvent B was 100% ACN with 0.1% formic acid while solvent A consisted of 98% water and 2% acetonitrile with 0.1% formic acid. The separated N-glycans were infused to Velos LTQ Orbitrap hybrid mass spectrometer (Thermo Scientific, San Jose, CA) through a nano-ESI source. The capillary temperature was kept at 300°C while capillary voltage was maintained at 1.5 kV thus allowing desolvation of LC separated sample. The mass spectrometer was operated in an automated data-dependent acquisition mode with the eight most abundant ions were subjected to CID MS/MS scan. The *m/z* full scan range was set to 500-2000 *m/z*. Tandem

MS conditions were set to 0.250 Q-value, 20 ms activation time, and 35% normalized collision energy.

6.2.7 Data Processing and Quantitation using MultiGlycan-ESI

The generated raw files were processed with MultiGlycan-ESI software. MultiGlycan-ESI provides a built-in N-glycan list (Default list). Also, users can compose their own glycan list file in CSV format and use it for glycan annotation. The software matches the LC-ESI-MS ions with the default or user-defined glycan list. The THRASH algorithm was utilized to basic peak processing and de-isotope isotopic distributions in MultiGlycan-ESI. In this study, reduced and permethylated N-glycan masses were selected to be searched. The mass tolerance was set to 5 ppm. The search retention time window was set to 5 minute. Different charge states and different adducts, including ammonium and sodium, were defined to be merged. The minimum peak width of an LC peak was set to 0.2 minute while the minimum abundance was set to 10,000.

6.3 Results and Discussion

The development of a data analysis tool is of great importance to achieve high-throughput glycomic quantitation. Here, a recently developed software tool, MultiGlycan-ESI, was utilized for glycomic quantitation. **Figure 6.1** listed the workflow of software based quantitation strategy. Briefly, N-glycans were released from glycoproteins and then reduced. The reduced glycans were then permethylated and subjected to nanoLC-ESI-MS analysis. The LC-MS raw data was uploaded to MultiGlycan-ESI. The whole scan range was searched to identify isotopic distributions of N-glycan peaks. User-defined glycan list was uploaded for searching reduced and permethylated N-glycans. Different adducts, including proton ions, ammonium ions and

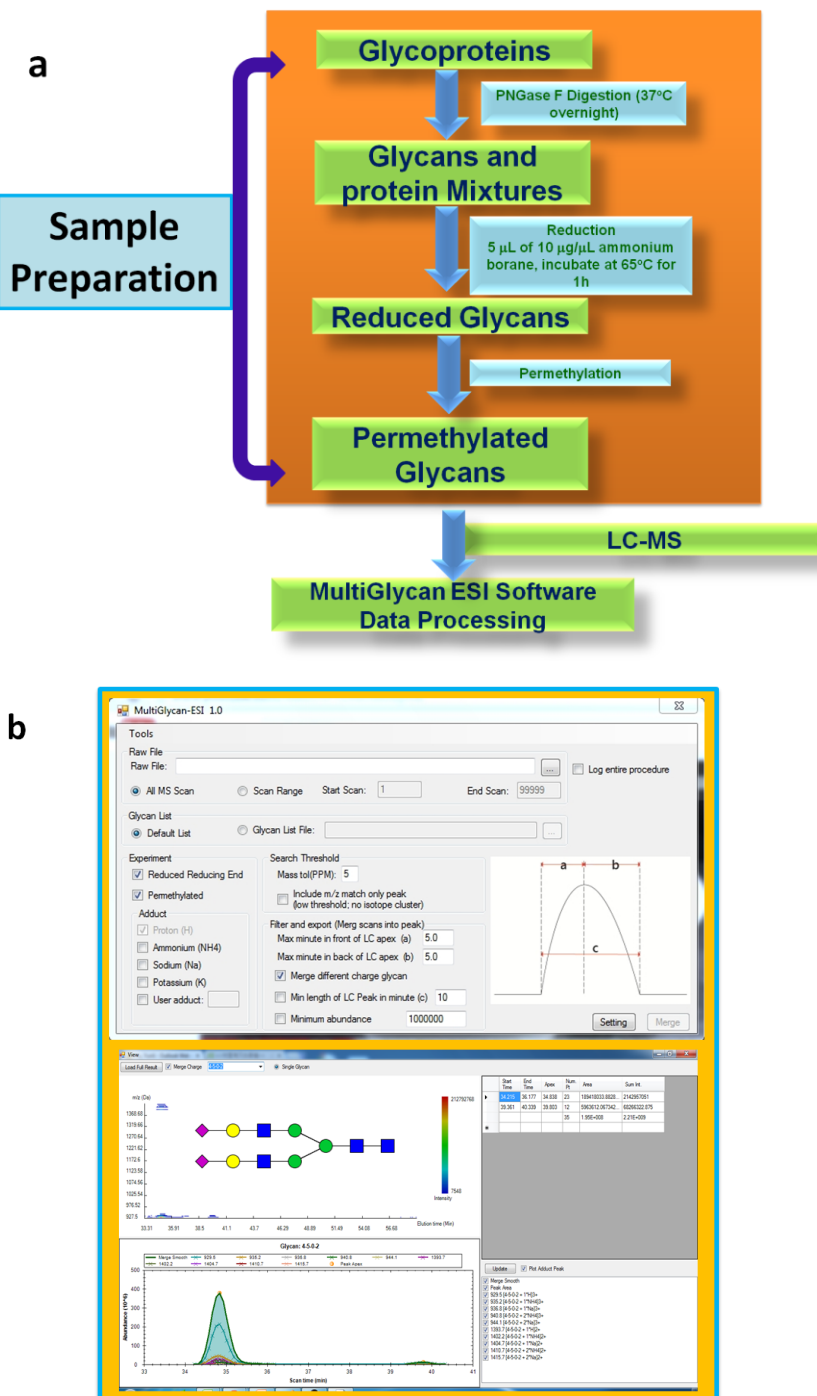


Figure 6.1 Workflow of MultiGlycan-ESI based automatic quantitation strategy. a) Permethylated N-glycan preparation workflow; b) Software annotation and quantitation method.

sodium ions, were selected for processing. Mass tolerance of peak searching was defined to 5 ppm, which was in alignment with the high-mass accuracy of an Orbitrap instrument used in this study. Different charge states and adduct of the same glycan were merged. The criteria of merged LC peak were minimum peak width of 0.2 minute, maximum peak width of 5 minute, and minimum abundance of 10,000. The total ion intensity of different charge states reported in the output file. The default peak processing parameter was utilized. Two csv files were output after data processing: one csv file provides a summary list of annotated glycan structures and merged intensity, and the other csv file containing a full list of annotated glycans can be uploaded into elution profile viewer (an internal function of the MultiGlycan-ESI software) to extract ion chromatograms.

The performance of MultiGlycan-ESI was evaluated by comparing the peak intensity generated by the software with the extracted peak area using Xcalibur from Thermo Scientific, referred to here as manual integration. The LC-MS data acquired from three injections of permethylated N-glycans derived from 500 ng fetuin were utilized for comparison. For manual integration, the extracted peak areas of different adducts and charge states were added up. In the case of MultiGlycan-ESI, the intensities of first monoisotopic peaks of different adducts and charge states were added. The comparison results are summarized in **Table 6.1**. The absolute intensities calculated using the two integration methods were not comparable because different quantitation scales were used in each case. However, the relative intensities of N-glycans calculated from the two integration methods were consistent with less than 5% differences, indicating a good agreement among the software integration and the manual integration. Therefore, the software is reliable for automated quantitation of LC-MS data.

Table 6.1 Integrated areas of permethylated N-glycans derived from fetuin, calculated by manual or MultiGlycan-ESI integration

N-glycan structure	Intensity	Intensity	Relative	Relative	Difference
	Manual	MultiGlycan ESI	intensity of Manual integration	intensity of MultiGlycan ESI	(%)
	(2.60±0.05)e8	(4.45±0.1)e7	0.57%	0.58%	1.71%
	(8.65±0.2)e9	(1.41±0.02)e9	19.02%	18.43%	3.13%
	(2.20±0.3)e7	(3.72±0.6)e7	0.05%	0.05%	0.61%
	(1.74± 0.005)e9	(3.08± 0.03)e9	3.83%	4.01%	4.57%
	(2.62±0.06)e10	(4.40±0.06)e10	57.57%	57.40%	0.30%
	(8.62±0.5)e9	(1.50±0.03)e9	18.95%	19.53%	2.97%

One advantage of utilizing MultiGlycan-ESI is the ability to automatically merge the different adducts and charge states corresponding to the same glycan. Manually adding the intensities of all adducts for each structure is laborious as most of the glycans have multiple m/z values. The necessity of adding all adducts for quantitation was demonstrated in **Figure 6.2**. As illustrated in **Figure 6.2**, the RSD of 15 injections can be as high as 67% for sodium adducts and ammonium adducts. When all adducts were added for quantitation, RSD of 15 injections was less than 25%. Moreover, the relative intensity distribution of one adduct is different from the distribution of all adducts summation, which indicating that for reliable quantitation all adducts and charges states need to be accounted for.

6.3.1 Quantitation of Glycomics using MultiGlycan-ESI

MultiGlycan-ESI was also utilized to assess the reproducibility of injection and on-line purification of permethylated glycans. Same amount of glycans derived from fetuin were injected at different injection volumes. Three injections were made for each injection volume. **Figure 6.3** shows the comparison of five groups of different injection volumes as well as the average of five groups. The concentrations of the five groups were 500 ng/ μ L, 250 ng/ μ L, 166.7 ng/ μ L, 125 ng/ μ L and 100 ng/ μ L. To achieve the final injection amount of 500 ng in each of these cases, the injection volumes were 1 μ L, 2 μ L, 3 μ L, 4 μ L and 5 μ L, respectively. For each group, the RSD was determined to be less than 15%. The RSD of all 15 injections is less than 25%. As the LC-MS RSD can be as high as 15%,¹⁸⁶ the variation contributed by sample handling and injection is less than 10%, which is a value analytically acceptable.

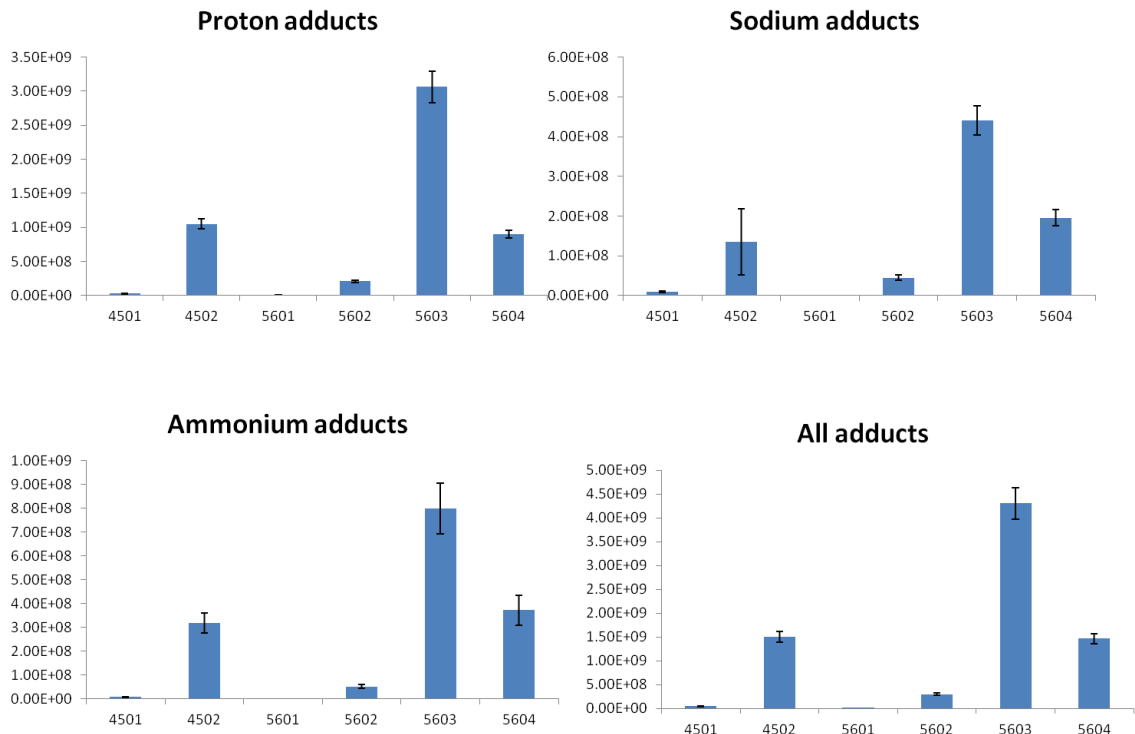


Figure 6.2 Bar graph of different adducts of permethylated N-glycans derived from fetuin.

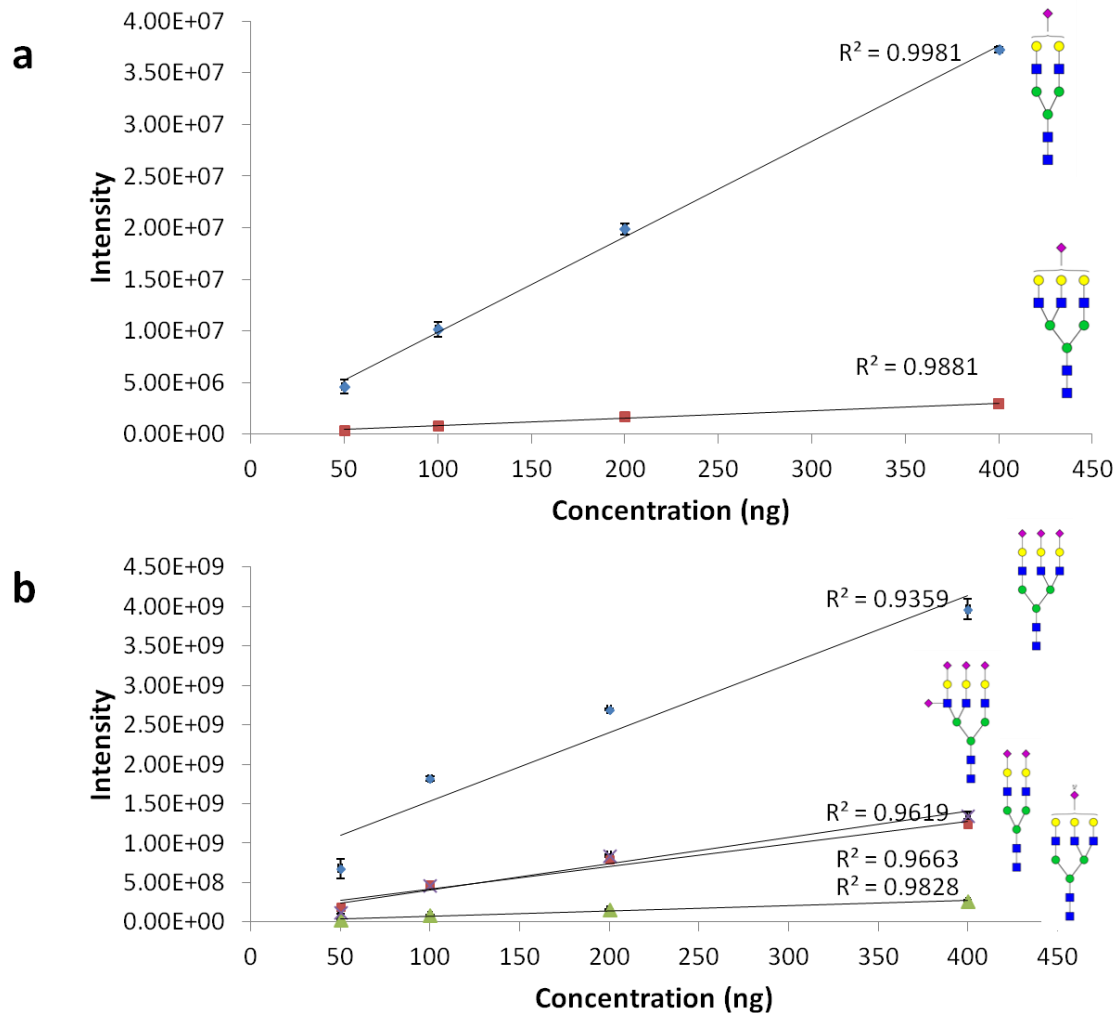


Figure 6.3 A plot of the linear relationship of the permethylated N-glycans derived from fetuin. Triplicate injections of four groups from 50 ng-400 ng of fetuin were made. Symbols: as in **Figure 2.1**

6.3.2 Label-Free Quantitation of N-glycans Derived from Fetusin Glycomics

Different concentration of permethylated N-glycans derived from fetusin was also subjected to LC-MS analysis. The dynamic range of six N-glycan derived from fetusin was more than two orders of magnitude. Triplicate injections of four different amounts spanning from 50 ng to 400 ng were made. All six N-glycans were detected even at the lowest injection amount. The intensities of N-glycans were calculated using MultiGlycan-ESI as described above. The relationship of injected fetusin amount to observed intensity was plotted in **Figure 6.4**. **Figure 6.4a** shows the relationship of fetusin concentration to the intensity of two low-abundance glycans. Both of them show good linear response with the increase of glycan amount. The correlation coefficients (R^2) of HexNAc4Hex5NeuAc1 and HexNAc5Hex6NeuAc1 are 0.998 and 0.988, respectively. The four relatively high-abundance N-glycans derived from fetusin were shown on **Figure 6.4b**. The linearity of the high-abundance glycans is decreased, which might be partially due the detector saturation. R^2 is higher than 0.93 for all six N-glycan derived from fetusin, indicating a good linear response between glycan amount and intensity.

6.3.3 Label-Free Quantitation of N-glycans Derived from Fetusin Spiked in HBS Sample

Different amount of N-glycans derived from fetusin were spiked into permethylated N-glycans derived from HBS to test the efficiency of MultiGlycan-ESI for the quantitation of complex biological sample. Six different amounts (0-200ng) of fetusin samples were spiked to N-glycans derived from 0.2 μ L HBS. Triplicate injections were made for each amount. **Figure 6.5** shows the relationship of fetusin concentration to the intensity. HexNAc5Hex6NeuAc3 and HexNAc5Hex6NeuAc4 show good linear response

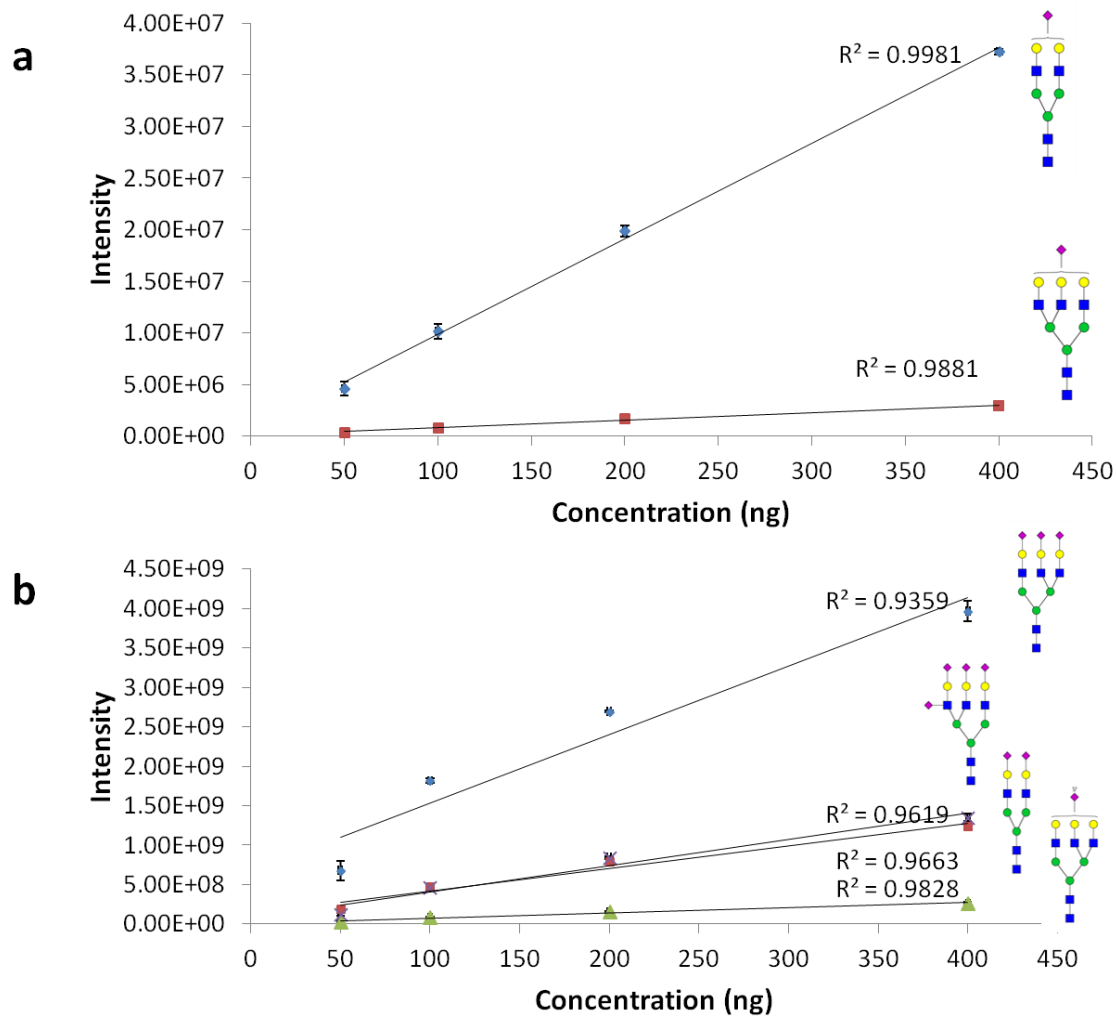


Figure 6.4 A plot of the linear relationship of the permethylated N-glycans derived from fetuin. Triplicate injections of four groups from 50 ng-400 ng of fetuin were made. Symbols: as in **Figure 2.1**

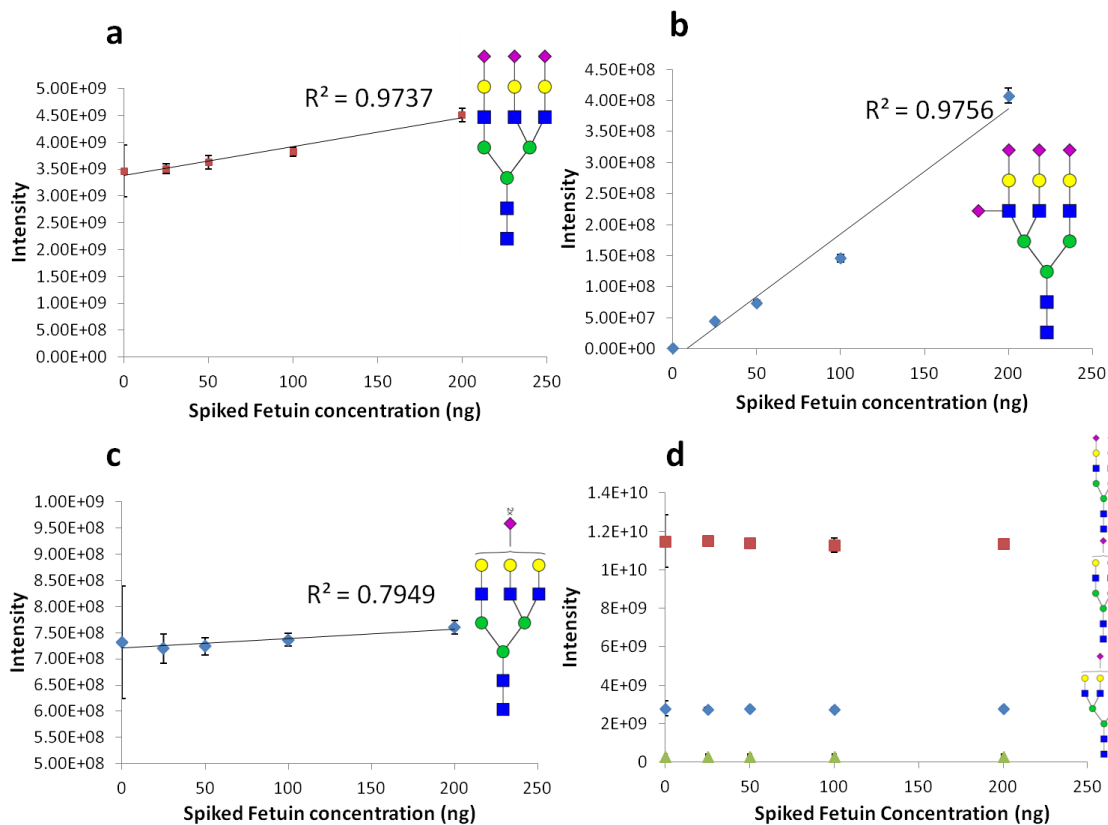


Figure 6.5 A plot of the permethylated N-glycans derived from fetuin spiked into 0.2 μ L HBS. Triplicate injections of five groups from 0 ng-200 ng fetuin spiked into HBS were made. Symbols: as in **Figure 2.1**

between the spiked amount to intensity, with the R^2 of 0.974 and 0.976, respectively. Due to the contribution of the “zero” point, the overall linearity (R^2) of HexNAc5Hex6NeuAc2 is 0.795 (**Figure 6.5c**). 200 ng of the fetuin sample contains less than 10% of the HexNAc5Hex6NeuAc2 concentration in HBS. Thus, the contribution of increased intensity may be outweighed by the instability of ESI. As it is shown in **Figure 6.5d**, there is no obvious increase of the intensity with the increase of spiked fetuin amount for other three N-glycan structures. This also can be explained as the spiked amount of glycans derived from fetuin is lower than 20% of the glycan in HBS. Similarly, a change of intensity is outweighed by the ESI variation.

To further confirm this assumption, same amount of fetuin was spiked to a 0.002 μ L HBS. As shown in **Figure 6.6**, all six glycans exhibit a linear relationship between N-glycan amount and intensity with R^2 higher than 0.94. For each structure, the spiked fetuin amount is higher than 20% of HBS sample amount. Thus, linear relationships for all six glycans were observed.

6.4 Conclusion

Due to the complexity and quantity of glycomics LC-MS data, informatics solutions are in demanding. Currently, most of the software processing tools of glycomics only enable the automated annotation of MALDI-MS data. The completely automated annotation and quantitation of LC-ESI MS data are still lacking. MultiGlycan-ESI is a recently developed glycan LC-ESI data quantitation tool. MultiGlycan-ESI provides a user-friendly interface and allows the summation of all different adducts and charge states of one glycan. The report file provides the structure information as well as the

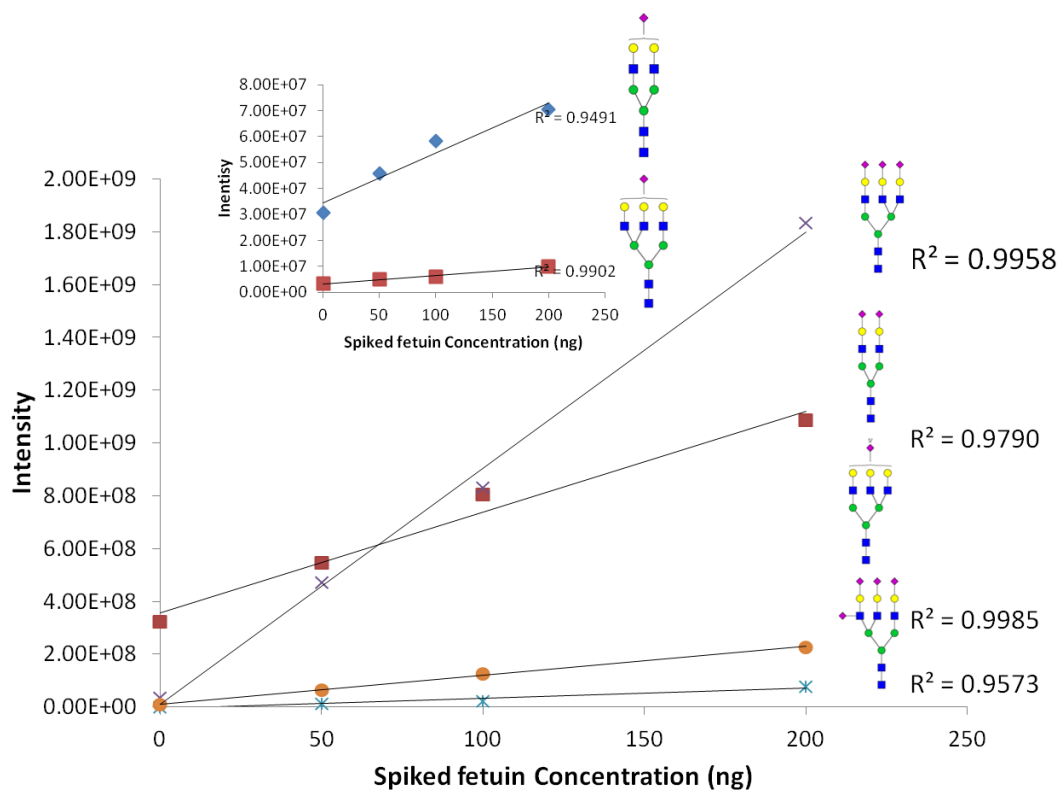


Figure 6.6 A plot of the permethylated N-glycans derived from fetuin spiked into 0.002 μ L HBS. Triplicate injections of five groups from 0 ng-200 ng fetuin spiked into HBS were made. Symbols: as in **Figure 2.1**

intensity. Extracted ion chromatogram can be generated when the full results were loaded to the built-in elution profile viewer.

The quantitation ability of MultiGlycan-ESI is demonstrated by comparing the relative intensities of manual integration to that of software. Although different integration methods were utilized, the overall difference was determined to be less than 5%.

The software proved to be a reliable tool for the quantitation of N-glycans derived from fetuin. A linear relationship was observed with the increase of the fetuin concentration. Moreover, the software revealed limitation of glycomic quantitation by using ESI-MS. As the detection variance in ESI-MS can be as high as 20%, it is accurate to detect small amount of abundance change of glycans. Furthermore, for the high abundant glycans, the detector saturation will affect the linear response in ESI-MS. Overall, MultiGlycan-ESI proved to be a reliable tool for glycomics quantitation, and can be utilized in high-throughput glycomics study.

CHAPTER VII

N-LINKED GLYCAN PROFILING IN NEUROBLASTOMA CELL LINES

Y. Hu, A. Mayampurath, S. Khan, J. K. Cohen, Y. Mechref, S. L. Volchenboum in preparation

7.1 Introduction

Neuroblastoma (NBL) is the most common extra-cranial solid tumor in children and is responsible for 10-15% of pediatric cancer-related deaths.¹⁸⁷ A key attribute of this disease is heterogeneity with completely different responses to treatment in patients with similar tumor onset. Current means of stratifying patients into risk-categories include a combination of clinical markers such as age, tumor stage, and histology and genetic markers such as loss of chromosome 1p and *MYCN* oncogene amplification.¹⁸⁸ However, discordance between *MYCN* amplification and other prognostic factors have been reported, thereby making optimal treatment difficult to undertake.¹⁸⁹ Among high-risk NBL, the death rate is currently at 50%, which demand the need for better therapeutics. Studies at molecular levels such as genomic, miRNA and proteomic profiling have provided powerful insights in neuroblastoma biology. Examples include identification of mutations and variations in genetic markers such as ALK and PHX2B¹⁹⁰, greater incidence of loss of heterozygosity events in tumor cells,¹⁹¹ detection of differences in protein phosphorylation within *MYCN* amplified and non-amplified neuroblastoma,¹⁹² derivation of a small set of differentially regulated genes¹⁹³ and proteins¹⁹⁴ within a study involving neurotrophin tyrosine kinase receptors etc. However, these are yet to be translated to clinical mechanisms of disease stratification.

Protein glycosylation is a post-translational modification where a glycan gets attached to specific amino acids. Glycans are sugar chains comprised of monosaccharides that form structures that show tremendous variety in branching, stereoremeric configuration and flexible glycosidic bonds. As one of the most common post-translational modifications of proteins, glycosylation is responsible for many protein attributes such as tertiary structure formation, mediating intercellular communication and immune response to pathogen infections.¹⁹⁵ N-linked glycosylation (or N-glycosylation) involves the attachment of a sugar chain to any Asn in the motif Asn-Xaa-Ser/Thr (where Xaa can be any amino acid except Proline). Another distinguishing characteristic of N-glycosylation is that all N-linked glycans share a common “pentamer” core structure consisting of two N-acetylglucosamine residues (GlcNAc) and three Mannose (Man) residues. The attachment occurs prior to folding, implying that N-glycosylation affects the tertiary structure and stability of the glycoprotein. Quantitative changes in glycosylation have been associated with many human diseases, including hereditary disorders, cardiovascular disease, and cancer. Additionally, glycomic changes have been observed to be associated with transition from non-lethal non-cancerous diseases to oncogenic equivalents.^{196,197} Liquid-chromatography mass-spectrometry (LC-MS) platforms, being high-throughput and high-sensitive, are routinely used to detect and monitor glycomic differences between healthy and disease individuals.^{13,161} Within neuroblastoma, monoclonal antibodies targeting GD2 digangliosides have been recently used as treatment in high-risk version of the disease.¹⁹⁸ Additionally, alterations in both N- and O-linked glycosylated sites in molecules such as ICAM-2 and cell-surface mucins have been linked to NBL¹⁹⁹ and through associations with ALK phosphorylation²⁰⁰ which

is one of the key signaling pathways in NBL. However, a comprehensive glycomic profiling of NBL cells has not yet to be performed. In this study, we detected and compared profiles of N-linked glycans between *MYCN* amplified NLF and *MYCN* non-amplified SY5Y cell lines using a combination of enzymatic release using PNGaseF, permethylation, liquid-chromatography (LC) separation and tandem mass spectrometry (MS/MS). Out of 47 glycans detected and quantified, 16 glycans showed significant variation (*p*-value < 0.05) in abundance. Network analysis and statistical testing revealed increased abundance particularly in larger, sialylated structures within *MYCN* amplified NLF cells that are associated with aggressive neuroblastoma. Further profiling these select glycans could provide the means to distinguish between high-risk *MYCN* amplified neuroblastoma from its low-risk, non-amplified counterpart, thereby opening up additional avenues of therapy in this disease.

7.2 Experiment

7.2.1 Materials

NLF and SY5Y cell lines were obtained from Dr. Garrett Brodeur at the Children's Hospital in Philadelphia. Borane-ammonia complex, sodium hydroxide beads, DMSO, iodomethane, MS-grade formic acid were purchased from Sigma-Aldrich (St. Louis, MO). Acetonitrile were obtained from Fisher Scientific (Pittsburgh, PA) and HPLC grade water was obtained from Mallinckrodt Chemicals (Phillipsburg, NJ). N-Glycosidase peptide purified from *Flavobacterium meningosepticum* (PNGase F) was procured from New England Biolabs Inc. (Ipswich, MA).

7.2.2 Cell Lysis

Both cell lines were collected and resuspended in 100 μL of PBS buffer. To insure efficient cell lysis, collected cells were frozen and thawed for several cycles. Then, the cell lines were sonicated in an ice bath for 1 h. The lysed cells were denatured at 80°C for another hour.

7.2.3 Release of N-linked Glycans

PNGase F was used for enzymatic release of N-glycans from glycoproteins. The denatured samples were mixed prior to the addition of 2.4- μL aliquot of PNGase F. Then, samples were incubated 37°C water bath for 18 h.

7.2.4 Dialysis and Reduction

The released N-glycans were purified by dialysis through cellulose ester (CE) membrane of molecular cut-off of 500 Da-1000 Da. An in-house built dialysis device was utilized for removing excess salts. The dialyzed samples were collected and dried under vacuum. Then, fresh ammonium-borane complex (10 $\mu\text{g}/\mu\text{L}$) was prepared and a 10- μL aliquot of aqueous was added to N-glycans. The samples were placed at 65 °C water bath for 1h before adding 10 μL acetic acid (10%). Then, the reaction mixtures were dry under vacuum. 300 μL of methanol was added into each sample and place in concentrator to dry the samples. This step was repeated several times to remove all borane complexes.

7.2.5 Permetylation

The reduced samples were further permethylated to increase the ionization efficiency of the native glycans. The permethylation was conducted according to published guidelines.^{48,66,67} Briefly, the reduced N-glycans were resuspended in 30 μL

DMSO, 20 μ L iodomethane, and 1.2 μ L water. The reaction mixtures were applied to sodium hydroxide beads filled spin column. The spin column was kept at room temperature for 25 min. Another 20 μ L iodomethane was applied to the top of the column and reacted for another 20 min. After reaction, the samples were spun down. 50 μ L of acetonitrile was applied to the top of the column and spinned down to elute the entire sample.

7.2.6 LC-MS/MS Conditions

Permethylated N-glycans were separated by nano-LC (Thermo Scientific, San Jose, CA) on reverse phase Acclaim[®] PepMap capillary column (150 mm x 75 μ m i.d) packed with 100 \AA C₁₈ bounded phase (Thermo Scientific). Separation was attained using a two solvent system; solvent A consisted of 2% acetonitrile and 98% water with 0.1% formic acid, while solvent B consisted of acetonitrile and 0.1% formic acid. Gradient conditions accomplished with 43%-60% solvent B over 32min at flow rate of 350 nL/min. LC separation was operated at 60°C. Nano-LC system interfaced to a Velos LTQ Orbitrap hybrid mass spectrometer (Thermo Scientific, San Jose, CA), thus allows mass spectrometry analysis after separation. The mass spectrometer was operated in an automated data-dependent acquisition mode in which the scan mode switched between MS full scan (m/z from 500-2000) and CID MS/MS scan which was conducted on the 4 most abundant ions with a 0.250 Q-value, 20 ms activation time, and 35% normalized collision energy. HCD MS/MS scan was conducted on the 4 most abundant ions with 0.1 ms activation time and 45% normalized collision energy. Analysis was performed in replicates of three per group (i.e. SY5Y and NLF).

7.2.7 Glycan Structural Assignment

The Xcalibur Qual Browser (Thermo Fisher Scientific) software was used to generate extracted-ion chromatograms from the full MS scans using glycan monoisotopic masses with a set mass tolerance of 10 ppm. A seven-point boxcar smoothing was enabled to improve the derived peak quality. Tandem mass spectra corresponding to glycan ions were manually annotated and diagnostic fragment ions were utilized to confirm the glycan structures.

7.2.8 Glycan Quantitation, Plotting and Statistical Characterization

Abundance values of glycans in each of the three replicates within SY5Y and NLF samples were obtained from their eXtracted Ion Chromatograms (XIC). Peak areas of different charge states and ion adducts were summed and used as a measure for glycan quantitation. Scatter plots built using the R statistical framework was used to confirm reproducibility in terms of correlation of glycan abundance between the replicates within each group. SPSS IBM Statistics software was used to perform a t-test in order to detect glycans with significant variation (p -value < 0.05) between SY5Y and NLF. A heatmap describing glycomic abundance profiles was built using heatmap.2 function in R (gplots package). Hierarchical clustering was performed using the hclust() function in R, on normalized glycan abundances (z-score normalized within each sample), using correlation as the similarity measure and method set to complete linkage.

Additionally, a glycan graph was built using Java Jtree library, where a pair of glycans were linked by a directed edge if the difference between their total monosaccharide counts increased by 1 in exactly one position, with the direction indicating increase in monosaccharide count. Node color and outline color was used to

indicate NLF versus SY5Y abundance variation. Finally, statistical testing for dependence of *MYCN* amplification on the total number of HexNAc and Hex monosaccharides, the number of sialic acid molecules, and the presence of fucosylation was conducted using linear-regression based on a generalized linear mixed model (glm function) in R. The response variable was set to 1 or 0 depending on whether the glycan was significantly increased in abundance in NLF as compared to SY5Y (*p*-value < 0.05). Covariate *p*-value estimates, based on the null hypothesis of the covariate being zero, was used to determine which of the dependent variables listed above had an effect on *MYCN* amplification.

7.3 Results and Discussion

7.3.1 Identification of Glycans in SY5Y and NLF Neuroblastoma Cell Lines

LC/ESI-MS data were processed using Xcalibur Qual Browser. The monoisotopic mass of each N-glycan structure was used to generate extracted-ion chromatograms. Mass tolerance was set to 10 ppm. There were 47 N-glycans derived from all three replicates within NFL and SY5Y cell lines that were detected by LC-MS according to their accurate mass. Glycan structures were annotated based on their accurate mass and tandem mass spectra. 38 N-glycans were confirmed through MSMS while the remaining seven have the *m/z* match with mass accuracy better than 2 ppm. The N-glycans with no tandem MS data were also confirmed through their retention time. HCD of sodium precursor ions yield more fragment information for N-glycan structure elucidation.

7.3.2 Quantitative Glycomic Profiling between SY5Y and NLF Cell Lines

Glycans were quantified using XIC values, after summation of peak areas across all adducts and charge states. **Figure 7.1** depicts the scatter plot of correlation scores

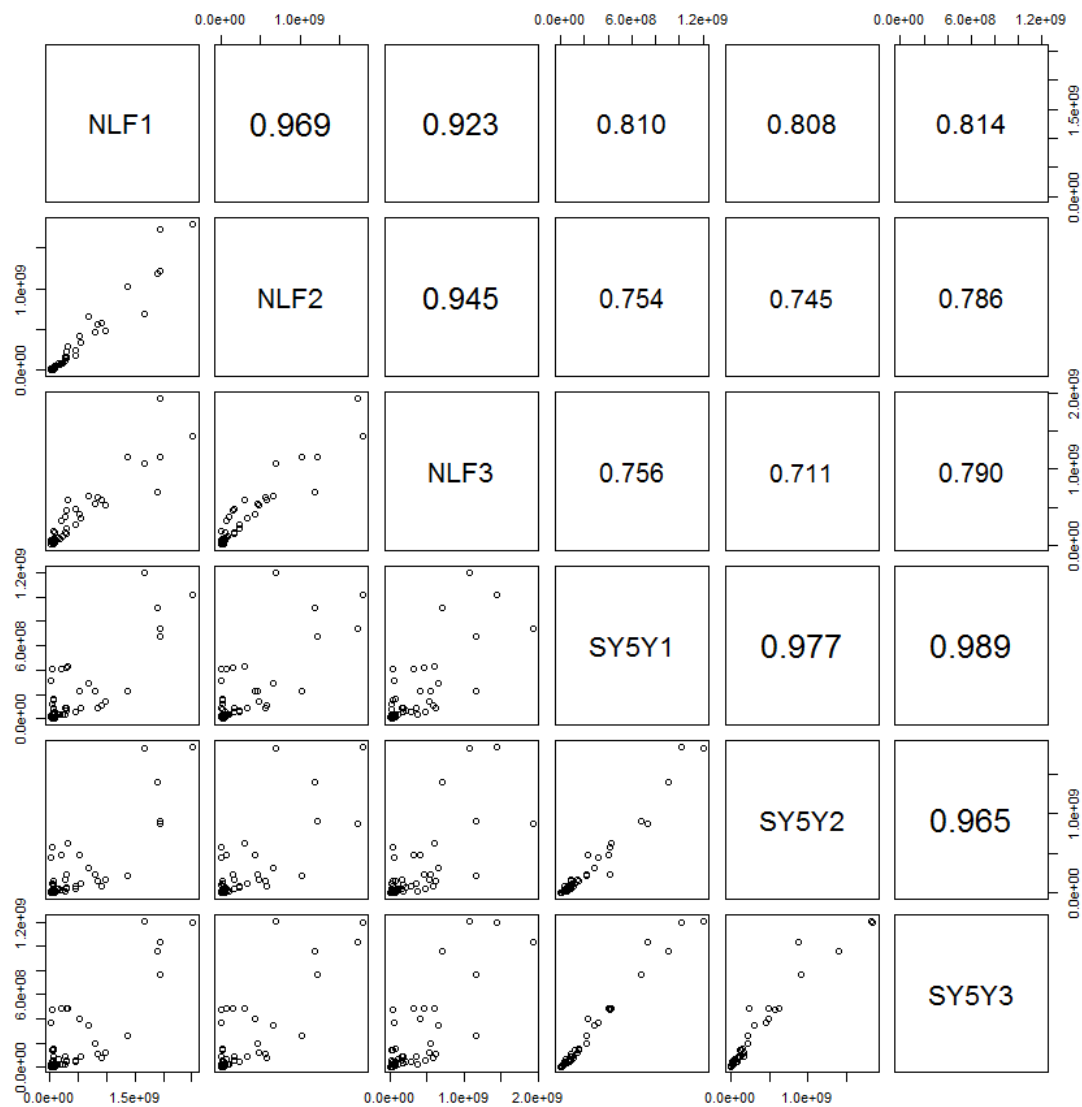
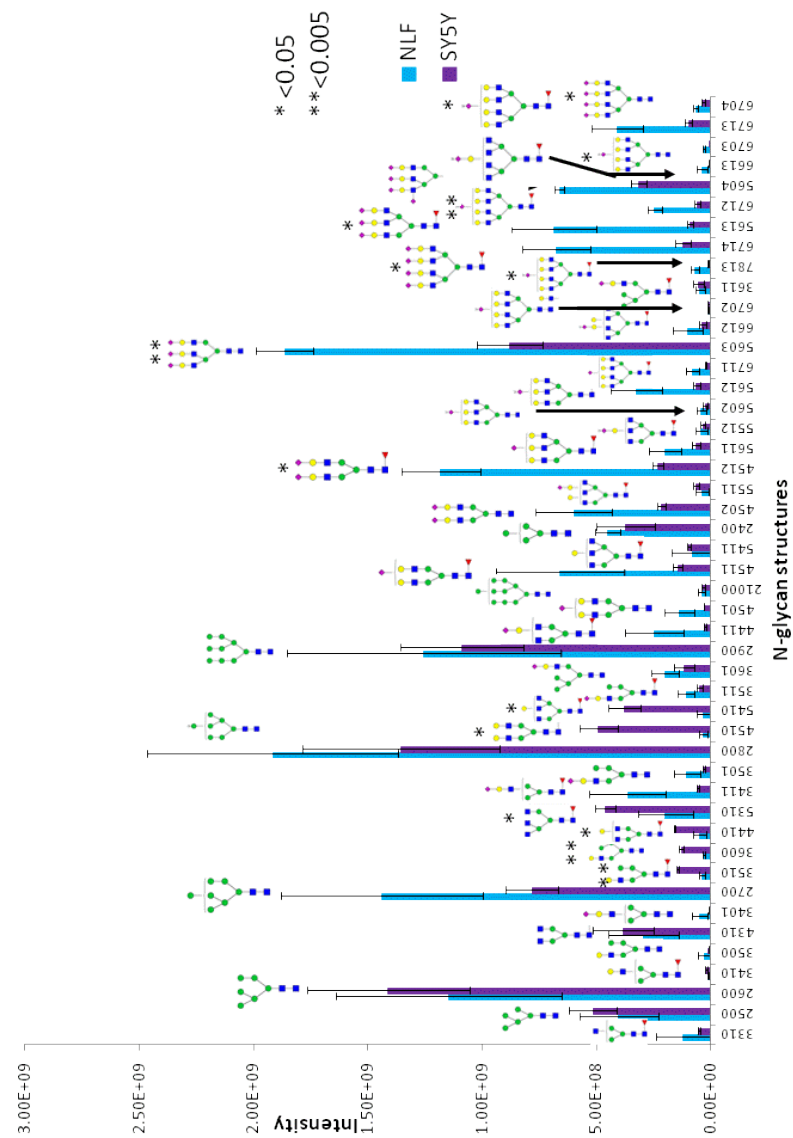


Figure 7.1 Scatter plot of detected glycan abundances (measured as XICs) within and across NLF and SY5Y cell lines. The plot trends along with cross-correlation measures depict high correlation between cell lines (indicative of good reproducibility) and low correlation across cell lines (indicative of change).

between abundance profiles of 47 glycans indicative of variation in both within and across cell lines. As can be seen the abundance values show high correlation (> 0.9) within cell lines, indicative of very high reproducibility. A lower correlation (0.7-0.8) was observed between glycan abundance across cell lines. Quantitative results of 47 glycans are shown in **Figure 7.2** and **Table 7.1**. In SY5Y, the top 3 most abundant glycans detected were all high-mannose glycans, HexNAc2Hex6, HexNAc2Hex7, and HexNAc2Hex8. The high-mannose glycan HexNAc2Hex8 was also the most abundant in NLF, with the triantenary tri-sialylted glycan HexNAc5Hex6NeuAc3 detected as a very close second and HexNAc2Hex7 third in abundance. Also shown in **Figure 7.2** are glycans with significant variation between SY5Y and NLF, as detected through using the t-test and indicated in Figure 2 by *. Table 1 depicts all 47 glycan in the order of increasing p-value. As can be seen, a total of 16 glycans were found to be differential expressed with significance (p-value < 0.05). The glycans that display the most significant increase in abundance in NLF when compared to SY5Y include HexNAc5Hex6NeuAc4 (p-value 8E-04), HexNAc5Hex6NeuAc3 (p-value 1E-03), and HexNAc6Hex7DeHex1NeuAc2 (p-value 3E-03), all which were sialylated. In contrast, the top glycans that display the most significant increase in abundance in SY5Y as compared to NLF include HexNAc3Hex6 (with p-value 1E-03), HexNAc3Hex5DeHex1 (p-value: 2E-03), and HexNAc5Hex4DeHex1 (p-value 8E-03), all of which were non-sialylated.

Figure 7.3 depicts the result of hierarchical clustering on normalized glycomic abundances. A clear division is observed at the highest split node of the hierarchical tree



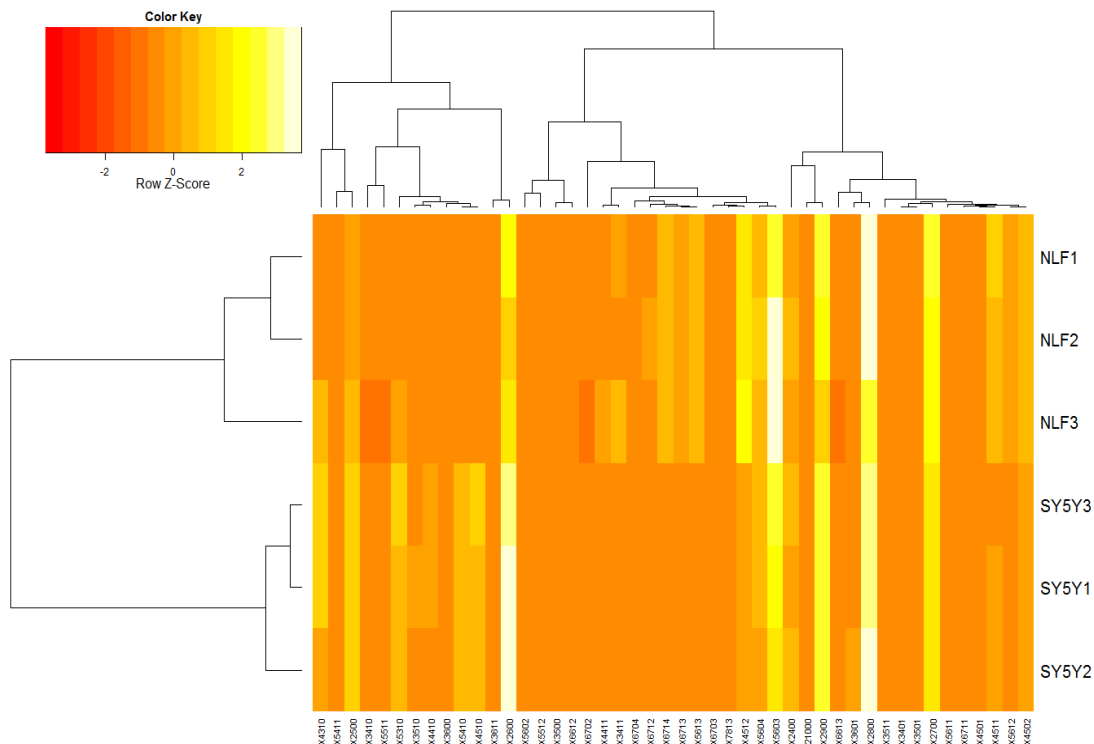


Figure 7.3 Hierarchical clustering of glycomic abundances. Each column is a glycan indicated as in a X-HexNAc-Hex-DeHex-NeuAc format. As can be observed, there is a split between glycans that are more abundant in SY5Y versus glycans that are more abundant in NLF. This illustrates that this particular glycan signature could be used for detecting *MYCN* amplification within neuroblastoma, and consequently for risk-stratification.

Table 7.1 List of N-glycans derived from NFL and SY5Y, along with derived topologies and p-values from a t-test comparison between groups. Glycans that show significant change in abundance between SY5Y and NFL cell lines are indicated by *.

Glycan	Composition	N-glycan Structure	p-value
1	HexNAc5Hex6NeuAc4		3E-04*
2	HexNAc3Hex6		1E-03*
3	HexNAc5Hex6NeuAc3		1E-03*
4	HexNAc3Hex5DeHex1		2E-03*
5	HexNAc6Hex7DeHex1NeuAc2		3E-03*
6	HexNAc5Hex4DeHex1		6E-03*
7	HexNAc6Hex7NeuAc3		8E-03*
8	HexNAc4Hex5DeHex1		9E-03*

Table 7.1 Continued

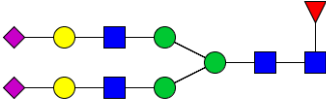
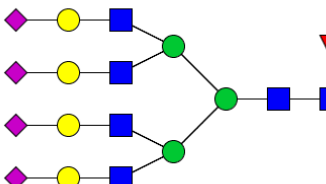
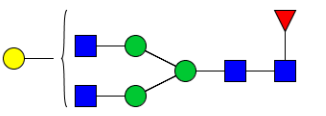
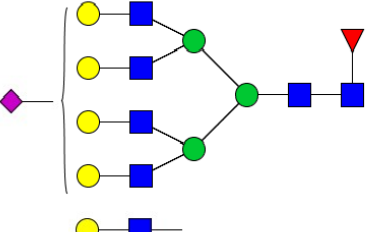
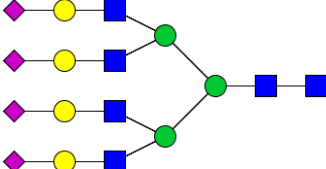
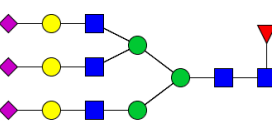
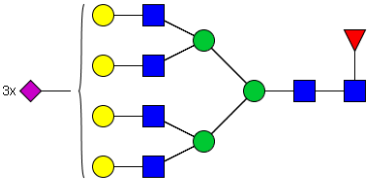
Glycan	Composition	N-glycan Structure	p-value
9	HexNAc4Hex5DeHex1N euAc2		0.010*
10	HexNAc6Hex7DeHex1N euAc4		0.019*
11	HexNAc4Hex4DeHex1		0.020*
12	HexNAc7Hex8DeHex1N euAc3		0.022*
13	HexNAc6Hex7NeuAc4		0.025*
14	HexNAc5Hex6DeHex1N euAc3		0.030*
15	HexNAc6Hex7DeHex1N euAc3		0.038*

Table 7.1 Continued

Glycan	Composition	N-glycan Structure	p-value
16	HexNAc5Hex3DeHex1		0.049*
17	HexNAc5Hex6DeHex1N euAc2		0.054
18	HexNAc4Hex5NeuAc2		0.057
19	HexNAc5Hex6DeHex1N euAc1		0.070
20	HexNAc3Hex4DeHex1		0.083
21	HexNAc6Hex7DeHex1N euAc1		0.083
22	HexNAc3Hex4DeHex1N euAc1		0.085
23	HexNAc4Hex5DeHex1N euAc1		0.085
24	HexNAc3Hex5DeHex1N euAc1		0.089

Table 7.1 Continued

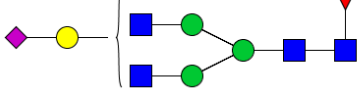
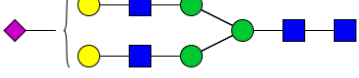
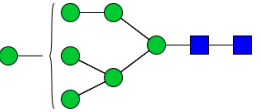
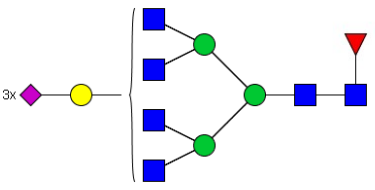
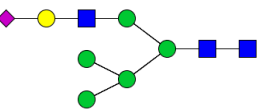
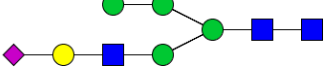
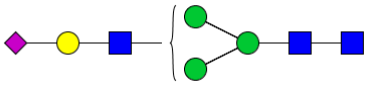
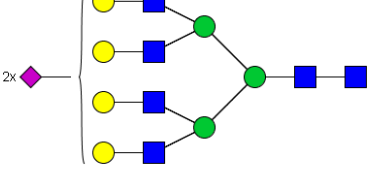
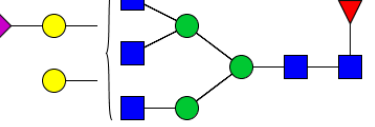
Glycan	Composition	N-glycan Structure	p-value
25	HexNAc4Hex4DeHex1N euAc1		0.095
26	HexNAc4Hex5NeuAc0		0.109
27	HexNAc2Hex7		0.116
28	HexNAc6Hex6DeHex1N euAc3		0.119
29	HexNAc3Hex6NeuAc1		0.128
30	HexNAc3Hex5NeuAc1		0.152
31	HexNAc3Hex4DeHex0N euAc1		0.168
32	HexNAc6Hex7NeuAc2		0.177
33	HexNAc5Hex5DeHex1N euAc1		0.225

Table 7.1 Continued

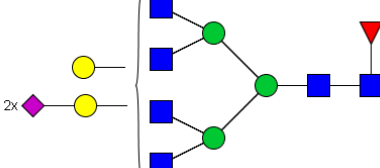
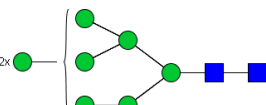
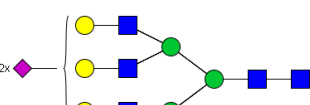
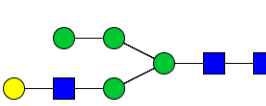
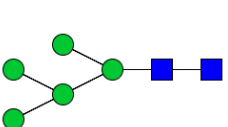
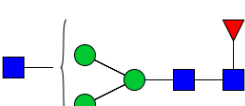
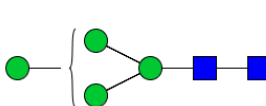
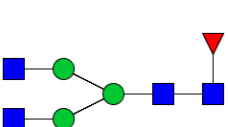
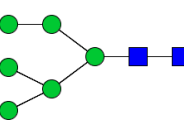
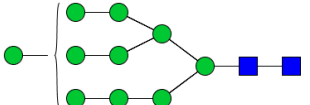
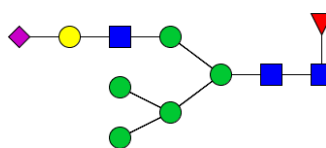
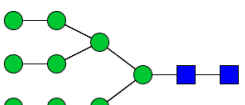
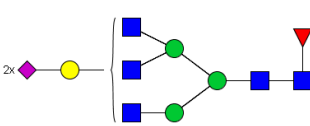
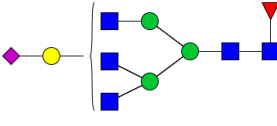
Glycan	Composition	N-glycan Structure	p-value
34	HexNAc6Hex6DeHex1NeuAc2		0.225
35	HexNAc2Hex8		0.239
36	HexNAc5Hex6NeuAc2		0.288
37	HexNAc3Hex5		0.389
38	HexNAc2Hex5		0.392
39	HexNAc3Hex3DeHex1		0.412
40	HexNAc2Hex4		0.413
41	HexNAc4Hex3DeHex1		0.488
42	HexNAc2Hex6		0.498

Table 7.1 Continued

Glycan	Composition	N-glycan Structure	p-value
43	HexNAc2Hex10		0.512
44	HexNAc3Hex6DeHex1N euAc1		0.622
45	HexNAc2Hex9		0.690
46	HexNAc5Hex5DeHex1N euAc2		0.712
47	HexNAc5Hex4DeHex1N euAc1		0.803

indicating that glycans that are more abundant in SY5Y versus glycans fall on one side as opposed to glycans that are more abundant in NLF which are located in the opposite cluster. This indicates that glycomic profiling could serve as a means for establishing a diagnostic signature towards risk-stratification in neuroblastoma.

7.3.3 MYCN Amplification Relationship with Monosaccharide Count and Sialylation

From **Figure 7.2**, it was observed that increased expression in larger glycans (i.e glycans with larger number of monosaccharides), along with increase in sialylation might be associated with *MYCN* amplification. To study this further, we created a ‘glycan graph’ as shown in **Figure 7.4** to illustrate relationship between glycan topology and *MYCN* amplification. Each node is a glycan and each directed edge signifies an increase in monosaccharide composition count by one in exactly one position among the monosaccharides. Glycans are layered according to total monosaccharide count, and thus each layer or tier of the graph is comprised of glycans with the same number of monosaccharides. The glycan graph is different from a glycan reaction network which indicates a stepwise addition and deletion of monosaccharides based on enzyme activity. For example, it is not possible to go from HexNac4Hex5DeHex1NeuAc1 to the glycan HexNAc5Hex5DeHex1Neu1 in a single reaction. The glycan graph is a useful means to illustrate relationship between glycan topology and abundance variations.

The smallest detected glycan HexNAc2Hex4 is situated in the top layer and the largest glycan HexNac6Hex7DeHex1NeuAc4 (with one non-terminal NeuAc) is at the lowest layer of the graph. Each node is colored according to whether the variation between SY5Y and NLF was significant ($p\text{-value} < 0.05$, yellow) or not ($p\text{-value} \geq 0.05$,

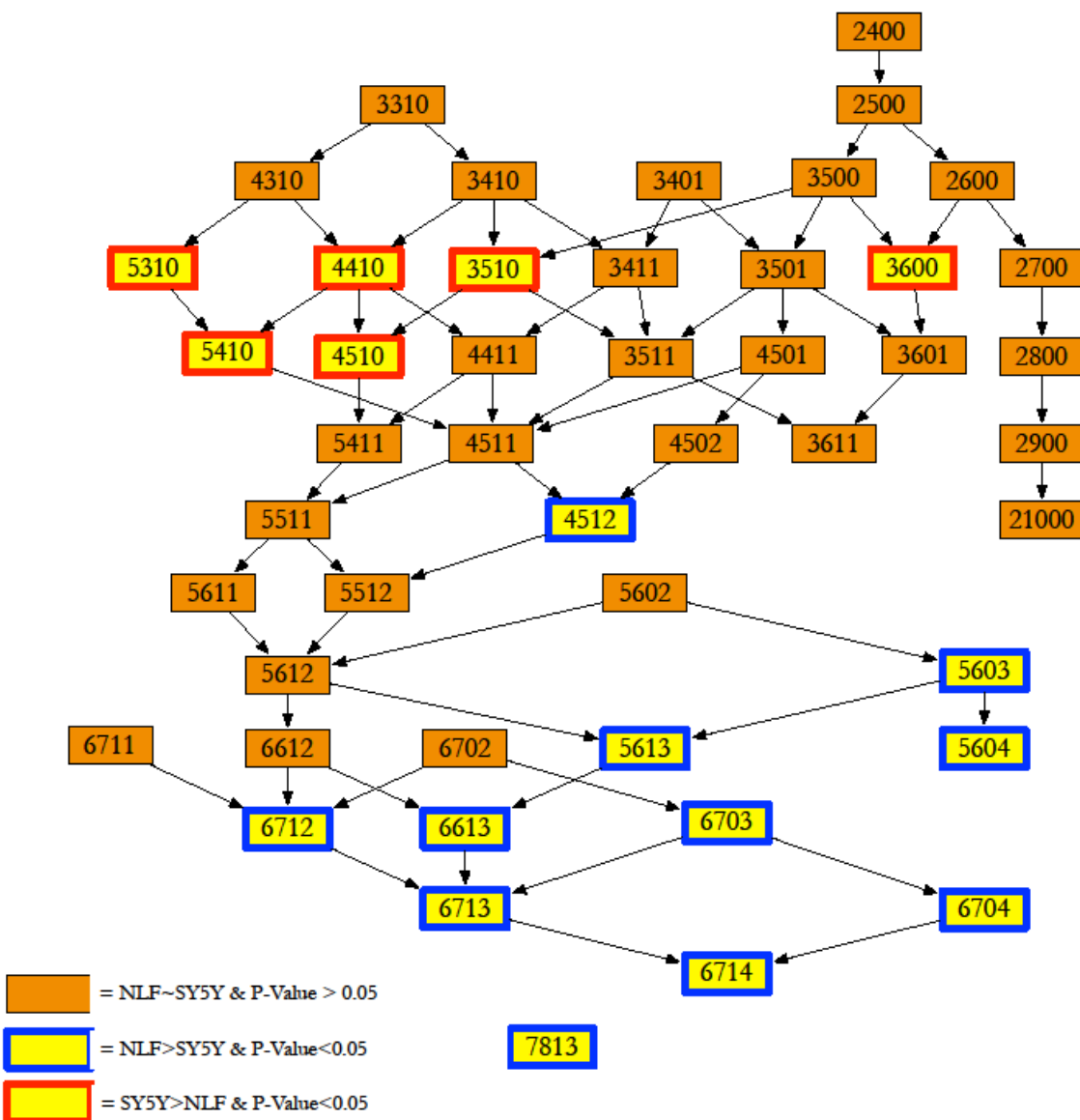


Figure 7.4 Glycan graph arranged according to total monosaccharide count. Each node is a glycan and two nodes are linked by a directed edge if the difference in monosaccharide count is +1 in only one position in the HexNAc-Hex-DeHex-NeuAc format. The glycan HexNAc7Hex8DeHex1Fuc3 was a single node without any edge connections. Orange boxes do not show significant change between SY5Y and NLF, where yellow boxes indicate glycans that show significant (p -value < 0.05) change in expression. The node color for the yellow boxes indicates if the glycan was more abundant in SY5Y (red) or NLF (blue). From the graph, there is evidence that bigger glycans and glycans with more sialylated structures are more abundant in *MYCN*-amplified NLF cells.

orange). For the glycans displaying significant change in abundance, the node outline is used to indicate greater abundance in SY5Y (red outline) or NLF (blue outline). Through this process, all glycans were mapped into the glycan graph (**Figure 7.4**) except for the largest glycan, HexNAc7Hex8DeHex1NeuAc3, which was a singleton without any connections. Interestingly, glycans that show a significant increase in expression in SY5Y are located at the top of the glycan graph, while glycans that show a significant increase in expression in NLF are located towards the bottom^{5,21}, but this study suggests the association between increased expression in larger glycans and *MYCN* amplification in neuroblastoma.

According to the graph, the first glycan that shows a statistically significant increase in NLF was HexNac4Hex5DeHex1NeuAc2. Interestingly, while both its parents (connected nodes directly above) do not show statistically significant difference in abundance, the trends are same: HexNAc4Hex5NeuAc2 and HexNac4Hex5DeHex1NeuAc1 are greater in NLF. Moving up the graph, we see that the path from HexNAc4Hex4DeHex1 - HexNAc4Hex4DeHex1NeuAc1-HexNAc4Hex5DeHex1NeuAc1 - HexNAc4Hex5DeHex1NeuAc2 indicates a gradual transition from a statistically increase in abundance in SY5Y to an increase abundance in NLF. Targeted studies aimed at these four glycans along with a study of sialyltransferase (in particular ST6GAL1 enzyme) activity should reveal more on this particular transition.

The association of increased sialylation with *MYCN* amplified NLF cells seems to be an overall effect, since glycans with 3 and 4 sialic acid molecules are situated at the bottom as opposed to 1 or no sialic acid terminations. In an attempt to estimate the effects of glycan size, increased sialylation and fucosylation in NLF cells, we performed a linear

regression using a generalized linear model (GLM). The binary response variable was set to 1 or 0 depending on whether the glycan showed a significant increase in abundance in NLF samples. The response was modeled as being dependent of HexNAc+Hex, number of NeuAc and presence of Dehex. The resulting p-values for parameter estimates depicted that the number of sialic acids (p-value = 0.0194, Table 2) was significant to *MYCN* amplification in neuroblastoma. A log-likelihood-based analysis of variance (ANOVA) comparison against a glm model considering only size and presence of fucose as covariates resulted in p-value (measured as chi-squared with 1 degree of freedom) of 2E10-3 (data not shown), thereby confirming the effect of increased sialic acid to *MYCN* amplification. Similar to glycan size, the relationship between increased sialylation and cancer has been well established^{5,201} and avenues of targeting aberrant sialylation are currently being explored.^{ENREF_200} Our results implicate that a study aimed at analyzing increased sialylation in neuroblastoma, by analyzing tumor samples and/or comparing glycomic abundances with sialyltransferase activity, could reveal potential targets for therapy.

7.4 Conclusion

In this study, we performed N-linked glycomic profile comparison between *MYCN* non-amplified SY5Y and *MYCN* amplified NLF neuroblastoma cell lines. Through a combination of LC-ESI-MS analytical platform and statistical analysis, a total of 47-glycans were profiled out of which sixteen depicted statistically significant differences between SY5Y and NLF. Further, preference for larger glycans and increased sialylation was detected in NLF samples. In particular, increased sialylation showed a statistical association with *MYCN* amplification in neuroblastoma. The results of this

study serve as a foundation for exploring aberrant glycosylation for risk-diagnosis as well as for therapeutic purposes in neuroblastoma, which is an avenue hitherto unexplored.

CHAPTER VIII

CONCLUSION AND FUTURE WORK

Glycosylation is the most popular PTMs which plays an important role in many biological processes. The development of analytical methods for glycomics study may help to elucidate the biological processes. Also, the glycosylation changes related to different disease states and progression may be used as potential biomarkers for disease diagnosis and prognosis. Full structural elucidation of glycoproteins may facilitate the development of therapeutic protein.

In this study, sample preparation steps were optimized to facilitate the sensitive detection of N-glycans by MS. The different ionization methods, MALDI and ESI, were compared for the detection of N-glycans. LC-ESI permits the detection of 73 glycans derived from HBS, while LC-MALDI allows the detection of 53 glycans. This indicates higher detection sensitivity of ESI compared to MALDI. Also, reliable quantification strategy which introduces isotopic reagents through permethylation and analyzed using LC-MS was developed. Iodomethane and deuterium iodomethane was incorporated into glycan and allows the relative quantification of four different samples. In the future work, ^{13}C can be introduced into the isotopic iodomethane reagents. Thus, an eight-plex MC-GlycoMAP, which allows the simultaneous relative quantification of eight different samples, will be developed. The mass difference of two reagents ($^{12}\text{CH}_2\text{DI}$ and $^{13}\text{CH}_3\text{I}$) labeled sample is between 30ppm to 50ppm, which depends on the labeling sites. Mass spectrometer with resolution of 100K is required for base line separation of two nearby peaks.

Another relative quantification strategy, TMT, has been introduced for the labeling of glycans. However, reliable quantification using TMT has not been accomplished. The major limitation is the low intensity of report ions, which is partially due to the overlap of glycan fragments and report ions. Improving MSMS reporter ions fragments is critical to achieve the reliable relative quantification of this method. Several parameters, such as collision energy and activation time can be optimized. Moreover, the fragmentation pattern of sodium adducts, potassium adducts and proton adducts can be evaluated to achieve high report ions efficiency.

The chromatogram behavior of permethylated N-glycans was investigated in this study. This study revealed there is a linear relationship between molecular weight and retention time for each glycan subgroup. This study aided in understanding the chromatographic mechanism governing the separation of permethylated glycans on C₁₈ column and utilized the model for N-glycan structure prediction. However, conducting the LC separation under room temperature limited the separation of structure isomers. In the future work, LC separation will be conducted at high temperature to improve the separation N-glycan isomers. The interaction of C₁₈ media and glycans under high temperature will be studied to better understand the separation mechanism. The relationship between the retention time and molecular weight may be utilize for the prediction of isomeric structures.

A new glycan sample preparation strategy was developed for N-glycan profiling of tissue sections. With this new developed strategy, 43 glycans were detected using mouse brain tissue section. N-glycan profiling of mouse brain tissue sections was accomplished at 1.5 mm diameter tissue surface. The surface is kept wet by manually

adding water every twenty minutes. However, this process increases the standard deviation between samples as a result of droplet diffusion size and inconsistent surface interactions between the pipette and glass. To eliminate the droplet diffusion and acquire the spatial resolution of tissue section, a microliter deposition device will be used in the future for on surface digestion. The microliter deposition device consists of a teflon template, a teflon tape backing, aluminum backing and metal framework. The teflon template has an arrangement of holes of fixed diameter in which the enzyme will be placed to react with the tissue sample underneath. When assembled, the Teflon template will be placed on the top of glass slide with tissue sections. The Teflon tape backing and aluminum backing will be placed under the tissue sections. The metal framework will hold all of these components together. The bottom of the metal framework has 48 Teflon-tip set screws arranged in a grid pattern. These screws enable the tight between Teflon template and glass and prevent the diffusion of the enzyme droplet. The microliter deposition device may facilitate the high throughput sample preparation and also provide a convenient way to increase the reproducibility of sample preparation. Moreover, the spatial resolution will be increased by decreasing the droplet size.

REFERENCE

- [1] N. Blom, T. Sicheritz-Ponten, R. Gupta, S. Gammeltoft, S. Brunak, *Proteomics* 4 (2004) 1633-1649.
- [2] R. S. Haltiwanger, J. B. Lowe, *Annu. Rev. Biochem.* 73 (2004) 491-537.
- [3] A. Helenius, M. Aebi, *Science* 291 (2001).
- [4] A. Varki, *Glycobiology* 3 (1993) 97-130.
- [5] D. H. Dube, C. R. Bertozzi, *Nature Reviews Drug Discovery* 4 (2005) 477-488.
- [6] B. J. Campbell, L. G. Yu, J. M. Rhodes, *Glycoconjugate Journal* 18 (2001) 851-858.
- [7] R. Malhotra, M. R. Wormald, P. M. Rudd, P. B. Fischer, R. A. Dwek, R. B. Sim, *Nature Medicine* 1 (1995) 599-599.
- [8] J. Z. Wang, I. GrundkeIqbali, K. Iqbal, *Nature Medicine* 2 (1996) 871-875.
- [9] A. Botella-Lopez, F. Burgaya, R. Gavin, M. S. Garcia-Ayllon, E. Gomez-Tortosa, J. Pena-Casanova, J. M. Urena, J. A. Del Rio, R. Blesa, E. Soriano, J. Saez-Valero, *Proceedings of the National Academy of Sciences of the United States of America* 103 (2006) 5573-5578.
- [10] S. Hakomori, *Cancer Research* 45 (1985) 2405-2414.
- [11] Y. J. Kim, A. Varki, *Glycoconjugate Journal* 14 (1997) 569-576.
- [12] C. A. Reis, H. Osorio, L. Silva, C. Gomes, L. David, *Journal of Clinical Pathology* 63 (2010) 322-329.
- [13] Y. Mechref, Y. Hu, A. Garcia, A. Hussein, *Electrophoresis* 33 (2012) 1755-1767.
- [14] M. N. Christiansen, J. Chik, L. Lee, M. Anugraham, J. L. Abrahams, N. H. Packer, *Proteomics* 14 (2014) 525-546.
- [15] U. M. Abd Hamid, L. Royle, R. Saldova, C. M. Radcliffe, D. J. Harvey, S. J. Storr, M. Pardo, R. Antrobus, C. J. Chapman, N. Zitzmann, J. F. Robertson, R. A. Dwek, P. M. Rudd, *Glycobiology* 18 (2008) 1105-1118.
- [16] C. Kirmiz, B. S. Li, H. J. An, B. H. Clowers, H. K. Chew, K. S. Lam, A. Ferrige, R. Alecio, A. D. Borowsky, S. Sulaimon, C. B. Lebrilla, S. Miyamoto, *Molecular & Cellular Proteomics* 6 (2007) 43-55.
- [17] R. Saldova, J. M. Reuben, U. M. A. Hamid, P. M. Rudd, M. Cristofanilli, *Annals of Oncology* 22 (2011) 1113-1119.
- [18] J. A. Goetz, Y. Mechref, P. Kang, M.-H. Jeng, M. V. Novotny, *Glycoconjugate Journal* 26 (2009) 117-131.
- [19] W. R. Alley, Jr., M. Madera, Y. Mechref, M. V. Novotny, *Analytical Chemistry* 82 (2010) 5095-5106.
- [20] W. R. Alley, Jr., M. V. Novotny, *Journal of Proteome Research* 9 (2010) 3062-3072.
- [21] Z. Kyselova, Y. Mechref, P. Kang, J. A. Goetz, L. E. Dobrolecki, G. W. Sledge, L. Schnaper, R. J. Hickey, L. H. Malkas, M. V. Novotny, *Clinical Chemistry* 54 (2008) 1166-1175.
- [22] I. O. Potapenko, V. D. Haakensen, T. Luders, A. Helland, I. Bukholm, T. Sorlie, V. N. Kristensen, O. C. Lingjaerde, A. L. Borresen-Dale, *Mol. Oncol.* 4 (2010) 98-118.
- [23] J. Renkonen, T. Paavonen, R. Renkonen, *Int. J. Cancer* 74 (1997) 296-300.
- [24] S. Hundt, U. Haug, H. Brenner, *Onkologie* 31 (2008) 65-65.
- [25] M. Trinchera, N. Malagolini, M. Chiricolo, D. Santini, F. Minni, A. Caretti, F. Dall'Olio, *International Journal of Biochemistry & Cell Biology* 43 (2011) 130-139.
- [26] R. S. Bresalier, S. B. Ho, H. L. Schoeppner, Y. S. Kim, M. H. Sleisenger, P. Brodt, J. C. Byrd, *Gastroenterology* 110 (1996) 1354-1367.

- [27] A.-S. Vercoutter-Edouart, M.-C. Slomianny, O. Dekeyzer-Beseme, J.-F. Haeuw, J.-C. Michalski, *Proteomics* 8 (2008) 3236-3256.
- [28] R. Goldman, H. W. Ressom, R. S. Varghese, L. Goldman, G. Bascug, C. A. Loffredo, M. Abdel-Hamid, I. Gouda, S. Ezzat, Z. Kyselova, Y. Mechref, M. V. Novotny, *Clinical Cancer Research* 15 (2009) 1808-1813.
- [29] D. Isailovic, R. T. Kurulugama, M. D. Plasencia, S. T. Stokes, Z. Kyselova, R. Goldman, Y. Mechref, M. V. Novotny, D. E. Clemmer, *Journal of Proteome Research* 7 (2008) 1109-1117.
- [30] A. Takada, K. Ohmori, T. Yoneda, K. Tsuyuoka, A. Hasegawa, M. Kiso, R. Kannagi, *Cancer Research* 53 (1993) 354-361.
- [31] F. Dall'Olio, M. Chiricolo, A. D'Errico, E. Gruppioni, A. Altimari, M. Fiorentino, W. F. Grigioni, *Glycobiology* 14 (2004) 39-49.
- [32] B. Li, H. J. An, C. Kirmiz, C. B. Lebrilla, K. S. Lam, S. Miyamoto, *Journal of Proteome Research* 7 (2008) 3776-3788.
- [33] H. J. An, S. Miyamoto, K. S. Lancaster, C. Kirmiz, B. Li, K. S. Lam, G. S. Leiserowitz, C. B. Lebrilla, *Journal of Proteome Research* 5 (2006) 1626-1635.
- [34] T. I. Williams, D. A. Saggese, D. C. Muddiman, *Journal of Proteome Research* 7 (2008) 2562-2568.
- [35] E. Machado, S. Kandzia, R. Carilho, P. Altevogt, H. S. Conradt, J. Costa, *Glycobiology* 21 (2011) 376-386.
- [36] V. Tretter, F. Altmann, L. Marz, *European Journal of Biochemistry* 199 (1991) 647-652.
- [37] S. M. Haslam, G. C. Coles, E. A. Munn, T. S. Smith, H. F. Smith, H. R. Morris, A. Dell, *Journal of Biological Chemistry* 271 (1996) 30561-30570.
- [38] H. Geyer, R. Geyer, *Biochimica et biophysica acta* 1764 (2006) 1853-1869.
- [39] D. M. Carlson, *Biol. Chem.* 243 (1968) 616-626.
- [40] Y. Huang, Y. Mechref, M. V. Novotny, *Anal. Chem.* 73 (2001) 6063-6069.
- [41] Y. Mechref, M. V. Novotny, *Chem. Rev.* 102 (2002) 321-369.
- [42] J. A. Goetz, M. V. Novotny, Y. Mechref, *Anal. Chem.* 81 (2009) 9546-9552.
- [43] A. H. Merry, D. C. A. Neville, L. Royle, B. Matthews, D. J. Harvey, R. A. Dwek, P. M. Rudd, *Analytical Biochemistry* 304 (2002) 91-99.
- [44] M. F. Verostek, C. Lubowski, R. B. Trimble, *Analytical Biochemistry* 278 (2000) 111-122.
- [45] C. E. Costello, J. M. Contado-Miller, J. F. Cipollo, *Journal of the American Society for Mass Spectrometry* 18 (2007) 1799-1812.
- [46] M. L. A. de Leoz, H. J. An, S. Kronewitter, J. Kim, S. Beecroft, R. Vinall, S. Miyamoto, R. d. V. White, K. S. Lam, C. Lebrilla, *Disease Markers* 25 (2008) 243-258.
- [47] S. R. Kronewitter, H. J. An, M. L. de Leoz, C. B. Lebrilla, S. Miyamoto, G. S. Leiserowitz, *Proteomics* 9 (2009) 2986-2994.
- [48] P. Kang, Y. Mechref, I. Klouckova, M. V. Novotny, *Rapid Commun. Mass Spectrom.* 19 (2005) 3421-3428.
- [49] S. Hase, T. Ikenaka, Y. Matsushima, *Biochemical and biophysical research communications* 85 (1978) 257-263.
- [50] K. R. Anumula, *Anal. Biochem.* 220 (1994) 275-283.
- [51] J. C. Bigge, T. P. Patel, J. A. Bruce, P. N. Goulding, S. M. Charles, R. B. Parekh, *Anal. Biochem.* 230 (1995) 229-238.

- [52] D. Maury, F. Couderc, J. Czaplicki, J. C. Garrigues, V. Poinsot, Biomedical chromatography : BMC 24 (2010) 343-346.
- [53] G. Okafu, J. Langridge, S. North, A. Organ, A. West, M. Morris, P. Camilleri, Anal. Chem. 69 (1997) 4985-4993.
- [54] K. Kakehi, T. Funakubo, S. Suzuki, Y. Oda, Y. Kitada, Journal of chromatography. A 863 (1999) 205-218.
- [55] K. Nakajima, Y. Oda, M. Kinoshita, T. Masuko, K. Kakehi, The Analyst 127 (2002) 972-976.
- [56] H. Schwaiger, P. J. Oefner, C. Huber, E. Grill, G. K. Bonn, Electrophoresis 15 (1994) 941-952.
- [57] N. K. Karamanos, T. Tsegenidis, C. A. Antonopoulos, J Chromatogr 405 (1987) 221-228.
- [58] W. Vondern, W. S. York, P. Albersheim, A. G. Darvill, Carbohydr Res 201 (1990) 135-144.
- [59] D. Sugahara, J. Amano, T. Irimura, Anal Sci 19 (2003) 167-169.
- [60] E. Lattova, H. Perreault, Journal of chromatography. B, Analytical technologies in the biomedical and life sciences 793 (2003) 167-179.
- [61] T. J. P. Naven, D. J. Harvey, Rapid Commun. Mass Spectrom. 10 (1998) 829-834.
- [62] G. C. Gil, Y. G. Kim, B. G. Kim, Anal. Biochem. 379 (2008) 45-59.
- [63] J. W. Gouw, P. C. Burgers, M. A. Trikoupis, J. K. Terlouw, Rapid Commun Mass Sp 16 (2002) 905-912.
- [64] S. H. Walker, L. M. Lilley, M. F. Enamorado, D. L. Comins, D. C. Muddiman, Journal of the American Society for Mass Spectrometry 22 (2011) 1309-1317.
- [65] C. I. Kerek, I. Ciucanu, Carbohydrate Res. 131 (1984) 209-217.
- [66] P. Kang, Y. Mechref, M. V. Novotny, Rapid Commun. Mass Spectrom 22 (2008) 721-734.
- [67] Y. Mechref, P. Kang, M. V. Novotny In *Glycomics: Methods and Protocols*; Packer, N. H., Karlsson, N. G., Eds. 2009; Vol. 534, p 53-64.
- [68] J. A. Saba, X. D. Shen, J. C. Jamieson, H. Perreault, Journal of Mass Spectrometry 36 (2001) 563-574.
- [69] L. A. Gennaro, J. Delaney, P. Vouros, D. J. Harvey, B. Domon, Rapid Commun Mass Sp 16 (2002) 192-200.
- [70] F.-T. Chen, R. A. Evangelista, Electrophoresis 19 (1998) 2639-2644.
- [71] R. A. Evangelista, F.-T. Chen, A. Guttmann, Journal of chromatography. A 745 (1996) 273-280.
- [72] A. Guttmann, F.-T. A. Chen, R. Evangelista, A., N. Cooke, Anal. Biochem. 233 (1996) 234-242.
- [73] A. Guttmann, F.-T. Chen, R. A. Evangelista, Electrophoresis 17 (1996) 412-417.
- [74] A. Guttmann, T. Pritchett, Electrophoresis 16 (1995) 1906-1911.
- [75] H. Suzuki, O. Mueller, A. Guttmann, B. L. Karger, Anal. Chem. 69 (1997) 4554-4559.
- [76] Y. Mechref, J. Muzikar, M. V. Novotny, Electrophoresis 26 (2005) 2034-2046.
- [77] M. Wuhrer, C. A. M. Koeleman, A. M. Deelder, C. N. Hokke, Analytical Chemistry 76 (2004) 833-838.
- [78] J. Zhao, W. Qiu, D. M. Simeone, D. M. Lubman, Journal of Proteome Research 6 (2007) 1126-1138.

- [79] H. Geyer, M. Wuhrer, A. Resemann, R. Geyer, *Journal of Biological Chemistry* 280 (2005) 40731-40748.
- [80] T. S. Mattu, L. Royle, J. Langridge, M. R. Wormald, P. E. Van den Steen, J. Van Damme, G. Opdenakker, D. J. Harvey, R. A. Dwek, P. M. Rudd, *Biochemistry* 39 (2000) 15695-15704.
- [81] B. Garner, A. H. Merry, L. Royle, D. J. Harvey, P. M. Rudd, J. Thillet, *Journal of Biological Chemistry* 276 (2001) 22200-22208.
- [82] M. P. Campbell, L. Royle, C. M. Radcliffe, R. A. Dwek, P. M. Rudd, *Bioinformatics* 24 (2008) 1214-1216.
- [83] M. Pabst, F. Altmann, *Analytical Chemistry* 80 (2008) 7534-7542.
- [84] M. Pabst, J. S. Bondili, J. Stadlmann, L. Mach, F. Altmann, *Analytical Chemistry* 79 (2007) 5051-5057.
- [85] S. H. Walker, B. C. Carlisle, D. C. Muddiman, *Analytical Chemistry* 84 (2012) 8198-8206.
- [86] F. G. Hanisch, S. Muller, *Methods Mol. Biol.* 534 (2009) 107-115.
- [87] B. Stahl, M. Steup, M. Karas, F. Hillenkamp, *Analytical Chemistry* 63 (1991) 1463-1466.
- [88] B. Stahl, S. Thurl, J. R. Zeng, M. Karas, F. Hillenkamp, M. Steup, G. Sawatzki, *Analytical Biochemistry* 223 (1994) 218-226.
- [89] J. O. Metzger, R. Woisch, W. Tuszyński, R. Angermann, *Fresen J Anal Chem* 349 (1994) 473-474.
- [90] J. Yuan, N. Hashii, N. Kawasaki, S. Itoh, T. Kawanishi, T. Hayakawa, *Journal of chromatography. A* 1067 (2005) 145-152.
- [91] A. M. Hitchcock, C. E. Costello, J. Zaia, *Biochemistry* 45 (2006) 2350–2361.
- [92] J. M. Prien, B. D. Prater, Q. Qin, S. L. Corckrill, *Anal. Chem.* 82 (2010) 1498-1508.
- [93] R. Lawrence, S. K. Olson, R. E. Steele, L. Wang, R. Warrior, R. D. Cummings, J. D. Esko, *J. Biol. Chem.* 283 (2008) 33674-33684.
- [94] M. J. Bowman, J. Zaia, *Anal. Chem.* 79 (2007) 5777-5784.
- [95] M. J. Bowman, J. Zaia, *Anal. Chem.* 82 (2010) 3023-3031.
- [96] P. Kang, Y. Mechref, Z. Kyselova, J. A. Goetz, M. V. Novotny, *Anal. Chem.* 79 (2007) 6064-6073.
- [97] J. A. Atwood III, L. Cheng, G. Alvarez-Manilla, N. L. Warren, W. S. York, R. Orlando, *J. Proteome Res.* 7 (2008) 367-374.
- [98] J. C. Botelho, J. A. Atwood III, C. L., G. Alvarez-Manilla, W. S. York, R. Orlando, *Int. J. Mass spectrom.* 287 (2008) 137-142.
- [99] K. Aoki, M. Perlman, J.-M. Lim, R. Cantu, L. Wells, M. Tiemeyer, *J. Biol. Chem.* 282 (2007) 9127-9142.
- [100] H. Hahne, P. Neubert, K. Kuhn, C. Etienne, R. Bomgarden, J. C. Rogers, B. Kuster, *Anal. Chem.* 84 (2012) 3716-3724.
- [101] B. Gong, E. Hoyt, H. Lynaugh, I. Burnina, R. Moore, A. Thompson, H. Li, *Anal. Bioanal. Chem.* 405 (2013) 5825–5831.
- [102] R. Orlando, J.-M. Lim, J. A. Atwood III, P. M. Angel, M. Fang, K. Aoki, G. Alvarez-Manilla, K. W. Moremen, W. S. York, M. Tiemeyer, M. Pierce, S. Dalton, L. Wells, *J. Proteome Res.* 8 (2009) 3816-3823.
- [103] M. A. Breidenbach, J. E. G. Gallagher, D. S. Kingc, B. P. Smarta, P. Wua, C. R. Bertozzia, *Proc. Natl. Acad. Sci. USA* 107 (2010) 3988–3993.

- [104] D. Goldberg, M. Sutton-Smith, J. Paulson, A. Dell, *Proteomics* 5 (2005) 865-875.
- [105] A. Ceroni, K. Maass, H. Geyer, R. Geyer, A. Dell, S. M. Haslam, *J. Proteome Res.* 7 (2008) 1650-1659.
- [106] N. Jaitly, A. Mayampurath, K. Littlefield, J. N. Adkins, A. G.A., R. D. Smith, *BMC Bioinformatics* 10.1 (2009) 87.
- [107] E. Maxwell, Y. Tan, Y. Tan, H. Hu, G. Benson, K. Aizikov, S. Conley, G. O. Staples, G. W. Slysz, R. D. Smith, J. Zaia, *PLoS One* 7.9 (2012) e45474.
- [108] P. M. Rudd, T. Elliott, P. Cresswell, I. A. Wilson, R. A. Dwek, *Science* 291 (2001) 2370-2376.
- [109] J. L. Stanta, R. Saldova, W. B. Struwe, J. C. Byrne, F. M. Leweke, M. Rothermund, H. Rahmoune, Y. Levin, P. C. Guest, S. Bahn, P. M. Rudd, *Journal of Proteome Research* 9 (2010) 5510-5510.
- [110] Y. Mechref, A. Hussein, S. Bekesova, V. Pungpapong, M. Zhang, L. E. Dobrolecki, R. J. Hickey, Z. T. Hammond, M. V. Novotny, *Journal of Proteome Research* 8 (2009) 2656-2666.
- [111] C. Chen, H. Schmilovtz-Weiss, X.-e. Liu, O. Pappo, M. Halpern, J. Sulkes, M. Braun, M. Cohen, N. Barak, R. Tur-Kaspa, V. Vanhooren, H. Van Vlierberghe, C. Libert, R. Contreras, Z. Ben-Arl, *Journal of Proteome Research* 8 (2009) 463-470.
- [112] P. Babu, S. J. North, J. Jang-Lee, S. Chalabi, K. Mackerness, S. R. Stowell, R. D. Cummings, S. Rankin, A. Dell, S. M. Haslam, *Glycoconjugate Journal* 26 (2009) 975-986.
- [113] K. Paschinger, E. Razzazi-Fazeli, K. Furukawa, I. B. H. Wilson, *Journal of Mass Spectrometry* 46 (2011) 561-567.
- [114] X. Wang, M. R. Emmett, A. G. Marshall, *Analytical Chemistry* 82 (2010) 6542-6548.
- [115] C. Bruggink, M. Wuhrer, C. A. M. Koeleman, V. Barreto, Y. Liu, C. Pohl, A. Ingendoh, C. H. Hokke, A. M. Deelder, *Journal of Chromatography B-Analytical Technologies in the Biomedical and Life Sciences* 829 (2005) 136-143.
- [116] G. Chataigne, F. Couderc, V. Poinsot, *Journal of Chromatography A* 1185 (2008) 241-250.
- [117] M. S. Bereman, T. I. Williams, D. C. Muddiman, *Analytical Chemistry* 81 (2009) 1130-1136.
- [118] L. Mauko, A. Nordborg, J. P. Hutchinson, N. A. Lacher, E. F. Hilder, P. R. Haddad, *Analytical Biochemistry* 408 (2011) 235-241.
- [119] J. Wohlgemuth, M. Karas, W. Jiang, R. Hendriks, S. Andrecht, *Journal of Separation Science* 33 (2010) 880-890.
- [120] M. P. Y. Lam, S. O. Siu, E. Lau, X. Mao, H. Z. Sun, P. C. N. Chiu, W. S. B. Yeung, D. M. Cox, I. K. Chu, *Analytical and Bioanalytical Chemistry* 398 (2010) 791-804.
- [121] M. S. Bereman, D. D. Young, A. Deiters, D. C. Muddiman, *Journal of Proteome Research* 8 (2009) 3764-3770.
- [122] Q. Luo, T. Rejtar, S.-L. Wu, B. L. Karger, *Journal of Chromatography A* 1216 (2009) 1223-1231.
- [123] G. O. Staples, M. J. Bowman, C. E. Costello, A. M. Hitchcock, J. M. Lau, N. Leymarie, C. Miller, H. Naimy, X. Shi, J. Zaia, *Proteomics* 9 (2009) 686-695.

- [124] J. M. Dreyfuss, C. Jacobs, Y. Gindin, G. Benson, G. O. Staples, J. Zaia, Analytical and Bioanalytical Chemistry 399 (2011) 727-735.
- [125] N. Kawasaki, S. Itoh, M. Ohta, T. Hayakawa, Analytical Biochemistry 316 (2003) 15-22.
- [126] M. Ninonuevo, H. J. An, H. F. Yin, K. Killeen, R. Grimm, R. Ward, B. German, C. Lebrilla, Electrophoresis 26 (2005) 3641-3649.
- [127] A. Dell, H. R. Morris, F. Greer, J. M. Redfern, M. E. Rogers, G. Weisshaar, J. Hiyama, A. G. C. Renwick, Carbohydr Res 209 (1991) 33-50.
- [128] A. Dell, J. Jang-Lee, P.-C. Pang, S. Parry, M. Sutton-Smith, B. Tissot, H. R. Morris, M. Panico, S. M. Haslam *Glycomics and Mass Spectrometry*; Springer: Heidelberg, 2008.
- [129] I. Ciucanu, C. E. Costello, Journal of the American Chemical Society 125 (2003) 16213-16219.
- [130] J. Delaney, P. Vouros, Rapid Commun Mass Sp 15 (2001) 325-334.
- [131] J. L. Desantos-Garcia, S. I. Khalil, A. Hussein, Y. Hu, Y. Mechref, Electrophoresis 32 (2011) 3516-3525.
- [132] Y. Mechref, M. V. Novotny, Analytical Chemistry 70 (1998) 455-463.
- [133] Y. Huang, Y. Mechref, M. V. Novotny, Analytical Chemistry 73 (2001) 6063-6069.
- [134] D. T. Fu, L. Chen, R. A. O'Neill, Carbohydr Res 261 (1994) 173-186.
- [135] J. Charlwood, H. Birrell, A. Organ, P. Camilleri, Rapid Commun Mass Sp 13 (1999) 716-723.
- [136] P. Deward, A. Koorevaar, J. P. Kamerling, J. F. G. Vliegenthart, Journal of Biological Chemistry 266 (1991) 4237-4243.
- [137] T. Tsuji, K. Yamamoto, T. Irimura, T. Osawa, Biochemical Journal 195 (1981) 691-699.
- [138] K. Yamamoto, T. Tsuji, T. Irimura, T. Osawa, Biochemical Journal 195 (1981) 701-713.
- [139] S. F. Wheeler, P. Domann, D. J. Harvey, Rapid Commun Mass Sp 23 (2009) 303-312.
- [140] R. Apweiler, H. Hermjakob, N. Sharon, Biochim. Biophys. Acta: Gen. Subjects 1473 (1999) 4-8.
- [141] G. W. Hart, R. J. Copeland, Cell 143 (2010) 672-676.
- [142] J. W. Dennis, M. Granovsky, C. E. Warren, Bioassays 21 (1999) 412-421.
- [143] J. W. Dennis, S. Laferte, C. Waghorne, M. L. Breitman, R. S. Kerbel, Science 236 (1987) 582-585.
- [144] S. Hakomori, Cancer Res. 56 (1996) 5309-5318.
- [145] S. Hakomori, Proc. Nat. Acad. Sci. U.S.A. 16 (2002) 10232-10233.
- [146] M. V. Dwek, H. A. Lacey, A. J. C. Leathem, Clin. Chim. Acta 271 (1998) 191-202.
- [147] R. A. Dwek, Chem. Rev. 96 (1996) 683-720.
- [148] H. J. An, S. R. Kronewitter, M. L. A. de Leoz, C. B. Lebrilla, Current Opinion in Chemical Biology 13 (2009) 601-607.
- [149] I. Brockhausen, J. M. Yang, J. Burchell, C. Whitehouse, J. Taylorpapadimitriou, European Journal of Biochemistry 233 (1995) 607-617.
- [150] B. Davidson, W. H. Gotlieb, G. Ben-Baruch, J. Kopolovic, I. Goldberg, J. M. Nesland, A. Berner, A. Bjamer, M. Bryne, Gynecologic Oncology 77 (2000) 35-43.

- [151] Z. Kyselova, Y. Mechref, M. M. Al Bataineh, L. E. Dobrolecki, R. J. Hickey, J. Vinson, C. J. Sweeney, M. V. Novotny, *Journal of Proteome Research* 6 (2007) 1822-1832.
- [152] B. Xia, C. L. Feasley, G. P. Sachdev, D. F. Smith, R. D. Cummings, *Analytical Biochemistry* 387 (2009) 162-170.
- [153] Y. Hu, Y. Mechref, *Electrophoresis* 33 (2012) 1768-1777.
- [154] V. N. Reinhold, B. B. Reinhold, C. E. Costello, *Analytical Chemistry* 67 (1995) 1772-1784.
- [155] P. M. Rudd, C. Colominas, L. Royle, N. Murphy, E. Hart, A. H. Merry, H. F. Hebestreit, R. A. Dwek, *Proteomics* 1 (2001) 285-294.
- [156] N. G. Karlsson, B. L. Schulz, N. H. Packer, J. M. Whitelock, *Journal of Chromatography B-Analytical Technologies in the Biomedical and Life Sciences* 824 (2005) 139-147.
- [157] M. Wuhrer, H. Geyer, M. von der Ohe, R. Gerardy-Schahn, M. Schachner, R. Geyer, *Biochimie* 85 (2003) 207-218.
- [158] A. Nicholls, K. A. Sharp, B. Honig, *Proteins* 11 (1991) 281-296.
- [159] R. S. Spolar, J. R. Livingstone, M. T. J. Record, *Biochemistry* 31 (1992) 3947-3955.
- [160] C. S. Chu, M. R. Ninonuevo, B. H. Clowers, P. D. Perkins, H. J. An, H. Yin, K. Killeen, S. Miyamoto, R. Grimm, C. B. Lebrilla, *Proteomics* 9 (2009) 1939-1951.
- [161] L. R. Ruhaak, C. Huhn, W.-J. Waterreus, A. R. de Boer, C. Neusuess, C. H. Hokke, A. M. Deelder, M. Wuhrer, *Analytical Chemistry* 80 (2008) 6119-6126.
- [162] K. A. Stumpo, V. N. Reinhold, *Journal of Proteome Research* 9 (2010) 4823-4830.
- [163] P. M. Drake, W. Cho, B. Li, A. Prakobphol, E. Johansen, N. L. Anderson, F. E. Regnier, B. W. Gibson, S. J. Fisher, *Clinical Chemistry* 56 (2010) 223-236.
- [164] Y. Mechref, Y. Hu, A. Garcia, S. Zhou, J. L. Desantos-Garcia, A. Hussein, *Bioanalysis* 4 (2012) 2457-2469.
- [165] Y. van Kooyk, G. A. Rabinovich, *Nature Immunology* 9 (2008) 593-601.
- [166] L. S. Kreisman, B. A. Cobb, *Glycobiology* 22 (2012) 1019-1030.
- [167] S. Hua, H. J. An, S. Ozcan, G. S. Ro, S. Soares, R. DeVere-White, C. B. Lebrilla, *The Analyst* 136 (2011) 3663-3671.
- [168] S. J. North, P. G. Hitchen, S. M. Haslam, A. Dell, *Current Opinion in Structural Biology* 19 (2009) 498-506.
- [169] N. H. Packer, M. A. Lawson, D. R. Jardine, J. W. Redmond, *Glycoconjugate J.* 15 (1998) 737-747.
- [170] X. Liu, D. J. McNally, H. Nothaft, C. M. Szymanski, J.-R. Brisson, J. Li, *Analytical Chemistry* 78 (2006) 6081-6087.
- [171] S. R. Kronewitter, M. L. A. de Leoz, K. S. Peacock, K. R. McBride, H. J. An, S. Miyamoto, G. S. Leiserowitz, C. B. Lebrilla, *Journal of Proteome Research* 9 (2010) 4952-4959.
- [172] K. O. Börnsen, M. D. Mohr, H. M. Widmer, *Rapid Commun. Mass Spectrom.* 9 (1995) 1031-1034.
- [173] C. S. Chao, M. C. Chen, S. C. Lin, K. K. Mong, *Carbohydr. Res.* 343 (2008) 957-964.
- [174] A. Dell, *Methods Enzymol.* 193 (1990) 647-660.
- [175] J. Colangelo, R. Orlando, *Analytical Chemistry* 71 (1999) 1479-1482.

- [176] L. A. Gennaro, D. J. Harvey, P. Vouros, Rapid Commun Mass Sp 17 (2003) 1528-1534.
- [177] D. R. Barnidge, M. K. Goodmanson, G. G. Klee, D. C. Muddiman, J. Proteome Res. 3 (2004) 664-652.
- [178] T. Yoshimura, G. Yamada, M. Narumi, T. Koike, A. Ishii, I. Selac, S. Mitrani-Rosenbaum, K. Ikenaka, Anal. Biochem. 423 (2012) 253-260.
- [179] T. Yoshimura, G. Yamada, M. Narumi, T. Koike, A. Ishii, I. Sela, S. Mitrani-Rosenbaum, K. Ikenaka, Analytical Biochemistry 423 (2012) 253-260.
- [180] D. J. Harvey, Journal of the American Society for Mass Spectrometry 11 (2000) 900-915.
- [181] M. S. Bereman, D. L. Comins, D. C. Muddiman, Chemical Communications 46 (2010) 237-239.
- [182] B. Domon, C. E. Costello, Glycoconjugate Journal 5 (1988) 397-409.
- [183] D. J. Harvey, Journal of Mass Spectrometry 35 (2000) 1178-1190.
- [184] G. Alvarez-Manilla, N. L. Warren, T. Abney, J. A. Atwood III, P. Azadi, W. S. York, M. Pierce, R. Orlando, Glycobiology 17 (2007) 677-687.
- [185] C.-Y. Yu, A. Mayampurath, Y. Hu, S. Zhou, Y. Mechref, H. Tang, Bioinformatics 29 (2013) 1706-1707.
- [186] P. Massaroti, L. A. B. Moraes, M. A. M. Marchioretto, N. M. Cassiano, G. Bernasconi, S. A. Calafatti, F. A. P. Barros, E. C. Meurer, J. Pedrazzoli, Anal. Bioanal. Chem. 382 (2005) 1049-1054.
- [187] J. M. Maris, M. D. Hogarty, R. Bagatell, S. L. Cohn, Lancet 369 (2007) 2106-2120.
- [188] J. R. Park, R. Bagatell, W. B. London, J. M. Maris, S. L. Cohn, K. M. Mattay, M. Hogarty, C. O. G. N. C. on behalf of the, Pediatric Blood & Cancer 60 (2013) 985-993.
- [189] A. Morales La Madrid, S. Volchenboum, J. M. Gastier-Foster, R. Pyatt, D. Liu, P. Pytel, C. Lavarino, E. Rodriguez, S. L. Cohn, Pediatric Blood & Cancer 59 (2012) 736-738.
- [190] J. M. Maris, New England Journal of Medicine 362 (2010) 2202-2211.
- [191] S. L. Volchenboum, C. Li, S. Li, E. F. Attiyeh, C. P. Reynolds, J. M. Maris, A. T. Look, R. E. George, Cancer Research 69 (2009) 4143-4149.
- [192] B. D. DeNardo, M. P. Holloway, Q. Ji, K. T. Nguyen, Y. Cheng, M. B. Valentine, A. Salomon, R. A. Altura, PLoS ONE 8 (2013) e82513.
- [193] J. H. Schulte, A. Schramm, L. Klein-Hitpass, M. Klenk, H. Wessels, B. P. Hauffa, J. Eils, R. Eils, G. M. Brodeur, L. Schweigerer, W. Havers, A. Eggert, Oncogene 24 (2004) 165-177.
- [194] B. Sitek, O. Apostolov, K. Stühler, K. Pfeiffer, H. E. Meyer, A. Eggert, A. Schramm, Molecular & Cellular Proteomics 4 (2005) 291-299.
- [195] A. Varki, R. D. Cummings, J. D. Esko, H. H. Freeze, P. Stanley, C. R. Bertozzi, G. W. Hart, M. E. Etzler *Essentials of Glycobiology*; Second ed.; Cold Spring Harbor Laboratory Press, 2008.
- [196] K. Kim, L. R. Ruhaak, U. T. Nguyen, S. L. Taylor, L. Dimpasoc, C. Williams, C. Stroble, S. Ozcan, S. Miyamoto, C. B. Lebrilla, G. S. Leiserowitz, Cancer Epidemiology Biomarkers & Prevention 23 (2014) 611-621.
- [197] I. Mitra, Z. Zhuang, Y. Zhang, C.-Y. Yu, Z. T. Hammoud, H. Tang, Y. Mechref, S. C. Jacobson, Analytical Chemistry 84 (2012) 3621-3627.

- [198] K. Parsons, B. Bernhardt, B. Strickland, *Annals of Pharmacotherapy* 47 (2013) 210-218.
- [199] N. Berois, E. Osinga, *Frontiers in Oncology* 4 (2014).
- [200] F. Del Gross, M. De Mariano, L. Passoni, R. Luksch, G. P. Tonini, L. Longo, *BMC Cancer* 11 (2011).
- [201] B. Adamczyk, T. Tharmalingam, P. M. Rudd, *Biochimica et Biophysica Acta (BBA) - General Subjects* 1820 (2012) 1347-1353.